UNIVERSITÀ DEGLI STUDI DI TRIESTE

XXXII CICLO DEL DOTTORATO DI RICERCA IN NANOTECNOLOGIE

MOLECULAR PROPERTIES OF CHITOSAN AND ITS DERIVATIVES AND THEIR POTENTIAL FOR BIOMEDICAL APPLICATIONS

Settore scientifico-disciplinare: BIO/10 - BIOCHIMICA

DOTTORANDO
FRANCO FURLANI

COORDINATORE
PROF. ALBERTO MORGANTE

SUPERVISORE DI TESI
PROF. IVAN DONATI

COSUPERVISORI DI TESI
PROF.SSA ELEONORA MARSICH
DOTT. PASQUALE SACCO

ANNO ACCADEMICO 2018/2019

UNIVERSITÀ DEGLI STUDI DI TRIESTE

XXXII CICLO DEL DOTTORATO DI RICERCA IN NANOTECNOLOGIE

MOLECULAR PROPERTIES OF CHITOSAN AND ITS DERIVATIVES AND THEIR POTENTIAL FOR BIOMEDICAL APPLICATIONS

Settore scientifico-disciplinare: BIO/10 - BIOCHIMICA

DOTTORANDO
FRANCO FURLANI

COORDINATORE
PROF. ALBERTO MORGANTE

SUPERVISORE DI TESI
PROF. IVAN DONATI

COSUPERVISORI DI TESI
PROF.SSA ELEONORA MARSICH
DOTT. PASQUALE SACCO

ANNO ACCADEMICO 2018/2019

PREFACE

This thesis is submitted in fulfilment to the requirements of the Graduate School of Nanotechnology for the academic title of Ph.D. in Nanotechnology at the University of Trieste. The work has been carried out mainly at the Department of Life Sciences at the University of Trieste under the supervision of Prof. Ivan Donati and co-supervised by Prof. Eleonora Marsich and Dr. Pasquale Sacco. Part of the activity was performed at the Center for Translational Medicine (CTM), International Clinical Research Center (ICRC) of St. Anne's University Hospital, Brno, Czech Republic under the supervision of Dr. Giancarlo Forte.

The thesis consists of a general introduction, aim of the study and a detailed discussion of results divided into four chapters.

SUMMARY

Macro- and micro/nano-hydrogels are highly hydrated networks consisting of polymers and solvents. They are widely studied for different applications, especially for biomedical ones. One of the most challenging uses of hydrogels regards cartilage regeneration. Indeed, cartilage degeneration represents a severe burden for the healthcare worldwide. None of the currently proposed treatments is able to fully satisfy patients' needs, probably since most of treatments lack of peculiar spatial complexity and mechanical properties of native tissues, *i.e.* a non-linear response to stress (strain hardening effect). One of the emerging approaches complies with the use of nano-composite networks consisting of hydrogels and nanoparticles embedding drugs. The main goals of the present thesis have tackled the fabrication and characterization - in terms of physical-chemical and biological properties - of hydrogels, nanoparticles and nanocomposite networks based on polysaccharides, *i.e.* chitosan, derivatives thereof and hyaluronan. To this aim, new approaches mimicking cartilage features have been devised.

In Chapter *I* is described the extensive characterization of macromolecular association and macromolecular re-arrangement between a lactose-modified chitosan, *i.e.* CTL, in the presence of a crosslinking agent, *i.e.* boric acid, in dilute conditions. Furthermore, the interaction sites between CTL and boric acid were identified. Switching to semi-dilute polymer samples, mechanical properties were deeply investigated. Peculiar mechanical properties of native tissues, *i.e.* a non-linear response to stress and strain hardening, were detected. This system displayed some features akin to natural occurring molecular motors, and in this case, energy can be provided by stress or heat in order to foster the reorganization of the network.

In Chapter *II* are reported two different strategies, which were developed to reduce the very fast kinetics of CTL/boron self-assembly, *i.e.* a pH- and a competitor-assisted gelation. Both strategies allowed forming homogeneous networks. Resulting matrices displayed self-healing ability, non-linear response to stress (strain-hardening effect), and were responsive towards different stimuli (*e.g.* presence of small molecules or temperature). Furthermore, the possibility to embed different cell types (*e.g.* stem cells) in such networks was studied.

Chapter *III* deals with the improvement of stability and performance of CTL-based networks by using a second stable covalent crosslinking agent, *i.e.* genipin. The binding between polymer and genipin and mechanical properties were monitored. The kinetics of genipin crosslinking resulted to be directly proportional to the time and temperature. Genipin, also at low concentrations, promoted the gelation of CTL in physiological conditions of pH and osmolarity. Resulting gels displayed a

strain hardening behavior, which was preliminary attributed to formation and reorganization of intermolecular low-energy bonds (*e.g.* hydrophobic interactions and hydrogen bounds).

In Chapter *IV* is described the characterization of a broad library of chitosan/hyaluronan nanoparticles (NPs). NPs were fabricated by using chitosans with different molecular properties, *i.e.* fraction of acetylated units (F_A in the range 0.02 - 0.63) and molecular weight ($\overline{M_v}$ in the range 10 000 - 500 000). Stability and shape of NPs were investigated, and the best performing formulation was identified, namely the one fabricated with chitosan with a medium molecular weight ($\overline{M_v}$ = 220 000) and partial acetylation (F_A = 0.16). Stable NPs displayed spherical shape and a diameter close to 220 nm. When diluted in media with physiological pH and osmolarity, *e.g.* PBS, osmotic swelling-driven forces promoted the increase of size and porosity of NPs. These NPs avoided engulfment during the early stage of incubation with macrophages and did not influence the biological response of neutrophils and of macrophages. This behavior was attributed to their peculiar physical-chemical properties (*e.g.* stability, shape and porosity). Stable NPs were also able to encapsulate different payloads. Finally, NPs were embedded in the CTL-based networks and resulting networks were able to promote a sustained release of drugs.

RIASSUNTO

Macro- e micro/nano-idrogeli sono strutture altamente idratate costituite da polimeri e solventi. Sono ampiamente studiati per diverse applicazioni, in particolare in ambito biomedico. Una delle possibili applicazioni per il loro impiego riguarda la rigenerazione della cartilagine. Infatti, la degenerazione della cartilagine è un grave problema per l'assistenza sanitaria in tutto il mondo e nessuno dei trattamenti attualmente proposti è in grado di soddisfare pienamente le esigenze dei pazienti, probabilmente anche poiché la maggior parte dei materiali non presenta le peculiari proprietà meccaniche dei tessuti nativi, ovvero una risposta non lineare allo stress e l'indurimento da sforzo. Un approccio emergente è l'uso di sistemi di nanocompositi costituiti da idrogeli e nanoparticelle in grado di incapsulare farmaci per avere un loro rilascio controllato. Gli obiettivi principali della tesi sono stati quelli di fabbricare e caratterizzare le proprietà fisico-chimiche e biologiche di idrogeli, nanoparticelle e sistemi nanocompositi a base di polisaccaridi, in particolar modo chitosano e suoi derivati e acido ialuronico. A tal fine, sono stati sviluppati nuovi approcci adatti ad ottenere idrogeli biomimetici in condizioni fisiologiche.

Nel capitolo *I* viene descritta ampiamente la caratterizzazione dell'associazione macromolecolare e la riorganizzazione macromolecolare in condizioni diluite tra un chitosano modificato con lattosio, cioè CTL, in presenza di un agente reticolante, cioè acido borico. Inoltre, sono stati identificati i siti di interazione tra CTL e acido borico. Dopodiché l'attenzione si è spostata sul sistema in fase semi-diluita. Sono state rilevate proprietà meccaniche peculiari dei tessuti biologici, ovvero una risposta non lineare allo stress e l'indurimento da sforzo. Tale sistema inoltre ha mostrato alcune caratteristiche simili ai motori molecolari e in questo caso l'energia sotto forma di forza meccanica o di calore può favorire la riorganizzazione dei complessi macromolecolari.

Nel capitolo *II* sono riportate due diverse strategie che sono state sviluppate per ridurre la cinetica molto veloce dell'interazione tra CTL e acido borico, vale a dire una gelificazione assistita da pH e una gelificazione assistita da competitori. Entrambe le strategie hanno permesso di avere idrogeli omogenei. Gli idrogeli ottenuti hanno mostrato capacità di *self-healing*, una risposta non lineare allo sforzo e indurimento da sforzo ed erano sensibili a diversi stimoli (ad es. la presenza di piccole molecole o variazioni di temperatura). Inoltre, è stata studiata la possibilità di incapsulare diversi tipi di cellule (ad es. cellule staminali e condrociti) negli idrogeli.

Il capitolo *III* riguarda il miglioramento della stabilità e delle prestazioni degli idrogeli a base di CTL utilizzando un secondo agente reticolante covalente, cioè la genipina. Sono stati monitorati il legame tra polimero e genipina e le proprietà meccaniche dei campioni ottenuti. La cinetica della reticolazione della genipina è risultata direttamente proporzionale al tempo e alla temperatura. La

genipina, anche a basse concentrazioni, ha promosso la gelificazione in condizioni fisiologiche di pH e osmolarità e gli idrogeli hanno mostrato un comportamento di indurimento da sforzo, che è stato attribuito alla formazione e alla riorganizzazione di legami intermolecolari a bassa energia (ad es. interazioni idrofobiche e legami idrogeno).

Nel capitolo *IV* è descritta la caratterizzazione di un'ampia libreria di nanoparticelle a base di chitosano e di acido ialuronico (NP). Le nanoparticelle sono state fabbricate usando chitosani con diverse proprietà molecolari, cioè frazione di unità acetilate (F_A nell'intervallo 0.02 – 0.63) e peso molecolare (M_v nell'intervallo 10 000 - 500 000). Sono state studiate la stabilità e la forma delle NP ed è stata identificata la formulazione con le migliori caratteristiche, ovvero quella fabbricata con un chitosano a peso molecolare medio (M_v = 220 000) e un'acetilazione limitata (F_A = 0.16). Le NP stabili sono risultate sferiche, con un diametro attorno ai 220 nm. Una volta diluite in solventi con pH e forza ionica fisiologici, come PBS, è stato rilevato un aumento delle dimensioni e della porosità a causa del richiamo di solvente all'interno delle NP. Queste NP hanno evitato il sequestro da parte dei macrofagi nelle prime fasi di interazione e non hanno influenzato la risposta biologica dei neutrofili e dei macrofagi. Tale comportamento è stato attribuito alle loro peculiari proprietà chimico-fisiche (ad es. stabilità, forma e porosità). Le NP stabili sono risultate anche in grado di incapsulare diverse molecole (una molecola modello e farmaci antinfiammatori). Infine, le NP sono state incluse negli idrogeli a base CTL e i sistemi nanocompositi sono stati in grado di promuovere un rilascio prolungato di farmaci.

LIST OF PAPERS

1. “Boric acid induced transient cross-links in lactose-modified chitosan (Chitlac)”. P. Sacco, F. Furlani, M. Cok, A. Travan, M. Borgogna, E. Marsich, S. Paoletti, I. Donati, *Biomacromolecules* **2017**, 8, 4206–4213
2. “Concepts for developing physical gels of chitosan and of chitosan derivatives”. P. Sacco, F. Furlani, G. de Marzo, E. Marsich, S. Paoletti, I. Donati, *Gels* **2018**, 4, 67 (1-29)
3. “Nucleation, reorganization and disassembly of an active network from lactose-modified chitosan mimicking biological matrices”, F. Furlani, P. Sacco, F. Scognamiglio, F. Asaro, A. Travan, M. Borgogna, E. Marsich, M. Cok, S. Paoletti, I. Donati, *Carbohydrate polymers* **2019**, 208, 451–456
4. “Chitosan acetylation degree influences the physical properties of polysaccharide nanoparticles: implication for the innate immune cells response”. F. Furlani, P. Sacco, E. Decleva, R. Menegazzi, I. Donati, S. Paoletti, E. Marsich, *ACS Applied Materials & Interfaces* **2019**, 11, 9794−9803
5. “pH-Assisted Gelation of Lactose-Modified Chitosan” P. Sacco, F. Furlani, S. Paoletti, I. Donati, *Biomacromolecules* **2019**, 20 (8), 3070-3075
6. “Biomimetic, Multi-Responsive and Self-Healing Lactose-modified Chitosan (CTL)-based Gels formed via Competitor-assisted Mechanism”, F. Furlani, P. Sacco, M. Cok, G. de Marzo, E. Marsich, S. Paoletti, I. Donati, *ACS Biomaterials Science & Engineering* **2019**, 5, 10, 5539-5547
7. “On the formation and stability of chitosan/hyaluronan-based complex coacervates”, F. Furlani, P. Parisse, P. Sacco, *Submitted*

CONTRIBUTION TO OTHER PUBLICATIONS NOT INCLUDED IN THE THESIS

1. "Highly monodisperse colloidal coacervates based on a bioactive lactose-modified chitosan: from synthesis to characterization". F. Furlani, P. Sacco, E. Marsich, I. Donati, S. Paoletti, *Carbohydrate polymers* **2017**, 174, 360-368
2. "Lactose-modified chitosan gold (III)-PEGylated complex–bioconjugates: from synthesis to interaction with targeted Galectin-1 protein". Q. Liu, P. Sacco, E. Marsich, F. Furlani, C. Arib, N. Djaker, M. L. de la Chapelle, I. Donati, J. Spadavecchia, *Bioconjugate Chemistry* **2018**, 29, 10, 3352-3361
3. "N-isopropyl chitosan. A pH- and thermo-responsive polysaccharide for gel formation", M. Cok, M. Viola, F. Vecchies, P. Sacco, F. Furlani, E. Marsich, I. Donati, *Carbohydrate polymers*, **2020**, 230, 115641

LIST OF PATENTS

- F. Furlani, P. Sacco, F. Scognamiglio, S. Paoletti & I. Donati, "Idrogeli omogenei da derivati oligosaccaridici del chitosano e loro applicazioni" (Homogeneous hydrogels from oligosaccharide derivatives of chitosan and their applications), 102019000006448, Italy, *Patent pending*

LIST OF ABBREVIATIONS

B – boric acid

CH – chitosan

DLS – Dynamic Light Scattering

DP – degree of polymerization

ECM – Extra Cellular Matrix

F_A – fraction of acetylation of chitosan

G_0 – shear modulus at zero strain

HA – hyaluronic acid

I – ionic strength

M – mannitol

pCB – 4-chlorophenylboronic acid

PDI – Polydispersity Index

$R_{G/N}$ – moles ratio between genipin and primary amine

$R_{M/B}$ – moles ratio between mannitol and boric acid

ROS – Reactive Oxygen Species

SAXS – Small Angle X-ray Scattering

TNF – Tumor Necrosis Factor

γ^* – critical strain

η_0 – zero shear viscosity

Table of contents

1 INTRODUCTION

1.1 Hydrogels

Hydrogels are highly hydrated three-dimensional networks consisting of two components, *i.e.* the liquid – the prevalent element – and the solute. The latter is usually a polymer, *e.g.* polysaccharides, able to retain a large amount of solvent, *i.e.* an aqueous solution (in the case of non-aqueous solution the more general term "gel" can be used). Although this description of hydrogels can seem simplistic, it could be quite difficult to appropriately define hydrogels. Probably the most complete definition of hydrogels needs to refer to their mechanical properties, in particular rheological ones. More in detail, rheological investigations of the system strained under oscillatory conditions for a large range of frequencies are necessary to define a hydrogel.(Lapasin, 2016) Generally, two different behavior can be detected: (*i*) viscous liquids display the storage modulus, *i.e.* G'; lower than the loss modulus, *i.e.* G", (*ii*) hydrogels display G' higher than G" in a large range of frequencies.

Hydrogels can be fabricated by exploiting different strategies, *i.e.* chemical and physical crosslinking. Physical crosslinking strategies include thermally induced entanglement of polymer chains, molecular self-assembly, ionic gelation and electrostatic interaction.(Zhang & Khademhosseini, 2017)

Hydrogels are widely used for different applications, spanning from biomedicine to soft electronics, sensors, and actuators.(Zhang & Khademhosseini, 2017) Some of the most advanced and studied applications of hydrogels deal with the biomedical field, *e.g.* regenerative medicine and drug delivery.(Jiang, Chen, Deng, Suuronen, & Zhong, 2014; Kim, Shin, & Lim, 2012; Tibbitt & Anseth, 2009; Webber, Khan, Sydlik, Tang, & Langer, 2015; Zhang & Khademhosseini, 2017) Regenerative medicine approaches require suitable networks able to mimic natural tissues properties, *e.g.* spatial composition, biochemical milieu and mechanical performance. Ideally, mimicking the biochemical and biomechanical behavior of the natural Extra Cellular Matrix (ECM) is a robust, widely sought strategy providing a solid rationale for biomaterials development. Different authors reported that both non-linear response to stress and strain-hardening behavior are the main features of the natural ECM.(Ma, Xu, Coulombe, & Wirtz, 1999; Storm, Pastore, MacKintosh, Lubensky, & Jamney, 2005; Jingyuan Xu et al., 1998) These peculiar characteristics act as mechanical stimuli for cells, which influence their fate, including proliferation and differentiation. Such conversion of mechanical external information into intracellular signaling is termed as "mechanotrasduction".(Chaudhuri, Gu, Darnell, et al., 2015; Chaudhuri et al., 2016; Nam, Hu, Butte, & Chaudhuri, 2016; Varelas et al., 2014)

Macro-, micro- and nano-gels are also widely used for drug delivery purposes. For these applications, appropriate systems should be biodegradable and biocompatible, without eliciting any immune response if implanted or administered. Naturally occurring biopolymers, *e.g.* polysaccharides are currently exploited to fabricate macro-, micro- and nano- ECM mimics, since they display most of the above mentioned properties.(Coviello, Matricardi, Marianecci, & Alhaique, 2007; Matricardi, Alhaique, & Coviello, 2016; Rowley, Madlambayan, & Mooney, 1999) In this scenario, chitosan and hyaluronic acid represent very attractive biopolymers both for regenerative medicine and drug delivery purposes.(Agnihotri, Mallikarjuna, & Aminabhavi, 2004; Bhattarai, Gunn, & Zhang, 2010; Croisier & Jérôme, 2013; Luo & Wang, 2014; Tripodo et al., 2015)

1.1.1 Mechanobiology in hydrogels

Mechanobiology deals with the study of mechanical cues, *i.e.* forces and mechanical properties of materials, in affecting cell function, *e.g.* adhesion, spreading and activation of cellular pathways.(Brusatin, Panciera, Gandin, Citron, & Piccolo, 2018; Huebsch, 2019; L. Li, Eyckmans, & Chen, 2017)

At first, attention was focused on investigating response of cells plated atop hydrogels. The matrix elasticity of hydrogels emerged as able to tune differentiation of Mesenchymal Stem Cells (MSCs) towards neural, muscle-like and bone cells, respectively on soft, intermediate and stiff substrates.(Engler, Sen, Sweeney, & Discher, 2006) Furthermore, rigidity and viscoelastic properties of substrate were reported to affect cell spreading.(Gong et al., 2018)

Nevertheless, cells, in natural conditions, are mainly distributed in three dimensional networks, *i.e.* Extra Cellular Matrix (ECM). Thus, attention moved to cells within 3D networks, able to recapitulate complexity of natural ECM.(Li et al., 2017) Networks elastic modulus stand out to tune MSCs differentiation towards osteocytes or adipocytes both *in vitro* and *in vivo*.(Huebsch, 2019; Huebsch et al., 2015; Oliver-De La Cruz et al., 2019) This behavior is associated to the activation of Hippo molecular pathway, governed by YAP/TAZ and affected by mechanical cues.(Brusatin et al., 2018; Chaudhuri, et al., 2016) Indeed, YAP/TAZ shuttling between nucleus and cytoplasm is a strong signal governing cell behavior.(Dupont et al., 2011; Johnson & Halder, 2014) More in detail, the activation of YAP/TAZ in the nucleus of MSCs drive them to osteogenic or chondrogenic differentiation. On the other hand, the inactivation of YAP/TAZ, confined in the cytoplasm, promote an adipogenic differentiation.(Brusatin et al., 2018)

Recently, the stress relaxation of ECM emerged as an important cue governing cell behavior. More in detail, faster relaxation entail higher proliferation, spreading, and osteogenic differentiation of MSCs.(Chaudhuri, Gu, Klumpers, et al., 2015) Furthermore, faster relaxation entail an higher

ability of chondrocytes to spread and to produce ECM.(Lee, Gu, Mooney, Levenston, & Chaudhuri, 2017)

1.2 Polysaccharides of medical interest

1.2.1 Chitosans

Chitosans are a family of biopolymers deriving from the partial/total deacetylation of chitin, the second most abundant polysaccharide on earth. Chitin is the main component of the exoskeleton of Arthropoda (*e.g.* crustaceans and insects), and it is present also in cell walls of certain fungi.(Vårum & Smidsrød, 2004) Chitin forms strong fibril-like structures and mostly play a structural role. From the structural point of view, chitosans are composed of two building β-1→4 linked sugars, *i.e.* glucosamine, $GlcNH_2$ (deacetylated, D unit) and *N*-acetyl-glucosamine, GlcNAc (acetylated, A unit) randomly or more blockwise distributed along the polysaccharide chain (Figure 1). The fraction of A units, F_A, determines the acetylation degree of chitosan. Chitosans with different fraction of acetylation can be produced by deacetylation both in alkaline and in acidic conditions by using chitin as raw material.(Vårum, Anthonsen, Grasdalen, & Smidsrød, 1991) On the other hand, highly deacetylated chitosans can be re-*N*-acetylated in hydroalcoholic media in order to tune their F_A.(Freier, Koh, Kazazian, & Shoichet, 2005; Sacco, Cok, Asaro, Paoletti, & Donati, 2018; Sorlier, Denuzière, Viton, & Domard, 2001)

The degree of acetylation influences important parameters, such as charge density, crystallinity, solubility and susceptibility to enzymatic degradation.(Vårum & Smidsrød, 2004) Chitosans behave as amphiphilic polymers since they display both hydrophobic (*N*-acetyl-glucosamine) and hydrophilic (glucosamine) units. Concerning solubility, all chitosans in acidic conditions, due to the protonation of amino groups at C2 position, behave as polyelectrolytes and are soluble. At neutral pH and above chitosans solubility is strictly dependent on F_A and molecular weight. Commonly used commercial chitosans, with F_A inferior to 0.3 and medium molecular weight, precipitate in such conditions. An highly deacetylated chitosan can be soluble at neutral pH only if the degree of polymerization, DP, is lower than 10.(Khong, Aarstad, Skjåk-Bræk, Draget, & Vårum, 2013) Conversely, medium/high molecular weight chitosans with acetylation degree approximately 40% and above, typically in the range $0.4 < F_A < 0.6$, are soluble at neutral pH.(Sannan, Kurita, & Iwakura, 1976; Vårum, Ottøy, & Smidsrød, 1994)

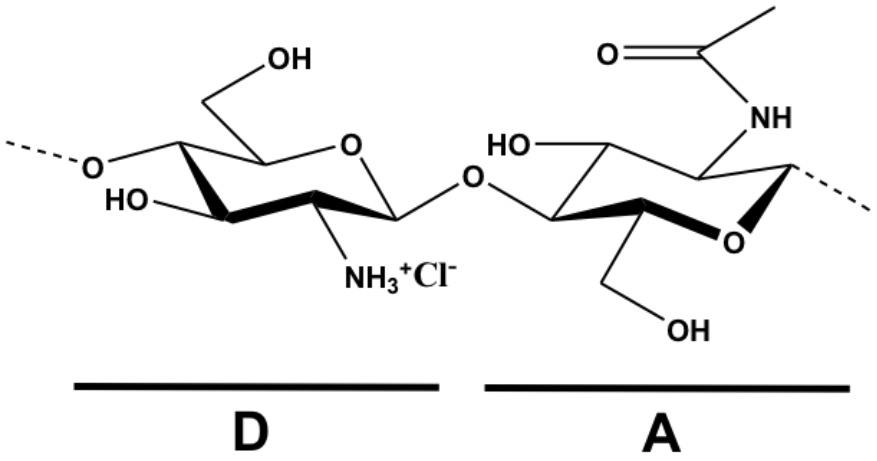

Figure 1. Schematic structure of hydrochloride chitosan. Glucosamine (D) and N-acetyl-glucosamine (A) units are reported.

Chitosans are low toxic, antimicrobic, non-immunogenic and biodegradable.(Nilsen-Nygaard, Strand, Vårum, Draget, & Nordgård, 2015) These biopolymers are extremely versatile, and can be used to develop different systems such as films, scaffolds, hydrogels, micro/nano-fibers, and micro/nano-particles.(Agnihotri et al., 2004; Aramwit, Ekasit, & Yamdech, 2015; Racine, Texier, & Auzély-Velty, 2017; Rinaudo, 2006; Sacco et al., 2014; Sacco, Brun, et al., 2018) Due to their interesting properties, chitosans are widely used for biomedical and pharmaceutical applications for the realization of systems able to encapsulate and deliver therapeutic molecules.(Aramwit et al., 2015; Calvo, Remuñán-López, Vila-Jato, & Alonso, 1997; de la Fuente, Seijo, & Alonso, 2008c, 2008a, 2008b; Elgadir et al., 2015; Janes & Alonso, 2003; Sacco, Brun, et al., 2018)

Chitosans display several interesting features, which have been discussed above. However, poor solubility at neutral pH, especially for medium/high molecular weight chitosans with $F_A < 0.4$ and lack of specific biological signals are severe limitations to its large-scale use in the biotechnological field where direct contact with cells and/or tissues is foreseen. An interesting approach for the modification of chitosan backbone is based on the introduction of sugars as flanking groups. Derivatization can be specific, involving the amino group ($-NH_2$) at C2 position, or nonspecific, involving hydroxyl groups (-OH) at C3 and C6 positions.(Rinaudo, 2006) One of the most widely used method to derivatize chitosan is the quaternization of the amino group as to improve its antibacterial properties.(Rabea, Stevens, Smagghe, & Steurbaut, 2003; Zambito, Felice, Fabiano, Di Stefano, & Di Colo, 2013) Another quite simple reaction on chitosan backbone is the reductive amination. The reaction can be performed in aqueous solutions under mild conditions yielding randomly distributed substituents along the chitosan chain.(Rinaudo, 2006) These chitosan

derivatives can display very peculiar properties. As an example, mannosylated chitosan was used for the specific recognition to antigen presenting cells such as B-cells, dendritic cells and macrophages.(Kim, Nah, Cho, Park, & Cho, 2006) Other sugar derivatives of chitosan have been reported to show antioxidant activities.(Ying, Xiong, Wang, Sun, & Liu, 2011)

1.2.1.1 Lactose-modified chitosan

Chitosan can be functionalized, by exploiting the amino group present on carbon 2, with lactose. The resulting semi-synthetic polysaccharide derived from the *N*-alkylation of chitosan in the presence of lactose is termed CTL (2-deoxy-2-lactit-1-yl chitosan, previously termed Chitlac and CTL60).(Donati et al., 2005) From the structural point of view, CTL are composed of three building β-1→4 linked sugars, *i.e.* glucosamine (D unit), *N*-alkylated glucosamine (lactitol-substituted D unit, L unit) and *N*-acetyl-glucosamine (A unit) randomly distributed along the polysaccharide chain (Figure 2).

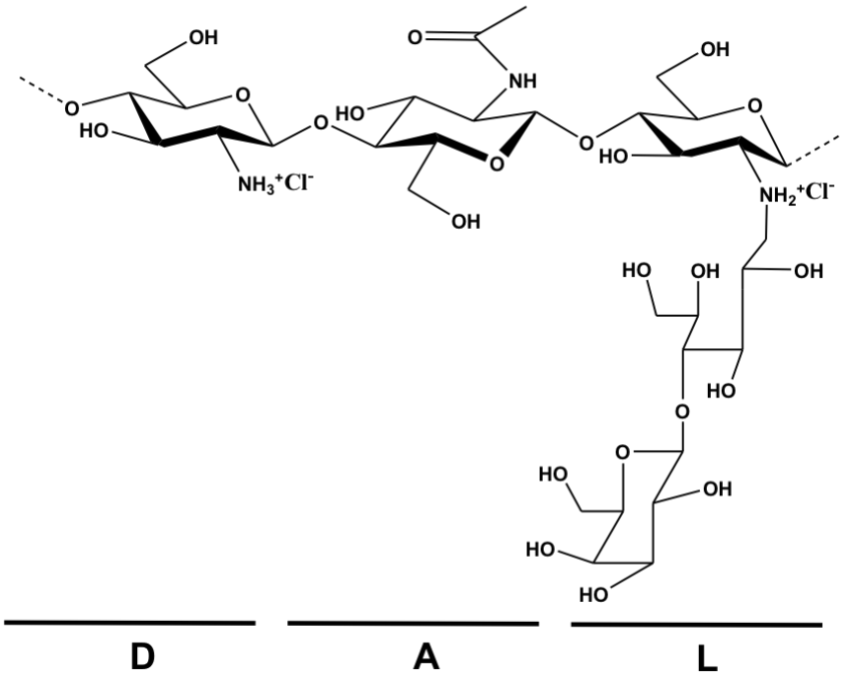

Figure 2. Schematic structure of hydrochloride lactose modified chitosan (CTL). Glucosamine (D), N-acetyl-glucosamine (A) and lactose-modified (L) units are reported. Reprinted from Furlani *et al.*(Furlani, Sacco, Marsich, Donati, & Paoletti, 2017)

The introduction of lactitol side chains on the chitosan backbone markedly modifies the physical-chemical properties of the polysaccharide rendering it soluble at neutral and basic pH and miscible with polyanions such as hyaluronan and alginate without eliciting any phase separation.(Patent No. WO135116A1, 2007) In the latter case, the interactions between the positive

charges on CTL and the negative ones on alginate lead to the formation, under controlled conditions, of soluble complexes which determine a synergistic behavior both in dilute and semi-dilute conditions.(Donati, Borgogna, Turello, Casàro, & Paoletti, 2007; Donati, Huag, et al., 2007) CTL was also used for the preparation of ternary mixtures with both alginate and hyaluronan.(Donati et al., 2011; Marsich et al., 2013) NMR and Molecular Dynamics analyses showed a higher flexibility of the lactitol side chain compared to the chitosan backbone.(D'Amelio et al., 2013) Furthermore, lactitol moieties display two different orientations with respect to the polysaccharide backbone, a folded and an extended conformation. In both conformations side chains show a good degree of water solvation.(Esteban et al., 2018)

CTL has recently emerged as intriguing examples of semi-synthetic biopolymers for potential applications in the field of drug delivery and regenerative medicine.(Furlani et al., 2017) CTL is able to form nanoparticles in the presence of tripolyphosphate (TPP, negatively charged multivalent ion) as crosslinker.(Furlani et al., 2017) Resulting colloids were found to be highly monodisperse but, at the same time, poorly stable in physiological conditions of ionic strength, pH and temperature. Some of aforementioned limitations have been overcome entailing medium molecular weight hyaluronan as additional crosslinker for chitosan.(Vecchies et al., 2018) The use of the anionic polysaccharide allowed for the synthesis of coacervates, which behave as pH-responsive carriers, thus suitable for potential applications in drug delivery. CTL has shown remarkable features in cell adhesion, proliferation and differentiation towards different cell types such as chondrocytes, osteoblasts and neural cells.(Donati et al., 2005; Medelin et al., 2018; Travan et al., 2012) CTL is prone for applications in orthopedics, and in particular for cartilage regeneration since it is able to support chondrocytes aggregation and proliferation.(Donati et al., 2005) In particular, CTL stimulate the production of collagen and glycosaminoglycans within an otherwise inert 3D architecture.(Marsich et al., 2008) Its biological significance has been traced back to the interaction with the ubiquitous Galectin 1, a protein dimer that displays two carbohydrate recognition domains.(Marcon et al., 2005) Recently, cell aggregation promoted by lactose modified chitosan emerged as crucial signal for differentiation of adipose-derived stem cells to the chondrogenic lineage.(Tan, Gao, Sun, Xiao, & Hu, 2013) Along this line, a lactose-modified chitosan was used to develop a hyaluronic acid-based hydrogel inducing stem cell aggregation during differentiation.(Tan et al., 2013) Similar biological activity has also been noticed on an osteoblast-like cell line.(Travan et al., 2012) CTL was also able to promote neuronal growth, differentiation, maturation and formation of synapses, thus representing a good candidate for the development of biomaterials for central nervous system regeneration.(Medelin et al., 2018)

1.2.1.2 Gelation of chitosan and its derivatives

Different research groups have extensively studied strategies to form chitosan-based hydrogels. The two main strategies are classified as physical and chemical gelation. Physical gelation exploits physical interactions such as hydrogen bonding, electrostatic interactions and hydrophobic interactions, and it is governed by chitosan molecular properties, *i.e.* molecular weight and fraction of acetylation, and by external parameters as pH and ionic strength. On the other hand, chemical gelation requires chemical reticulating molecules able to promote covalent bonds.

Physical chitosan hydrogels generally are more biocompatible, and it is possible to tune their gelation by varying physical-chemical parameters, *e.g.* temperature, pH and ionic strength. Usually, physical chitosan gels display lower mechanical properties compared to chemical ones.(Racine et al., 2017) Electrostatic, hydrophobic interactions and hydrogen bonds cooperate for the formation of networks. In the case of ionic interactions, pH and ionic strength play a key role. Chitosans behave as polyelectrolytes at acidic pH. In such conditions chitosans are able to interact with oppositely charged molecules forming coacervates in the micro- and nano-size range.(Luo & Wang, 2014) On the other hand, the process leading to homogeneous macro hydrogels is more demanding. An interesting approach was reported by Donati and collaborators.(Sacco et al., 2014) They reported an external gelation approach in order to finely tune gelation in the presence of negatively charged polyanions (*e.g.* tripolyphosphate). Resulting gels emerged as potential systems for drug delivery and regenerative medicine.(Sacco, Brun, et al., 2018) Other authors reported the production of hydrogels based on chitosan and anionic polymers in acidic conditions,(Patent No. EP2021408B1, 2009; Patent No. WO/2013/037965, 2013) thus limiting their use for biomedical applications. Hydrophobic interactions were widely exploited to have homogenous thermosensitive chitosan hydrogels. Thermo-sensitive gelling systems were devised by combining chitosans and polyol-phosphates (*e.g.* β-glycerophosphate), polyol bearing molecules (*e.g.* mannitol) or inorganic phosphate (*e.g.* ammonium phosphate).(Patent No. WO/2007/051311, 2007; Lavertu, Filion, & Buschmann, 2008; Supper, Anton, Boisclair, et al., 2014; Supper, Anton, Seidel, et al., 2014) These gels have shown great potential in biomedical applications including drug delivery and tissue engineering,(Chenite et al., 2000; Ta, Han, Larson, Dass, & Dunstan, 2009; L. Wang & Stegemann, 2010; Zhou, Jiang, Cao, Li, & Chen, 2015) nevertheless some authors reported limitations about stability and inadequate mechanical properties.(Huang et al., 2014; Ruel-Gariepy, Chenite, Chaput, Guirguis, & Leroux, 2000; Supper, Anton, Boisclair, et al., 2014; Supper, Anton, Seidel, et al., 2014) An alternative thermogelling system at human body temperature was reported for a system consisting of chitosan and nucleic acids.(Patent No. WO/2017/135498, 2017)

Chemical hydrogels can be produced by exploiting covalent bounds with amine and hydroxyl groups of chitosan. Molecules such as glutaraldehyde, diisocyanate or diacrylate are commonly used to promote chitosan gelation.(Patent No. WO/2009/056602, 2009; Racine et al., 2017) Unfortunately, most of them are toxic, thus limiting their use for biomedical applications.(Racine et al., 2017) An alternative naturally occurring crosslinking agent is genipin. Genipin resulted to be less toxic and it is able to promote gelation of blends of chitosan and other biopolymers.(Barbosa et al., 2010; Barbosa, Pêgo, & Amaral, 2011; Bi et al., 2011; Sung, Huang, Huang, & Tsai, 1999) Furthermore, genipin is able to efficiently promote gelation of chitosans derivatives, *e.g.* PEG grafted chitosan.(Bhattarai, Ramay, Gunn, Matsen, & Zhang, 2005)

The use of chemically modified chitosans was widely exploited to enhance performance of gels based on chitosan.(Patent No. US4424346A, 1984) For instance, chitosans grafted with water-soluble thermosensitive polymers were used to form thermosensitive hydrogels.(Argüelles-Monal, Recillas-Mota, & Fernández-Quiroz, 2017) Chitosans grafted with glycolic acid and phloretic acid were designed to obtain biodegradable injectable chitosan gels, through enzymatic cross-linking with horseradish peroxidase and H_2O_2, able to encapsulate chondrocytes.(Jin et al., 2009) An interesting use of chitosan and hyaluronic acid derivatives was proposed by Patil and collaborators.(Manna, Bharani, & Patil, 2009) Chitosan was grafted with adenine, whereas hyaluronic acid was modified with thymine and the self-assembly was obtained by means of hydrogen bonding between DNA base pairs substituted on the backbone of polymers.

1.2.2 Hyaluronic acid

Hyaluronic acid (HA) is a linear polysaccharide composed of alternating sequences of two building sugars, *i.e.* (β-1→4)glucuronic acid and (β-1→3)*N*-acetylglucosamine units, and it is usually present in its sodium salt form (Figure 3).(Kogan, Šoltés, Stern, & Gemeiner, 2007) Hyaluronic acid is a non sulphated glycosaminoglycan and it is mainly present in synovial fluid, connective tissues and the vitreous humor of the eye.(Kogan et al., 2007) In past decades, hyaluronic acid was extracted from the roosters' combs. Currently, HA is mainly produced by large scale fermentation of genetically modified bacteria, *e.g. Bacillus subtilis*, thus avoiding possible contamination by animals pathogens (*e.g. Streptococcus equi*).(Kim, Ravichandran, Khan, & Kim, 2008) Hyaluronic acid present in extracellular matrix displays an average molecular weight in the range 1-2 million.(Almond, 2007) The conformation adopted by hyaluronan can be described as a worm-like chain due to repulsion of negative charges and the polysaccharide is prone to bind positively charged molecules and water. Therefore, in aqueous solutions, hyaluronic acid is able to increase its volume

of 1 000 times. In hydrate form, hyaluronic acid is able to absorb loads and to lubricate.(Hardingham, 2004)

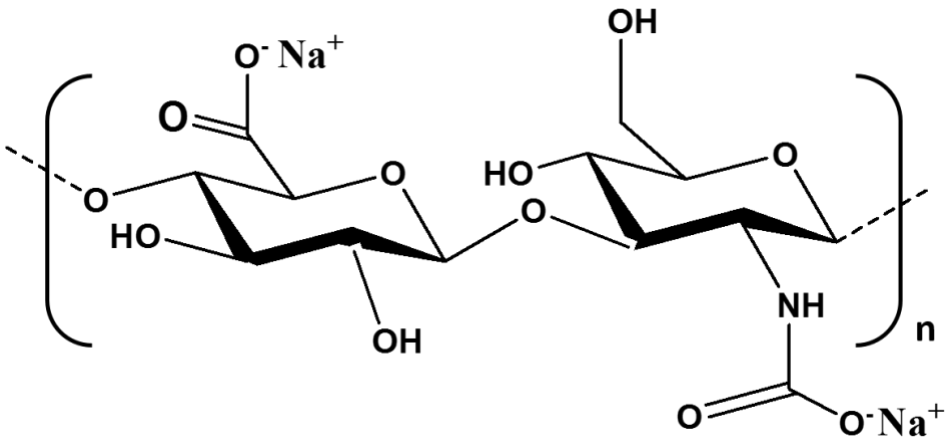

Figure 3. Schematic structure of sodium hyaluronan. Glucuronic acid and N-acetyl-glucosamine units are reported.

Hyaluronic acid plays key roles in the organization of the extracellular matrix, regulation of cell interactions, modulation of inflammation and wound healing.(Almond, 2007; Menzel & Farr, 1998) More in detail, hyaluronic acid is able to efficiently interact with the membrane receptor CD44, overexpressed in different types of cancer (*e.g.* breast and liver tumors).(Jiang, Liang, & Noble, 2007; Qin & Tang, 2002; Rao et al., 2015) This ability was exploited for specific drug delivery applications.(Almalik, Day, & Tirelli, 2013) Owing to its good biocompatibility, non-immunogenicity and viscoelastic properties, hyaluronic acid has been extensively used for the development of drug delivery systems and for regenerative medicine applications.(Highley, Prestwich, & Burdick, 2016; Tripodo et al., 2015)

Hyaluronic acid can be easily modified by exploiting its carboxylic and hydroxyl groups.(Tripodo et al., 2015) The conjugation of hyaluronic acid to hydrophobic residues can promote the self-assembly of the resulting modified polymer into biocompatible nanoparticles.(Montanari et al., 2013; Vafaei et al., 2016) Resulting nanoparticles emerged as excellent drug delivery system for hydrophobic compounds.(Montanari et al., 2019) Furthermore, the covalent conjugation of hyaluronic acid to bioactive molecules, *i.e.* HAylation, is able to increase solubility, stability and specific targeting of poor soluble drugs.(Mero & Campisi, 2014)

Hyaluronic acid and its derivatives can also be used to form hydrogels.(Burdick & Prestwich, 2011; Highley et al., 2016) Different strategies have been developed including covalent crosslinking and supramolecular interactions, *e.g.* host-guest interactions. Some of these strategies enabled the

efficient encapsulation of cells and bioactive molecules and are promising for regenerative medicine applications.(Highley et al., 2016)

1.2.3 Other polysaccharides of medical interest

Other polysaccharides used for biomedical applications include cellulose, alginate, agarose, carrageenan, starch, scleroglucan, dextran, xanthan, xyloglucan, gellan gum, guar gum, pullulan, and arabinogalactan.(Coviello et al., 2007; Silva et al., 2011)

One of the most widely used and studied is alginate, which derive from brown seaweed. This polymer is able to efficiently interact with bivalent cations, *e.g.* Ca^{2+}.(Rinaudo, 2008) This interaction can be exploited to form microparticles and hydrogels.(Kuo & Ma, 2001; Thu et al., 1996) Microparticles are suitable to encapsulate cells, *e.g.* pancreatic islets, preventing them from autoimmune response in diabetes.(Wang et al., 1997) Furthermore, alginate can be easily modified to improve its biomimetics.(Rowley et al., 1999)

Another widely used polysaccharide is agarose, which is extracted from red seaweed. This polymer can be used to form self-assembled thermosensitive hydrogels, suitable for cell encapsulation.(Mauck et al., 2000)

1.3 Polysaccharide-based nanoparticles

Polysaccharide-based nanoparticles can be devised by using natural and synthetic polysaccharides. Those based on natural polysaccharides, *e.g.* chitosan, hyaluronic acid and alginate, are the most attractive since, usually, are non-toxic, biocompatible, biodegradable and easy to functionalize.(Ali & Ahmed, 2018; Yang, Han, Zheng, Dong, & Liu, 2015) Polysaccharide-based nanoparticles can be produced by exploiting different techniques, including coacervation, and self-assembly.(Swierczewska, Han, Kim, Park, & Lee, 2016; Yang et al., 2015)

Coacervation defines a process in which a phase separation occurs, forming two phases: a polymer-rich phase, *i.e.* the coacervate, and the liquid phase. This phenomenon is promoted by the interaction between two oppositely charged molecules in right proportions. In the case of interactions between a macromolecule (*e.g.* chitosan or hyaluronan) and a small charged molecule (*e.g.* tripolyphosphate) as the term “simple” coacervation is used. On the other hand, the term “complex” coacervation is used when at least two different macromolecules are involved.

One of the most widely studied simple coacervate is based on chitosan and tripolyphosphate (TPP), as crosslinking agent. Coacervation and stability of resulting coacervates resulted to be

strongly affected by different physical chemical conditions such as the concentrations of chitosan and TPP, molecular properties of chitosan (*i.e.* molecular weight and F_A), pH and concentration of salt (*i.e.* NaCl).(Bi et al., 2011; Calvo et al., 1997; Huang, Cai, & Lapitsky, 2015; Huang & Lapitsky, 2011, 2012, 2017) Chitosan/TPP nanoparticles were extensively investigated as systems for drug, protein and gene delivery.(Abul Kalam, Khan, Khan, Almalik, & Alshamsan, 2016; Ajun, Yan, Li, & Huili, 2009; Calvo et al., 1997; De Campos, Sanchez, & Alonso, 2001; Janes & Alonso, 2003; Vimal et al., 2013; Wu, Yang, Wang, Hu, & Fu, 2005; Zhang, Oh, Allen, & Kumacheva, 2004) Resulting nanoparticles displayed an excellent ability to encapsulate and to release in a controlled way proteins and both hydrophilic and hydrophobic drugs.(Calvo et al., 1997; Masarudin, Cutts, Evison, Phillips, & Pigram, 2015; Niaz et al., 2016) Furthermore, the muco-adhesiveness ability of chitosan was exploited to treat mucus-rich sites, *e.g.* ocular and nasal sites.(De Campos et al., 2001; Janes & Alonso, 2003)

Complex coacervation was widely explored by using different natural polysaccharides such as chitosan, alginate, hyaluronan, carrageenan, dextran, in order to develop colloids suitable for protein and drug delivery.(Luo & Wang, 2014) Complex coacervation between positively charged polymers and negatively charged nucleic acids was also widely investigated for gene delivery applications.(Lallana et al., 2017; Raemdonck, Martens, Braeckmans, Demeester, & De Smedt, 2013) The driving forces for nanoparticles formations were attributed, beyond electrostatic interactions, also to the gain of entropy of the system following water and counterions release from both macromolecules.(de la Fuente et al., 2008c) One of the most investigated types of complex coacervate is based on chitosan and hyaluronic acid. Hyaluronic acid (HA) was exploited to promote the selective targeting of cells overexpressing its membrane receptor CD44,(Almalik, Karimi, et al., 2013) *e.g.* breast and liver tumors.(Qin & Tang, 2002; Rao et al., 2015) Similar nanoparticles were able to efficiently encapsulate bioactive molecules and to promote their release in a controlled fashion.(Oyarzun-Ampuero, Brea, Loza, Torres, & Alonso, 2009; Parajó, D'Angelo, Welle, Garcia-Fuentes, & Alonso, 2010; Sacco, Decleva, et al., 2017) Due to the high ability of chitosan to interact with nucleic acids, complex coacervates consisting of chitosan, hyaluronic acid and nucleic acids were devised.(Deng et al., 2014; Lallana et al., 2017) The nanoparticles ability to interact with cells was dependent on molecular properties of chitosan (molecular weight and F_A).(Almalik, Donno, et al., 2013; Lallana et al., 2017) Nevertheless, some authors reported some drawbacks on nanoparticles stability, thus limiting their use for biomedical applications.(Debele, Mekuria, & Tsai, 2016; Wu & Delair, 2015) Some research groups were able to improve the stability of resulting nanoparticles by exploiting metallic ions.(Giacalone et al., 2014; Wu & Delair, 2015)

Self-assembly is a strategy which use amphiphilic polymers, able to spontaneously self-assembly in water solutions into micelles with a controlled nanostructure.(Debele et al., 2016) Hydrophilic polysaccharides can be functionalized with hydrophobic groups, *e.g.* alkyl and deoxycholic acid. Resulting amphiphilic polymers in water undergo intra- and/or inter-molecular interaction between hydrophobic moieties, by enabling the spontaneous formation of micelles.(Yang et al., 2015) Some of the most widely used polysaccharides for such approach are chitosan and alginate.(Debele et al., 2016) Resulting nanoparticles are able to efficiently encapsulate both hydrophilic and hydrophobic drugs and they are promising for drug delivery applications.(Park, Saravanakumar, Kim, & Kwon, 2010)

1.4 Articular cartilage

Articular cartilage is a hyaline cartilage and is thick from 2 to 4 mm.(Eyre, 2002) It is composed of a dense extracellular matrix (ECM) with a sparse distribution of highly specialized cells, *i.e.* chondrocytes. The composition of ECM mainly consists of water, collagen, and proteoglycans. A limited amount of non-collagenous proteins and glycoproteins are also present.(Buckwalter, Hunzinker, & Rosenberg, 1988) This peculiar composition is able to retain a large amount of water, and the resulting tissue is able to absorb impacts and withstand significant loads. Articular cartilage can be subdivided in four zones with different strength as a function of the extension of collagen crosslinking and different cell distribution (Figure 4). These zones, with different fibrillar architecture are (*i*) superficial or tangential, (*ii*) intermediate or transitional, (*iii*) deep or radial, and (*iv*) calcified.(Eyre, 2002) In the superficial zone (thick ~200 μm) collagen fibrils tightly packed and are mainly parallel to the plane of the articular surface. In this zone the concentration of chondrocytes is relatively high. This zone is in contact with synovial fluid and it is responsible for protecting deeper layer from shear, tensile and compressive forces. Furthermore, lubricating molecules such as proteoglycan-4 allow for low-friction movement in joints.(Levett et al., 2014) In the transitional zone, collagen fibrils are oblique, and cells are spherical and at low density. The intermediate zone represents 40-60% of total cartilage volume and it provides resistance to compressive forces. In the deep zone, collagen fibrils display a high diameter and they are orthogonal to the articular surface, providing a high resistance to compressive forces. In this zone cells are parallel to fibrils in a column-like disposition. The deep zone account for around 30% of total cartilage volume and it consist of a high percentage of proteoglycans. The calcified zone welds the deep zone of cartilage to subchondral bone, enabling the transmission of loads to the underlying subchondral bone. In this zone, only a limited number of chondrocytes are present and they display a hypertrophic phenotype. The

molecular composition of the different zones is very similar, with the predominant fraction of collagen II (≥90%) and a small fraction of collagen IX (~1%) and XI (~3%); in the calcified zone collagen X is also present.(Eyre & Wu, 1987; Gannon et al., 1991)

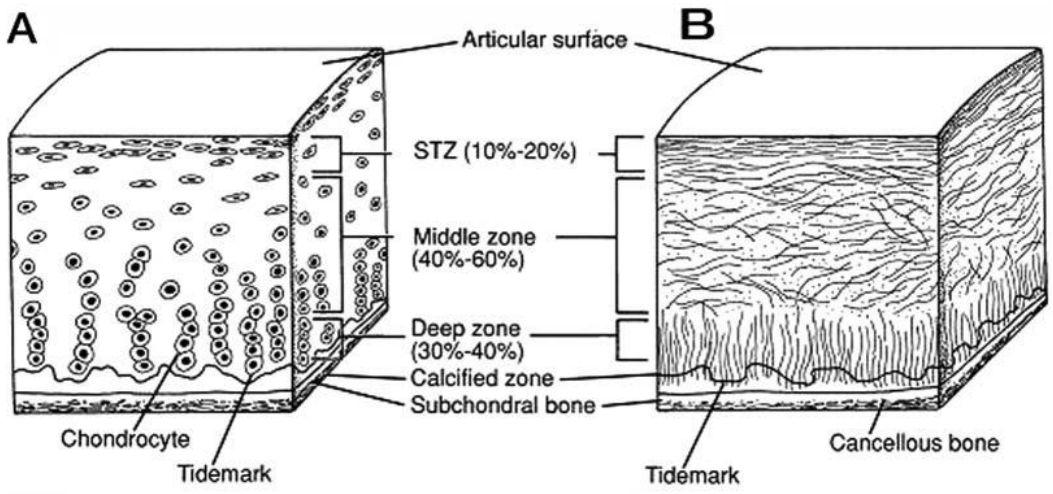

Figure 4. Schematic cross-section of cellular organization **(A)** and collagen fiber architecture **(B)** of articular cartilage. Reprinted with permission from Buckwalter *et al.*(Buckwalter et al., 1994) Copyright 1994, Wolters Kluwer Health.

Articular cartilage, differently from other tissues, does not have blood vessels or nerves. Chondrocytes depend mainly on anaerobic metabolism and nutrients come from the synovial fluid through diffusion. Chondrocytes synthesize ECM components and they are able to remodel them by means of metalloproteinases (*e.g.* collagenase and gelatinase) and cathepsins.

Articular cartilage is able to withstand high cyclic loads and this ability is attributed to its peculiar viscoelastic properties.(Buckwalter, 1998; Mankin, 1982) Cartilage can be considered as an hydrogel consisting of polymers (collagen, proteoglycans) and an aqueous solution accounting for up to 80% of the total weight; in the latter phase inorganic ions, *e.g.* calcium, sodium, potassium, and chloride are also present.(Ateshian, Warden, Kim, & Al., 1997) When forces are applied to joint, the increase in interstitial fluid pressure induce fluid flow out of the ECM.(Mow, Holmes, & Lai, 1984) When the force is removed, the fluid is able to flow back into the ECM. Furthermore, the two opposing bones and surrounding tissues confine the cartilage under load to limit mechanical deformation. This complex composition and organization provide cartilage a strain-hardening behavior.(Setton, Mow, & Howell, 1995; Woo, Mow, & Lai, 1987)

1.4.1 Arthritis and cartilage degeneration

Mature articular cartilage can undergo degeneration following severe injuries or degenerative diseases. Due to repetitive mechanical loading or inflammation, a progressive and irreversible degeneration of articular cartilage can occur. The resulting disease is called osteoarthritis (OA) and usually imply also changes in the surrounding synovial fluid and bone tissue. Osteoarthritis currently affects 250 million people worldwide, with a major incidence in elder people. With the combining factors of increasing aging and obesity of population, its incidence will grow further. Osteoarthritis can affect knee, hand and hip joints. The most common zone affected is knee, with an incidence in Europe, among people older at least 22 years, of 14% for men and 12% for women.(Hunter & Bierma-Zeinstra, 2019) People affected by osteoarthritis usually display a severe pain. These conditions have significant costs for patients affected and for the healthcare system. The medical cost of osteoarthritis in various high-income countries has been estimated to account for between 1% and 2.5% of the gross domestic product of these countries.(Hunter, Schofield, & Callander, 2014)

In the case of trauma, the native tissue try to repair the defect, albeit mature cartilage has little capacity of self-repair.(Vasiliadis, Wasiak, & Salanti, 2010) In the case of a partial-thickness injury, a limited amount of synovial fibroblasts migrate towards and into the defect.(Hunziker & Rosenberg, 1996) On the other hand, in the case of full-thickness injury, a large amount of cells from subchondral bone migrate in the defect. These cells form a fibrous or fibrocartilaginous reparative tissue. The resulting tissue lack of optimal mechanical properties and of the complex architecture of the native tissue and it is not able to bond with the remaining healthy cartilage.(Lietman, Miyamoto, Brown, Inoue, & Reddi, 2002; Steadman et al., 2003)

Osteoarthritis can occur also without any trauma. In this case, usually, an unpaired balance between matrix deposition and matrix degradation is present.(Torzilli, Grigiene, Borrelli, & Helfet, 1999) In the case of altered cartilage metabolism, chondrocytes can produce and excessive amount of enzymes, *e.g.* metalloproteinases, inducing a massive matrix degradation. This process can be induced by the presence of large amount of proinflammatory cytokines, *e.g.* TNF-α and IL-1.(Buckwalter, 1997) Similar phenomena can also be promoted by joint inactivity and insufficient dynamic loads.(Akizuki et al., 1986)

Articular cartilage can undergo degeneration also without trauma and with an early onset. Rheumatoid arthritis is an autoimmune disease that leads to inflammation and progressive degradation of cartilage. In this condition, immuno-complexes are present, which induce recruitment of neutrophils and consequently of macrophages. These cells release a large amount of pro-

inflammatory compounds which induce the onset of a chronic inflammation and the progressive degradation of articular cartilage.(Udalova, Mantovani, & Feldmann, 2016)

1.4.1.1 Strategies for cartilage regeneration

Due to articular cartilage poor regenerative and self-healing ability, different strategies have been studied in the last decades in order to improve cartilage regeneration. These techniques can be grouped in (*i*) bone marrow stimulation techniques, (*ii*) direct chondral replacement techniques, and (*iii*) culture-based techniques. Each of them can be associated with various materials and growth factors, leading to the development of a huge number of different techniques.(Correa & Lietman, 2017)

(*i*) Bone marrow stimulation technique includes drilling, abrasion and microfracture. These approaches entail the "damage" of remaining articular tissue in order to promote the release of mesenchymal stem cells from subchondral bone. Mesenchymal stem cells are able to form a fibrous tissue, nevertheless a significant symptomatic improvement was detected in most patients.(Steadman, Rodkey, Briggs, & Rodrigo, 1999) After a long term follow up, about 20% patients did not report any improvement.(Knutsen et al., 2007) Another variant of such techniques is termed Autologous Matrix Induced Chondrogenesis (AMIC). According to this procedure, after microfracture, a collagen scaffold is placed on the defect in order to hold in place the mesenchymal stem cells and help the repair process.(Jacobi, Villa, Magnussen, & Neyret, 2011)

(*ii*) Direct chondral replacement techniques include mosaicplasty, fresh osteochondral allograft transplantation and periosteal transplantation. In these techniques, the injured cartilage is replaced with osteochondral portions taken from non-load-bearing regions of the joints from the same patient (autograft) or from donors (allograft). These approaches were tested for both partial- and full-thickness lesions and results were satisfactory for most of patients in the medium term.(Leumann et al., 2009; Reguzzoni, Manelli, Ronga, M, Raspanti, & Grassi, 2005)

(*iii*) Culture-based techniques include Autologous Chondrocyte Implantation (ACI) and Matrix-induced Autologous Chondrocyte Implantation (MACI). Both strategies entail tissue engineering approaches. A full thickness biopsy is first harvested from the patient, then autologous chondrocytes are extracted from the biopsy (by using enzymes) and expanded in two-dimension cultures for about four weeks. Finally, chondrocytes are implanted in the patient. According to the first approach, *i.e.* ACI, chondrocytes are injected under a periosteal cover, which then is saturated onto the defect; at a later time, a collagen scaffold was used in place of the periosteal cover.(Richardson, Caterson, Evans, Ashton, & Roberts, 1999) In approximately 50% of cases, the repair tissue from ACI resembles fibrocartilage and is rich in collagen type I (instead of collagen type

II).(Vasiliadis et al., 2010) This is most likely due to chondrocytes de-differentiation during expansion in two-dimensional cultures. Therefore, at a later time, MACI procedures were developed (Figure 5). This approach entails cells seeding onto a scaffold a few days before implantation. Finally, the scaffold is trimmed in order to fit the patient defect and fixed in the damaged site by exploiting a fibrin glue.(Franceschi et al., 2008; Jacobi et al., 2011)

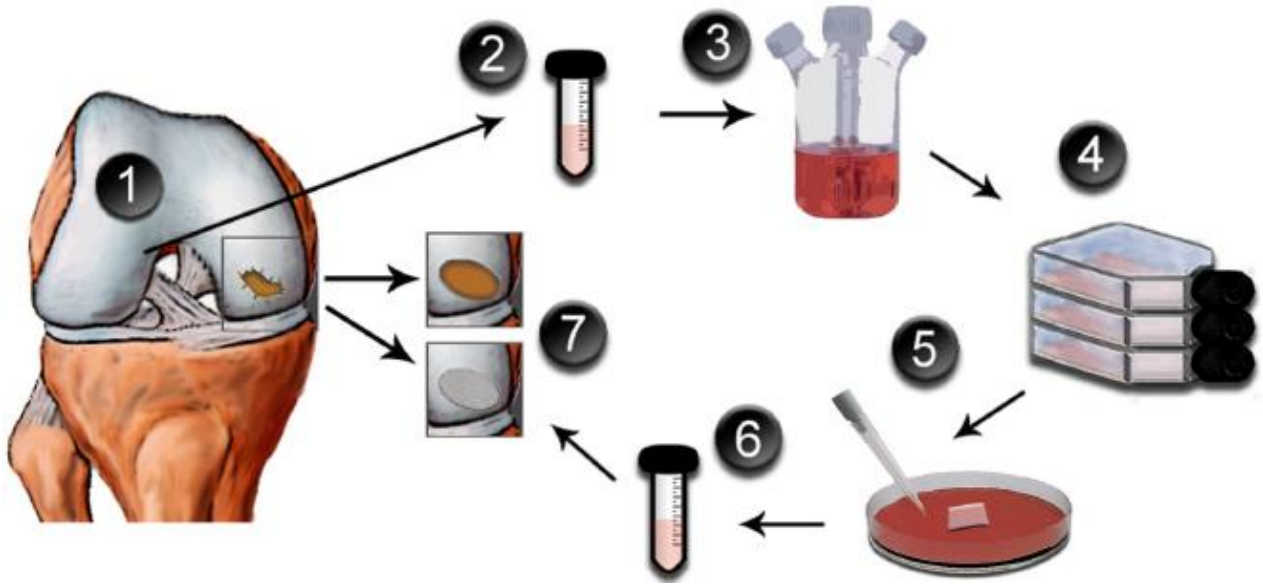

Figure 5. Schematic procedure of Matrix-induced Autologous Chondrocytes Implantation (MACI). Reprinted from Jacobi *et al.*(Jacobi et al., 2011)

One of the major limitations of currently proposed regenerative approaches for cartilage has been the inability to regenerate tissue with the original composition and structure of articular cartilage. Consequently, the repair tissue lacks the mechanical properties required to support loads.

Hydrogels, due to their structural similarity to natural tissues, are promising candidates for cartilage repair. Hydrogels can be tailored with adequate mechanical strength and porosity in order to form a biomimetic ECM environment.(Demoor et al., 2012; Knutsen et al., 2004) The design of biomaterials able to promote chondrogenic differentiation and guide cartilage extracellular matrix synthesis resulted as a promising approach to improve cartilage regeneration outcomes. Different chemically and physically crosslinked hydrogels based on synthetic or natural polymers have been developed in the last decades. Usually, synthetic based hydrogels, albeit appropriate as to mechanical properties, lack of bioactivity, *e.g.* the ability to promote chondrogenic differentiation.(Klein, Rizzi, Reichert, Georgi, N, Malda, & Schuurman, 2009) To improve the latter, different growth factors and peptides were embedded or grafted.(Albrecht et al., 2011; Nguyen, Kudva, Guckert, Linse, & Roy,

2011) On the other hand, hydrogels based on natural polymers, such as collagen, agarose, chitosan, alginate, gelatin, hyaluronic acid (HA), and chondroitin sulfate, showed excellent biological activity.(Klein et al., 2009) Recently, hydrogels based on chondroitin sulfate and polyacrylamide were reported to display an excellent adhesiveness to native tissue and a good ability to promote chondrogenic differentiation.(Han et al., 2018) Furthermore, hydrogels based on modified gelatin, hyaluronic acid and chondroitin sulfate (all of them methacrylated, in order to be photocurable) were devised and resulted to promote chondrogenesis and production of a biomimetic ECM.(Levett et al., 2014) Thermosensitive hydrogels based on chitosan were also able to promote differentiation of mesenchymal stem cells in chondrocytes.(Huang et al., 2014)

An emerging approach is the use of injectable hydrogels embedding biodegradable nanoparticles encapsulating anti-inflammatory drugs or growth factors, providing a sustained release of them over time. The resulting system should weaken the chronic inflammation and simultaneously support the regeneration of healthy articular cartilage.(Asadi et al., 2018; Jeznach, Kołbuk, & Sajkiewicz, 2018) For instance, chitosan based nanoparticles encapsulating drugs and embedded in an hydrogel based on chitosan, alginate and fibrin resulted to efficiently support chondrogenesis *in vivo* and to promote the production of a biomimetic ECM.(Deepthi, Gafoor, Sivashanmugam, Shantikumar, & Jayakumar, 2016)

2 AIM OF THE THESIS

The main aim of this research thesis deals with the production of polysaccharide-based nanocomposite networks to be potentially used as biomaterials for tissue engineering and regenerative medicine, with special focus on cartilage restoration. The specific objectives of the thesis are:

- **i.** Investigate macromolecular association and characterize networks based on CTL and boric acid as crosslinking agent;
- **ii.** Establish methods for forming homogeneous hydrogels;
- **iii.** Investigate the suitability of resulting hydrogels for cells colonization and proliferation;
- **iv.** Fabricate and characterize hydrogels based on chitosan and CTL by using a second covalent gelling agent, namely genipin;
- **v.** Evaluate the influence of different molecular properties of chitosan (*i.e.* fraction of acetylation and molecular weight) on physical-chemical properties of chitosan/hyaluronan nanoparticles;
- **vi.** Study how nanoparticles stability and physical-chemical properties can affect the innate immune system cells response;
- **vii.** Evaluate the possibility to use nanoparticles and nanocomposite networks as drug delivery systems.

3 EXPERIMENTAL SECTION

3.1 CHAPTER I: Preparation and characterization of networks based on a lactose-modified chitosan and boric acid

3.1.1 Aim of the work

In this chapter the main aims are (*i*) evaluate CTL structuring in the presence of boric acid, (*ii*) evaluate if energy, provided in different forms (*i.e.* stress and heat), can induce a network reorganization, (*iii*) investigate interaction sites of boric acid binding to CTL, (*iv*) evaluate mechanical properties of resulting networks as function of boric acid concentration.

3.1.2 Material and methods

3.1.2.1 Materials.

Lactose-modified chitosan (CTL or CTL)-hydrochloride form with fractions of: *N*-acetyl glucosamine (GlcNAc; "acetylated", A) (F_A) = 0.07; glucosamine ($GlcNH_2$; "deacetylated", D) (F_D) = 0.36; lactitol-substituted D unit (N-alkylated GlcLac; "lactitol", L) (F_L) = 0.57 was kindly provided by biopo*Life* S.r.L. (Trieste, Italy). The intrinsic viscosity, [η], at 25 °C was 470 mL/g and the weight average molar weight was $\overline{M_W}$ = 770 000 with a PI of 2.68 (SEC-MALLS, data not shown). Phosphate-buffered saline (PBS), boric acid (H_3BO_3), sodium chloride, deuterium oxide, 4-chlorophenylboronic acid (pCB), sodium hydroxide (NaOH), and deuterium oxide were all purchased from Sigma Aldrich (USA). All other reagents were from Sigma-Aldrich (USA). All reagents and chemicals were of high purity grade. Deionized (Milli-Q) water was used as solvent in all experiments.

3.1.2.2 Preparation of solutions and/or matrices.

Solutions were prepared at pH equal to 7.4 and pH was kept constant using Phosphate Buffered Saline (PBS) 1X. Briefly, for a sample with CTL final concentration equal to 10.0 g/L, 50 mg of polymer were solubilized in 3.5 mL of deionized water in a 5 mL beaker, then pH was adjusted to 7.4 by using NaOH (1 M). Finally, 450 µL of PBS 10X and water were added to have a final volume of 4.5 mL.

A typical synthesis was carried out as follows: 500 µL of a solution of boric acid with different concentration (from 0 to 320 mM) (PBS 1X as solvent and pH stabilized to 7.4) were added to 4.5 mL of CTL solution (PBS 1X as solvent and pH stabilized to 7.4) in 5 mL beakers under vigorous

magnetic stirring. The same ratio in volume between the two components was used for all experiments. After boric acid addition samples were sustainably stirred by using a magnetic stirrer to promote a homogeneous dispersion of the crosslinker. Resulting samples were allowed to equilibrate for 20 minutes at room temperature prior to further analyses.

3.1.2.3 Dynamic Light Scattering.

Dynamic Light Scattering was measured by means of a Zetasizer Nano ZS with 173° detection optics and incident light at 633 nm (Malvern Instruments) in PBS buffer (pH = 7.4) in disposable cuvettes. CTL solutions (1.5 mL, polymer concentration equal to 1.5 and 2.0 g/L) placed in disposable cuvette were titrated (3 µL injections) using an aqueous solution of boric acid (boric acid 500 mM, PBS 1X as solvent and pH 7.4) to gradually increase R_B. After each injection of cross-linking ion, the solution was vigorously shaken, and solutions were allowed to equilibrate one minute prior to measurements. Measured count rates were normalized for the attenuation factor to yield derived count rate. Data are reported as the relative scattering intensity (*i.e.* derived count rate) of the titrated solutions (I_{R_B}) and that of untreated polymer ($I_{R_B=0}$).

Measurements were also performed on CTL alone and in the presence of boric acid at 8.8 mM at 25 °C, corresponding to the sample in which was detected the maximum scattering intensity. Boric acid titration was performed at 25 °C. Then samples were analyzed at different temperatures, namely 25, 31, 37 and 43°C. As control a sample without boric acid was used. Data are reported as the difference in scattering intensity (*i.e.* derived count rate) (reported in %), by assuming equal to 0 the scattering intensity at 25°C of the respective sample.

Furthermore, measurements were performed on the same sample (CTL alone and in the presence of boric acid at 8.8 mM at 25 °C) and after a thermal curing during which the sample was measured at 25 °C, heated at 43 °C and measured at 43 °C, cooled at 25 °C and measured also at this latter temperature.

3.1.2.4 Capillary viscosity.

Reduced capillary viscosity at different R_B values (η_{r,R_B}) was measured at 25 °C by means of a Schott-Geräte AVS/G automatic measuring apparatus and an Ubbelohde type viscometer upon addition of boric acid at different concentrations. All measurements were performed at least in triplicate using PBS at pH 7.4 as buffer.

3.1.2.5 High-field NMR measurements.

700 µL of CTL solution (1 % w/v, 10% V/V D_2O, PBS, pH = 7.4) placed in a quartz tube were titrated (70 µL injections) using 4-chlorophenylboronic acid (pCB) solution (20 mM, PBS, pH 7.4).

After each pCB injection, the solution was vigorously shaken and allowed to equilibrate for few minutes before measurements. The ^{1}H-NMR, ^{13}C-NMR and ^{1}H-^{13}C-2D spectra were recorded on a Varian VNMRS (11.74 T) NMR spectrometer operating at 499.65 MHz for proton. All measurements were performed at 25 °C.

3.1.2.6 Rheological measurements.

Rheological tests for the CTL-boric acid systems were performed under continuous shear conditions to determine the extent of the steady viscosity values in the stress (τ) range 0.1 - 1000 Pa, as well as under oscillatory shear conditions to determine the extension of the linear viscoelasticity regime (stress sweep tests at 1 Hz) and the mechanical spectrum (frequency sweep, τ = 1 Pa, within the linear viscoelastic regime). The complex viscosity (η*), the storage (G') and loss (G") moduli were recorded in the frequency range 0.01 - 100 Hz. Continuous oscillatory shear tests were performed at ν =1 Hz and τ =1 Pa for 3 hours (10 800 s). All tests were carried out with the controlled stress rheometer Haake Mars III operating at 25 °C. A glass bell covering the measuring device was used to improve thermal control and limit evaporation. In the case of the system composed of CTL and boric acid 8 mM, a short stress sweep test was recorded at 25 °C and after a thermal curing (25 °C $\rightarrow$ 43 °C $\rightarrow$ 25 °C). For comparison, the short stress sweep of CTL alone was used.

3.1.2.7 Statistical analysis.

Statistical analysis and graph elaboration were performed using GraphPad Prism 8 (GraphPad Software, San Diego, CA).

3.1.3 Results and discussion

3.1.3.1 Macromolecular association

The interaction between CTL and boric acid was investigated by two complementary techniques, *i.e.* Dynamic Light Scattering (DLS) and capillary viscometry. Analyses were performed by using constant polymer concentrations and upon increasing the crosslinker concentration. By increasing the boric acid concentration, a gradual increase of the scattering was detected (Figure 6a), up to a maximum value, indicating polymer structuring. Then, by further increasing boric acid concentration the scattering intensity decreased, suggesting polymer reorganization. A symmetrical inverse trend was detected by evaluating relative viscosity values (Figure 6b). Considering both results together, the concentration of boric acid at which light scattering and relative viscosity exhibited onset of non-monotonic behavior corresponded to 7.9×10^{-3} ($\pm 1.6 \times 10^{-3}$) M boric acid.

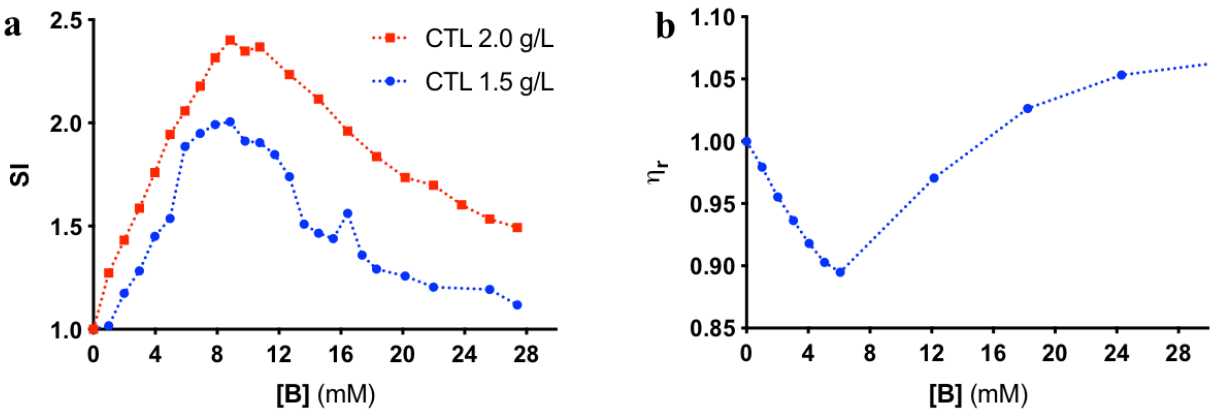

Figure 6. (a) Dependence of the normalized scattering intensity from boric acid concentration at CTL concentration of 2.0 g/L and 1.5 g/L. All measurements were performed at 25 °C in PBS at pH 7.4. Lines are drawn to guide the eye. **(b)** Dependence of the normalized relative viscosity from boric concentration at CTL concentration of 1.5 g/L. The dotted line is drawn to guide the eye. All measurements were performed at 25°C in PBS at pH 7.4.

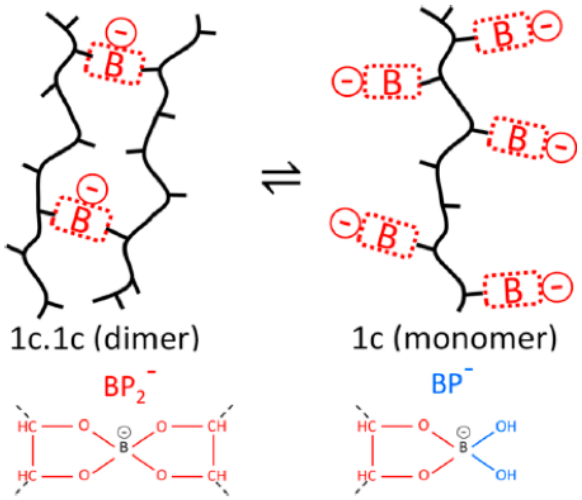

Scheme 1. Schematic representation of the formation of dimers of CTL chains (1c.1c) induced by the presence of boric acid and of the formation of single chains (1c). Reprinted with permission from Sacco *et al.*(Sacco et al., 2017) Copyright 2017 American Chemical Society.

This peculiar behavior was interpreted according to a two stage phenomenon: (*i*) at low boric acid concentrations, macromolecular CTL−boric acid complexes (indicated as BP_2^- in Scheme 1) form, increasing the mass per unit volume, and eliciting an increase in the scattering intensity and a parallel decrease of hydrodynamic volume following chain pairing, and (*ii*) at relatively high crosslinker concentrations, negative charges bore by boron elicit electrostatic repulsion between polymer chains (indicated as BP^- in Scheme 1), with complexes disentangling, and decrease of scattering intensity and increase of viscosity.

3.1.3.2 Interaction sites of boric acid to CTL

The side chains of CTL (Scheme 2) consist of an unmodified galactose linked to glucitol moiety, with various binding sites for boric acid, each of them with different binding constant when taken separately.(Peters, 2014; Wu et al., 2013) To investigate the interaction sites, high field NMR analyses were performed by exploiting a model divalent diol-binding molecule, *i.e. p*-chloro-phenyl-boronic acid (pCB), in order to avoid peak broadening due to polymer reticulation.

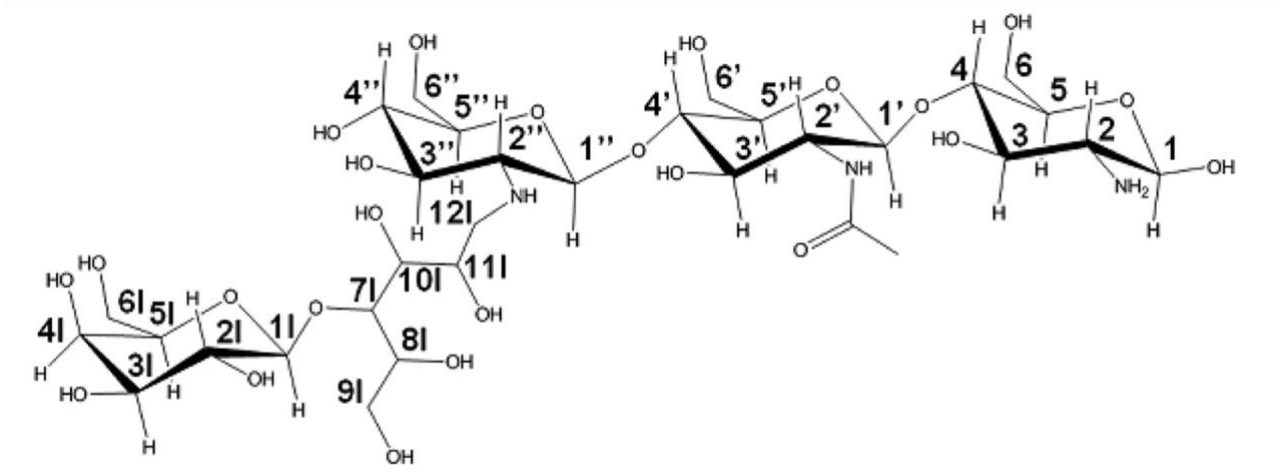

Scheme 2. Schematic representation of CTL with the labels for the different carbon atoms. Reprinted with permission from D'Amelio *et al.*(D'Amelio et al., 2013) Copyright 2013 American Chemical Society.

NMR analyses allowed to detect signals corresponding to free and bound pCB (Figure 7a). Upon increasing boronic acid concentration, a progressive increase of bound pCB was detected (Figure 7b). The saturation of binding sites was estimated to be 0.88, suggesting an approximately interaction of one boronic acid molecule for each lactitol moiety.

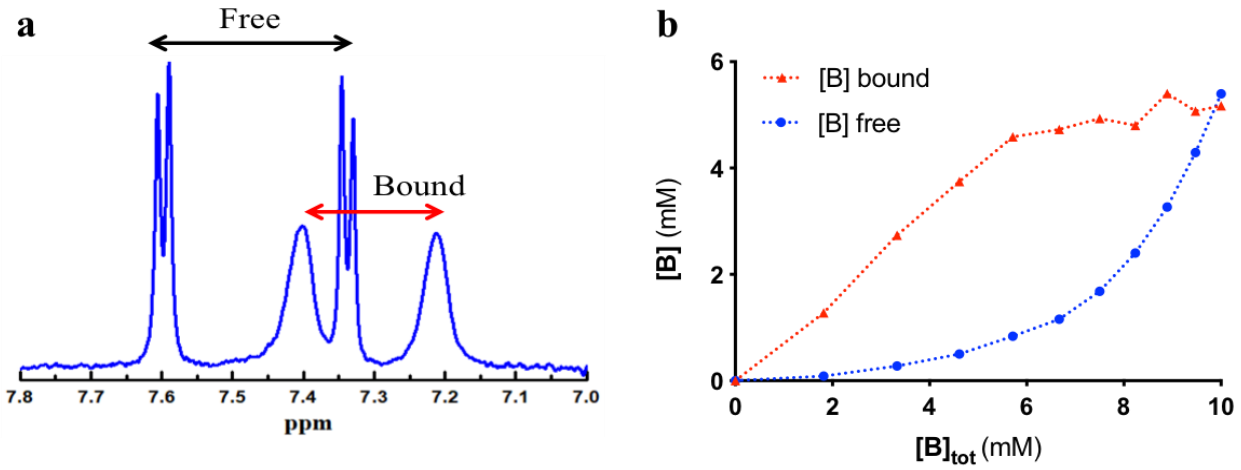

Figure 7. (a) Aromatic signals of bound and free pCB in the presence of CTL (10 mg/mL). **(b)** Saturation binding of pCB on CTL as determined by ^{1}H-NMR. Dependence of bound and free boronic acid on the total concentration of added pCB. Lines are drawn to guide the eye.

The effective binding sites of CTL were then investigated by evaluating modifications of its ^{1}H- and ^{13}C-NMR spectra.(D'Amelio et al., 2013) The schematic representation of CTL with the corresponding labelling of the different carbon atoms is reported in Scheme 2. Upon addition of pCB, several variations in the intensity and position of the ^{1}H-NMR signals were detected in the chemical shift range from 3.3 to 4.0 ppm (Figure 8).

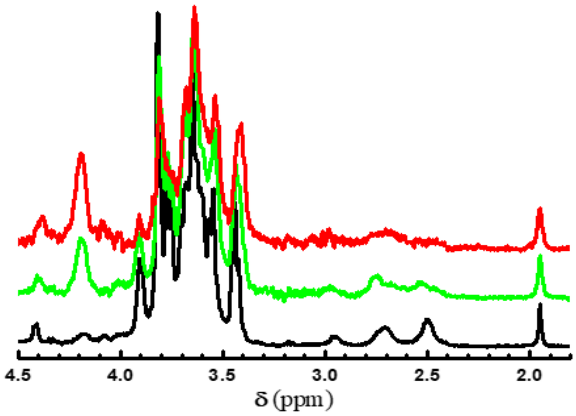

Figure 8. ^{1}H-NMR spectrum of CTL in the absence (black line) and in the presence of pCB at a concentration of 5.6 mM (green line) and of 8.6 mM (red line). Reprinted from Furlani *et al.*(Furlani, Sacco, Scognamiglio, et al., 2019)

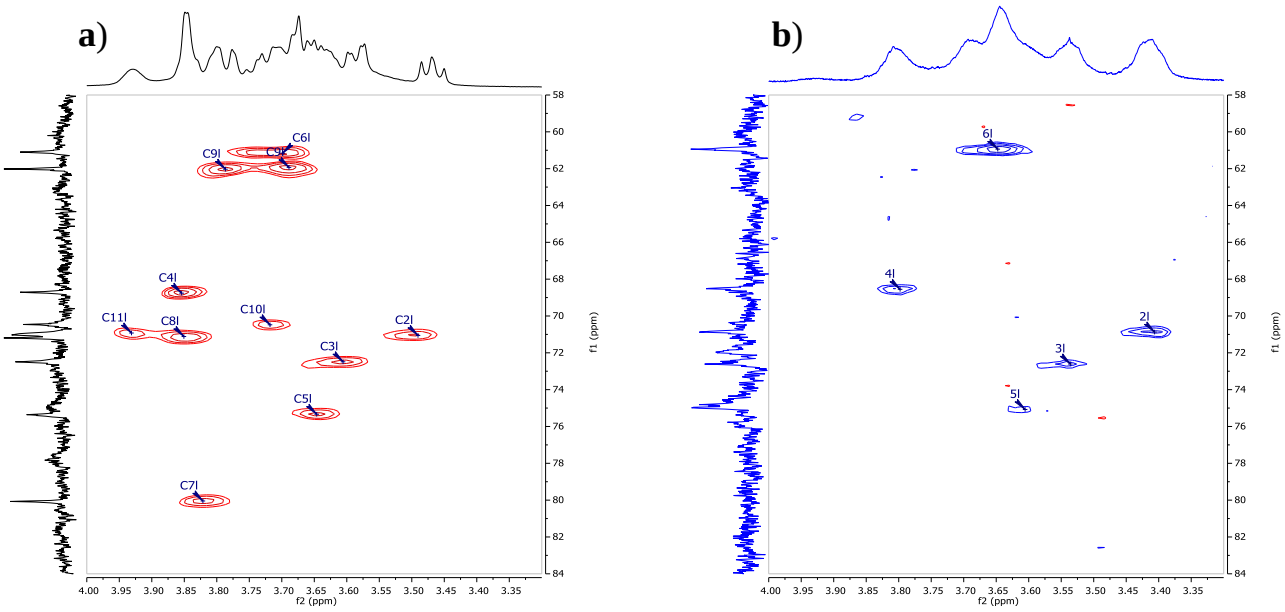

Figure 9. $_{1}$H-$_{13}$C HSQC spectra of CTL (1 % w/V) prior to **(a)** and after **(b)** the addition of pCB (19 mM). Spectral Width 5000.0 for 1H over 750 data points, 25125.6 Hz for 13C. 400 t1 increments, of 8scans each, were employed. The data matrix size after processing was 1024x1024. Reprinted from Furlani *et al.*(Furlani, Sacco, Scognamiglio, et al., 2019)

More in detail, upon increasing boronic acid, a decrease in the signal intensity of hydrogens C7*l*, C8*l*, C9*l* and C10*l* was detected. Furthermore, a shift of C11*l* from approximately 3.9 ppm to 4.2 ppm was detected. Hence, at low pCB concentrations, the boronic derivative mainly binds OH pair on vicinal carbons C10*l* and Cl1*1* of the side-chain moiety. By further increasing pCB, also C8*l*, C9*l* are involved. These results are in line with the prevalent involvement in binding CHOH groups of polyol compounds, which display a reduced freedom of rotation than the terminal CH_2OH groups.(Dawber, Green, Dawber, & Gabrail, 1988) $_{1}$H-NMR signals of galactose moiety were not affected by pCB. These results were supported by $_{1}$H-$_{13}$C 2D experiments (Figure 9). The only cross-peaks detectable in the presence of pCB are those of the galactose part of the flanking groups of CTL.

Upon increasing pCB, signals of the carbons C11*l* and C10*l* of CTL moved significantly in $_{13}$C-NMR analyses. The signal of C9*l* was not affected with limited pCB amount, whereas disappeared for higher boronic acid concentrations. On the other hand, it was not possible to follow the signal of C8*l* due to overlap (Figure 10); probably, at high pCB amount, it shifted to higher frequencies.

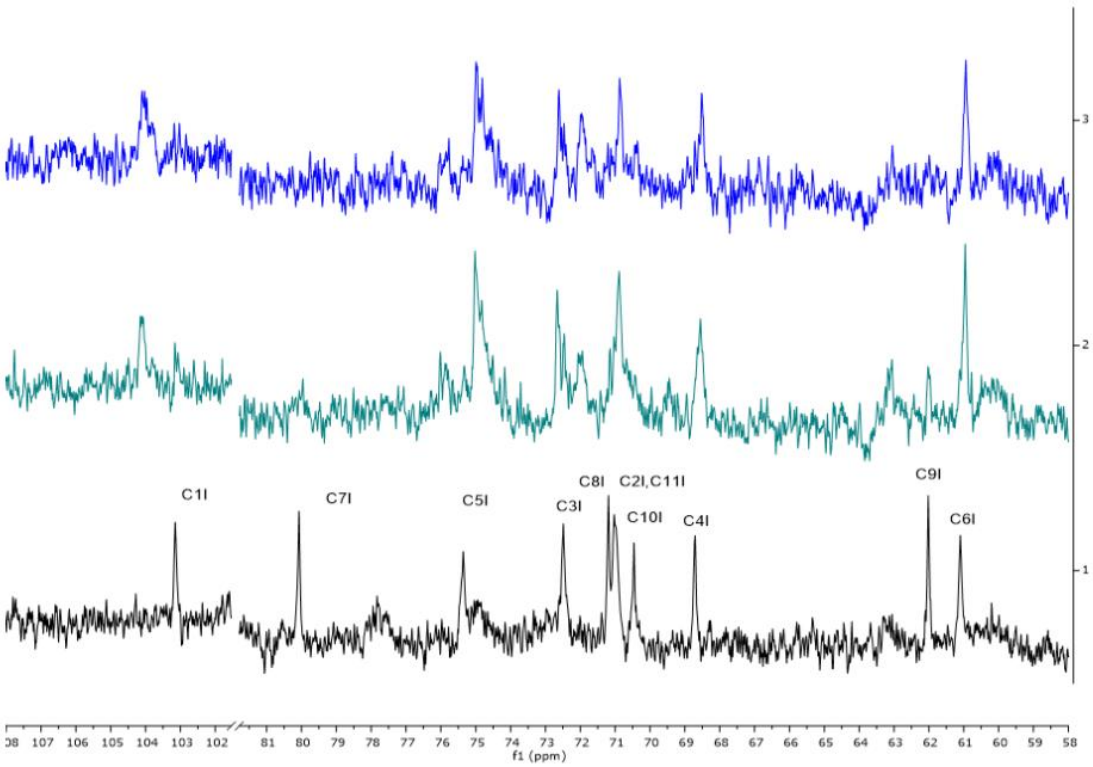

Figure 10. ^{13}C NMR signals of CTL for the samples: CTL 1% (black), CTL 0.55 % and pCB 8.6 mM (green), and CTL 1% and pCB 19 mM (blue). Reprinted from Furlani *et al.*(Furlani, Sacco, Scognamiglio, et al., 2019)

According to NMR results, the open glucose moiety of the side chain of CTL displays two binding sites for boron (Scheme 3) which seems to share the same thermodynamic features. Taking into account the stoichiometry 1:1 between boron and the lactitol moiety, a continuous shift between the two conditions can be hypothesized.

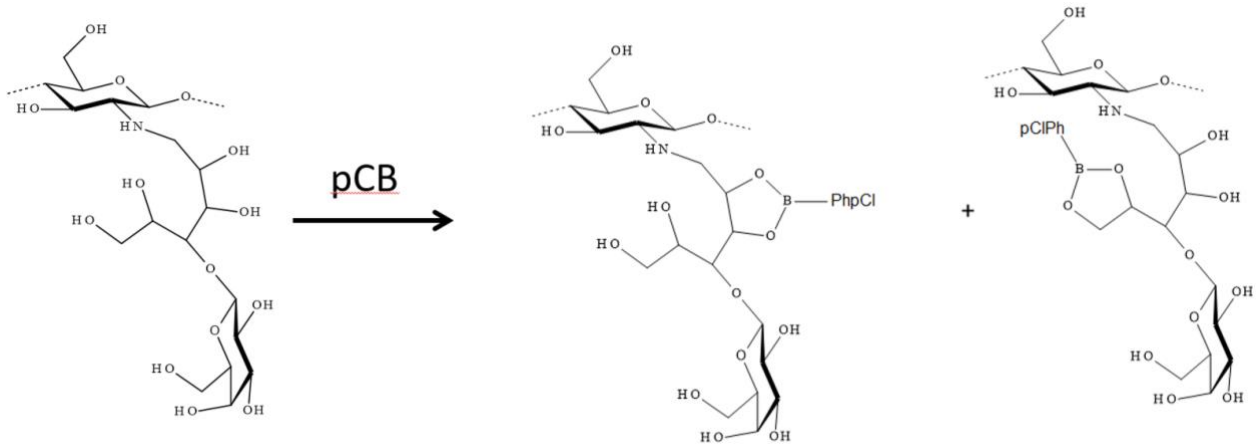

Scheme 3. Schematic representation of the pCB binding sites in CTL. Reprinted from Furlani *et al.*(Furlani, Sacco, Scognamiglio, et al., 2019)

3.1.3.3 Network nucleation and disassembly.

In order to study the role played by boric acid in modulating the mechanical properties of networks, rheological measurements were performed on systems with different amounts of boric acid, but with constant concentration of CTL.

Both G' and G" experimental data of mechanical spectra (frequency sweep tests) were nicely fitted by a combination of Maxwell elements, composed by a sequence of springs and dashpots in parallel:

$$G' = \sum_{i=1}^{n} G_i \frac{(\lambda_i \omega)^2}{1+(\lambda_i \omega)^2} \; ; \; G_i = \frac{\eta_i}{\lambda_i} \quad \text{(eq. 1)}$$

$$G'' = \sum_{i=1}^{n} G_i \frac{\lambda_i \omega}{1+(\lambda_i \omega)^2} \; ; \; G_i = \frac{\eta_i}{\lambda_i} \quad \text{(eq. 2)}$$

where *n* is the number of Maxwell elements considered, G_i is the spring constant, η_i is the dashpot viscosity and λ_i represent the relaxation time of *i*th Maxwell element.

Mechanical spectra were acquired at constant stress and different frequency values. All samples showed a crossover, *i.e.* an intersection between storage and viscous moduli curves. The only samples which did not display this peculiar viscoelastic response, *i.e.* the crossover, were those with a limited amount of boric acid and without any crosslinking agent. More in detail, above the cross-over frequency, G' > G", thus the system is more elastic than viscous. All spectra displayed similar trends of the G" - ν curve, with a clear maximum value (Figure 11a). This peculiar trend is due to the transient nature of boric acid induced reticulations.(Mayumi, Marcellan, Ducouret, Creton, & Narita, 2013)

The use of two Maxwell element is sufficient to accurately fit experimental data. According to equations 1 and 2 it is possible to determine the relaxation time, τ_{relax}, which ranges from 0.3 s to 2 s (data not shown). These data are in line reports on similar transient crosslinked networks.(Narita, Mayumi, Ducouret, & Hébraud, 2013) The increase of crosslinker and/or polymer concentrations bring an increase of relaxation time, reducing the transient nature of the networks.

In the case of the sample under oscillatory shear, eq. 1 was replaced by eq. 3, in which a purely elastic element, G_e, was added

$$G' = G_e + \sum_{i=1}^{n} G_i \frac{(\lambda_i \omega)^2}{1+(\lambda_i \omega)^2} \quad \text{(eq. 3)}$$

The number of the Maxwell elements was selected by a statistical procedure to minimize the product $\chi_2 \times N_p$, where χ_2 is the sum of the squared errors, while N_p indicates the number of fitting parameters.

An exponential dependence in shear modulus values, determined according to eq. 3, as function of the boric acid concentration was detected (Figure 11b). This can be easily explained considering that the increase of crosslinker amount increases the numbers of junction points between the CTL chains.

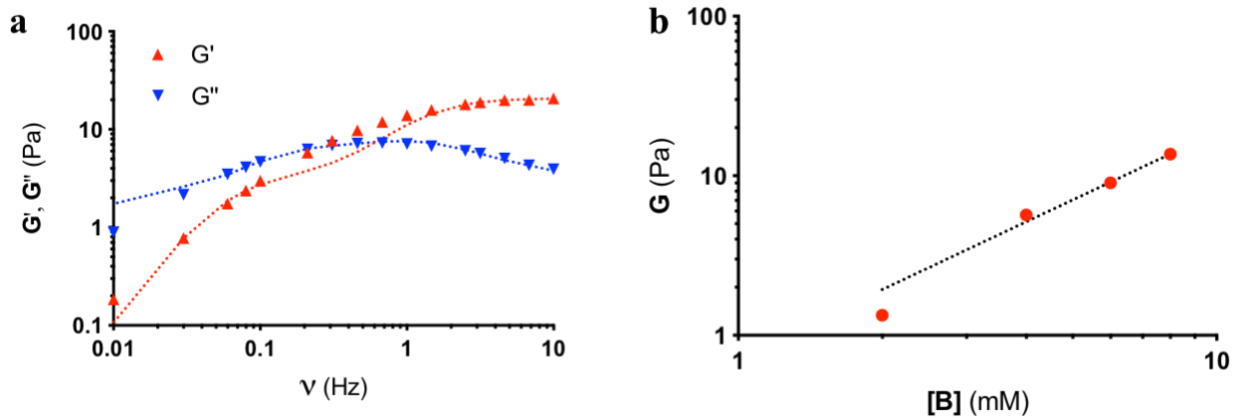

Figure 11. (a) Dependence of G' and G" on the frequency for CTL in the presence of boric acid 8 mM. Dotted lines represent the best-fit of the experimental data of G' and G" using Maxwell models (eq. 1 and eq. 2). **(b)** Dependence of the shear modulus (G), determined according to eq. 3, on concentration of boric acid. The dotted line is the best-fit of the experimental data points according to equation $G \propto [B]_{1.5}$ ($R_2 > 0.99$). Experimental conditions: [CTL] = 10 g/L, T = 25 °C, PBS 1X, pH 7.4.

Oscillatory stress-sweep experiments were then performed to investigate the extension of linear viscoelastic regime for CTL based networks. The stress/strain dependence resulted linear at least up to γ = 200%. At higher deformations, a strain hardening behavior was detected (Figure 12a). The experimental points in Figure 12a were nicely fitted using eq. 4

$$\tau = G_0 \, \gamma \, e^{\left(\left(\frac{\gamma}{\gamma^*}\right)^2\right)} \quad \text{(eq. 4)}$$

where τ is the applied stress, G_0 is the shear modulus at zero strain, γ is the experimental deformation and γ^* is the critical strain at which the deviation from linearity becomes dominant.(Erk, Henderson, & Shull, 2010)

Exponential dependence of G_0 and γ^* as function of boric acid concentrations were detected (Figure 12b).

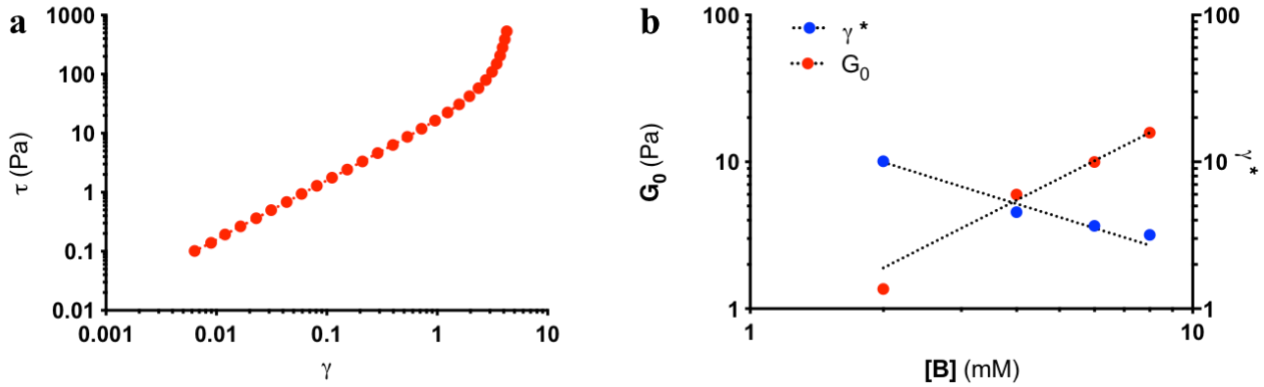

Figure 12. (a) Dependence of stress-strain response for CTL networks with boric acid 8 mM; the dotted line represents the best fit of experimental points according to eq. 4. **(b)** Dependence of the shear modulus at zero strain (G_0) and of the critical strain (γ^*) on boric acid concentration; dotted lines are the best-fit of the experimental data points according to equation $G_0 \propto [B]^{1.5}$ ($R_2 > 0.99$) and $\gamma^* \propto [B]^{-0.9}$ ($R_2 > 0.95$), respectively. Experimental conditions: [CTL] = 10 g/L, T = 25 °C, PBS 1X, pH 7.4.

The stress-strain curves of the networks were also fitted using the large deformation analysis proposed by different authors.(Carrillo, MacKintosh, & Dobrynin, 2013; Vatankhah-Varnosfaderani et al., 2017) This analysis has a premise that the onset of the non-linear elastic response is based on the bending deformation mode of network strands. Thus, the experimental points were nicely fitted using eq. 5

$$\sigma_{xy} = \frac{G\gamma}{3}\left(1 + 2\left(1 - \frac{\beta I_1(\gamma)}{3}\right)^{-2}\right) \text{ (eq. 5)}$$

where σ_{xy} is the shear stress, G is the shear modulus, $I_1(\gamma)$ is the first strain invariant for shear deformation and β is the chain elongation ratio.

$I_1(\gamma)$ is described by eq. 6

$$I_1(\gamma) = \gamma^2 + 3 \text{ (eq. 6)}$$

Whereas β is described by eq. 7

$$\beta = \frac{\langle R_{in}^2 \rangle}{\langle R_{max}^2 \rangle} \text{ (eq. 7)}$$

β is the ratio of the mean-square distance between cross-links ($\langle R_{in}^2 \rangle$) in the underformed network and the square of the end-to-end distance of the fully extended strands ($\langle R_{max}^2 \rangle$), where R_{max} equals *nl*, with *n* the number of repeating units and *l* their length.

The maximum network elongation γ_{max} is determined from eq. 8 (Vatankhah-Varnosfaderani et al., 2017)

$$\gamma_{Max} \approx \beta^{-0.5} \text{ (eq. 8)}$$

Boric acid displays the nucleation ability to promote reticulation of CTL. By exploiting the two approaches descripted above (eq. 4 and eq. 5), was possible to detect similar shear modulus (G) values and the same power law dependence as function of the crosslinker concentration, *i.e.* $G \propto [B]^{\alpha}$. This means that boric acid displays a crosslinking ability, *i.e.* the nucleation ability, directly proportional to its concentration.

Furthermore, the peculiar non-linear mechanical response of the networks consisting of CTL and boric acid 8 mM displays high affinity with other crosslinked natural biopolymers, *i.e.* collagen and neurofilaments (Figure 13a).(Storm et al., 2005) For CTL based networks, a power-law dependence of the shear modulus as function of the maximum elongation network, *i.e.* γ_{max}, was detected (Figure 13b). A similar trend was previously reported for elastomers in the E - λ_{max} dependence.(Vatankhah-Varnosfaderani et al., 2017) The lower mechanical performance and higher maximum elongation network for CTL based network can be traced back to the high flexibility of the CTL backbone.(D'Amelio et al., 2013) CTL based networks can consequently classified as "super-soft" materials, potentially suitable as *in vitro* biomimetics of ECM and for soft tissue engineering.

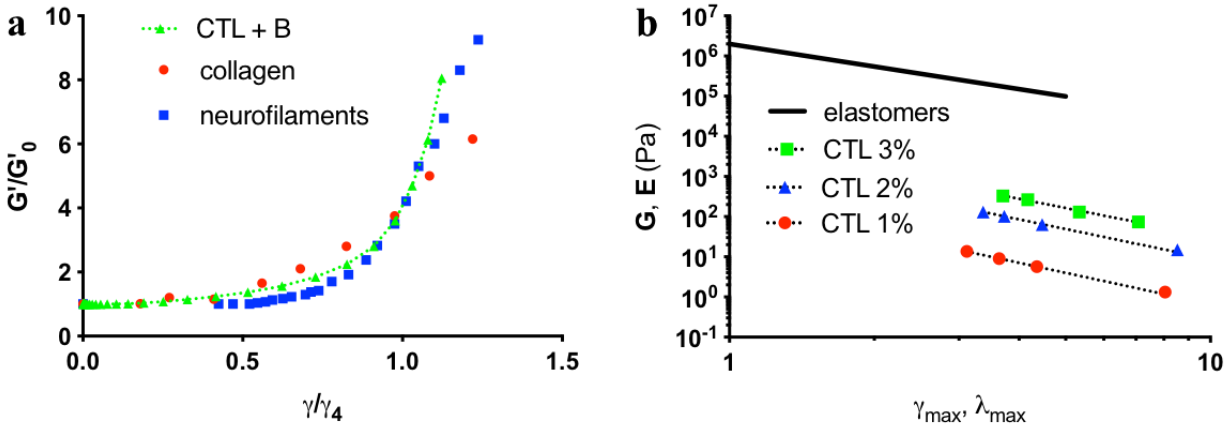

Figure 13. (a) Scaled modulus-strain curves for CTL 10 g/L in the presence of boric acid (8 mM), for collagen and neurofilaments. The latter two were replotted from Storm et al.(Storm et al., 2005) **(b)** Dependence of the shear modulus on the maximum shear (γ_{max}) of samples with different CTL concentration in the presence of different amounts of boric acid. Dotted lines represent the fitting of the experimental data by means of a power law $G \propto \gamma_{max}{}^{a}$, with *a* ranging from -2.2 to -2.4. Experimental conditions: T = 25 °C, PBS 1X, pH 7.4. For comparison, the dependence of the Young's modulus on the maximum strain for elastomers is also reported, taken from Vatankhah-Varnosfaderani *et al.*(Vatankhah-Varnosfaderani et al., 2017) (black solid line). Adapted from Furlani *et al.*(Furlani, Sacco, Scognamiglio, et al., 2019)

Flow curves experiments were also performed in the same experimental conditions. A marked non-linear response, with a shear-thickening, in the presence of boric acid was detected (Figure 14a). The experimental points in the linear part of the flow curve - *i.e.* at low values of the shear rate - were nicely fitted by a simplified version of the Cross equation (eq. 9) (Cross, 1965)

$$\eta = \frac{\eta_0}{1+(\gamma k)^n} \qquad \text{(eq. 9)}$$

where η_0 is the zero-shear viscosity, corresponding to the limiting Newtonian plateau for $\gamma \rightarrow 0$, k is a fitting parameter representing the characteristic relaxation time and n is a fitting parameter known as the Cross rate constant.(Marsich et al., 2013) Furthermore, the critical shear rate, $\dot{\gamma}_{crit}$, was defined as the shear rate at which the shear viscosity is $\eta_{\dot{\gamma}crit} = 1.2\ \eta_0$.(Sacco, Furlani, et al., 2017) A power law dependence, *i.e.* $\eta_0 \propto [B]^{3.1}$, of the zero-shear viscosity as function of boric acid was detected (Figure 14b). An opposite dependence in the critical shear rate, $\dot{\gamma}_{crit}$, was detected (Figure 14b). These results underline the role of boric acid a crosslinking agent.

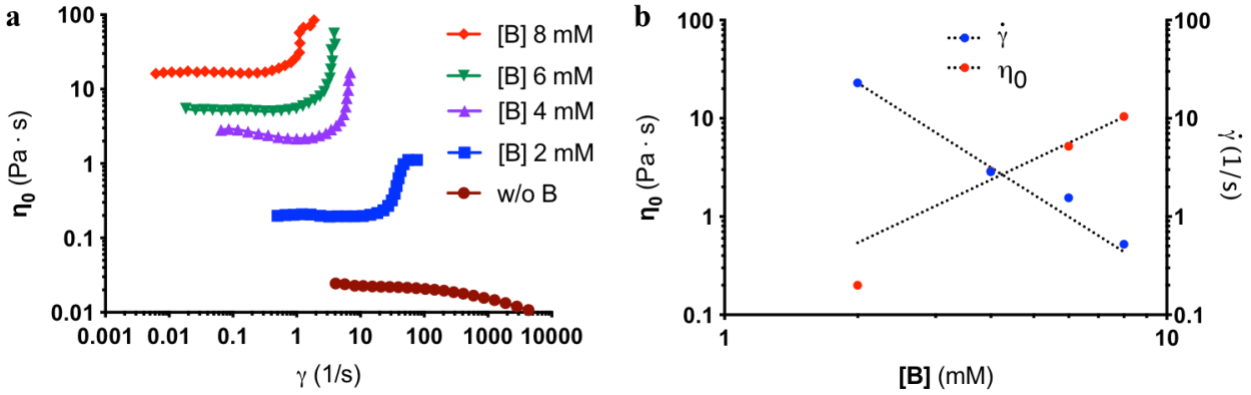

Figure 14. (a) Dependence of the shear viscosity, η, on shear rate; dotted lines are drawn to guide the eye. **(b)** Dependence of the zero-shear viscosity (η_0) of the critical shear rate ($\dot{\gamma}_{crit}$) on concentration of boric acid. Dotted lines are the best-fit of the experimental data points according to equation $\eta_0 \propto [B]_{3.1}$ ($R_2 > 0.99$) and $\dot{\gamma}_{crit} \propto [B]^{-2.6}$ ($R_2 > 0.99$), respectively. Experimental conditions: [CTL] = 10 g/L, T = 25 °C, PBS 1X, pH 7.4.

Shear thickening behavior was previously reported for hydrophobically modified polymers, in which the application of stress promoted the increase of mechanically active chains.(Tam, Jenkins, Winnik, & Bassett, 1998) For CTL based networks, shear thickening can be attributed to shear induced reorganization of bound boric acid and the formation of higher crosslinks, promoting viscosity increase.

Boric acid, at relatively high concentrations, *e.g.* 20 mM, induced a decrease in storage modulus in both frequency and stress sweep tests (Figure 15). This means that, depending on concentration, boric acid can act also as disassembling agent of the networks.

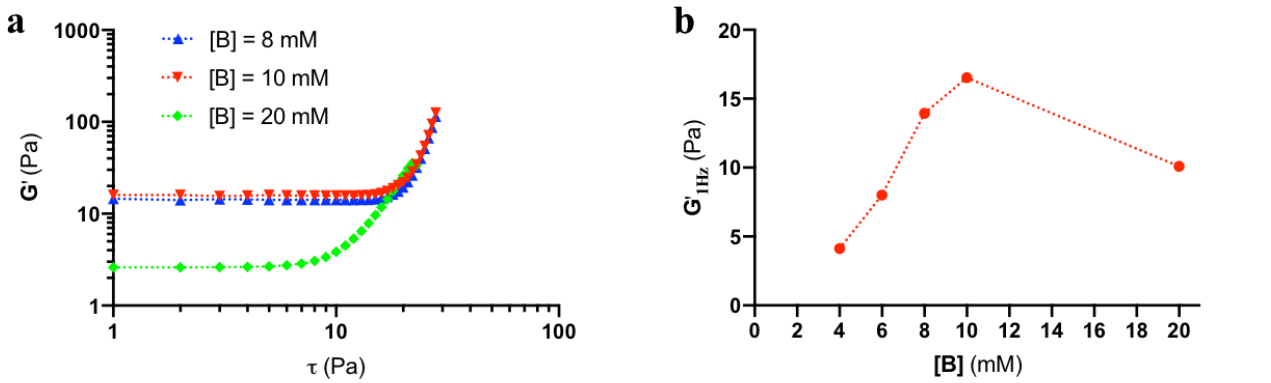

Figure 15. (a) Dependence of G' from the shear stress for samples with constant polymer concentration and different boric acid concentration; dotted lines are drawn to guide the eye. **(b)** Dependence of the value of G' at 1 Hz from the concentration of boric acid ([B]); the dotted line is drawn to guide the eye. Experimental conditions: [CTL] = 10 g/L, *T* = 25 °C, PBS 1X, pH 7.4.

3.1.3.3.1 Network reorganization

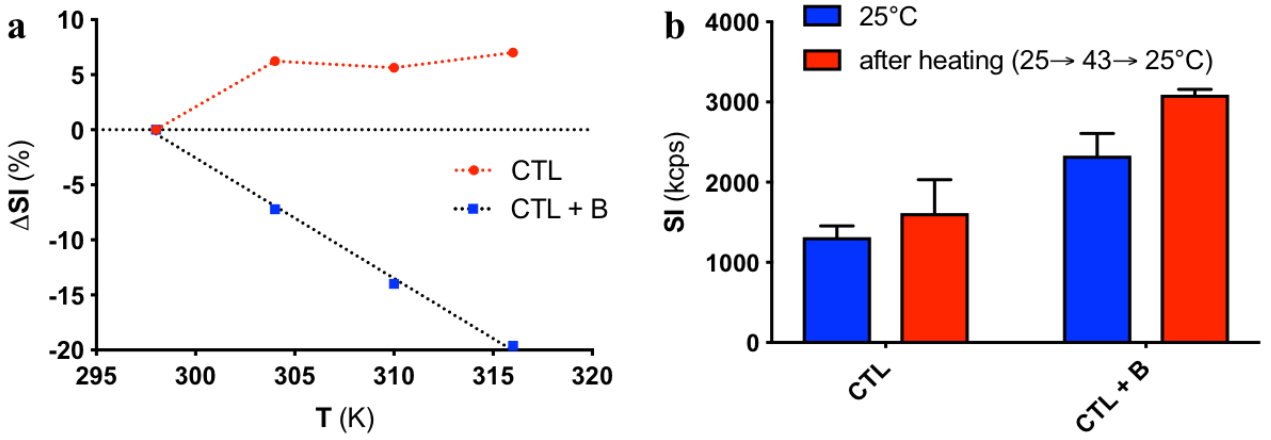

Figure 16. (a) Dependence of the relative variation (%) of the scattering intensity (SI) from the temperature in boric acid treated polymer (boric acid final concentration equal to 8.8 mM) and in the sole polymer. Both samples have the same polymer concentration (2.0 g/L). Lines are drawn to guide the eye. **(b)** Derived count rate for CTL and CTL in the presence of boric acid (boric acid 8.8 mM) at 25 °C (blue) and after the thermal curing (25 °C → 43 °C → 25 °C, red). All samples have the same polymer concentration (2.0 g/L). All measurements were performed in PBS at pH 7.4.

The thermal sensitivity of the interaction between CTL and boric acid was investigated by scattering intensity measures by DLS (Figure 16). In the case of boric acid treated samples the scattering intensity was markedly affected by temperature, whereas no difference was detected for the control sample (Figure 16a). This behavior reflects the unbinding of boric acid due to an increase in temperature. The same samples were heated, cooled, and then analyzed again. For boric acid crosslinked networks, a significant increase of the scattered light was detected after thermal curing (Figure 16b). No significant difference was detected for the control sample. These results suggest a temperature-induced macromolecular rearrangement in crosslinked networks, with an increase of bound boric acid after the thermal curing.

The network reorganization induced by temperature was detected also by rheological measurements. The thermal curing promoted a marked increase of elastic modulus, *i.e.* G', in boric acid crosslinked networks (Figure 17a). Storage modulus was almost constant for the sample without any crosslinking agent. Similar thermal curing behavior was previously reported for networks based on actin and actin binding proteins.(Lieleg et al., 2009)

Energy can also be transmitted by means of a continuous oscillatory shear.(Moghimi, Jacob, Koumakis, & Petekidis, 2017). In the presence of boric acid (8 mM) a marked increase (4-fold) of elastic modulus was detected, suggesting network reorganization (Figure 17b). At the end of the mechanical curing, the resulting sample displayed higher moduli than the unsolicited sample in both frequency and stress sweep (Figure 18a and 18b).

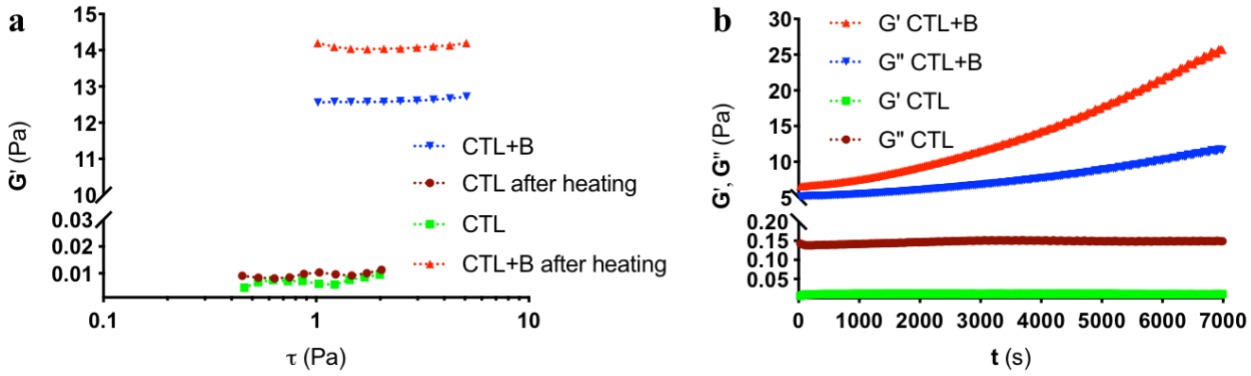

Figure 17. (a) Dependence of G' on stress (τ) for CTL alone and in the presence of boric acid 8 mM at 25 °C prior and after the thermal curing (25°C → 43 °C → 25 °C). **(b)** Time effect of continuous oscillatory shear on G' and G'' for CTL with boric acid 8 mM. For comparison, the time effect of mechanical solicitation on G' and G'' for CTL without boric acid is also reported. Experimental conditions: [CTL] = 10 g/L, [B] = 8 mM, *T* = 25 °C, PBS 1X, pH 7.4.

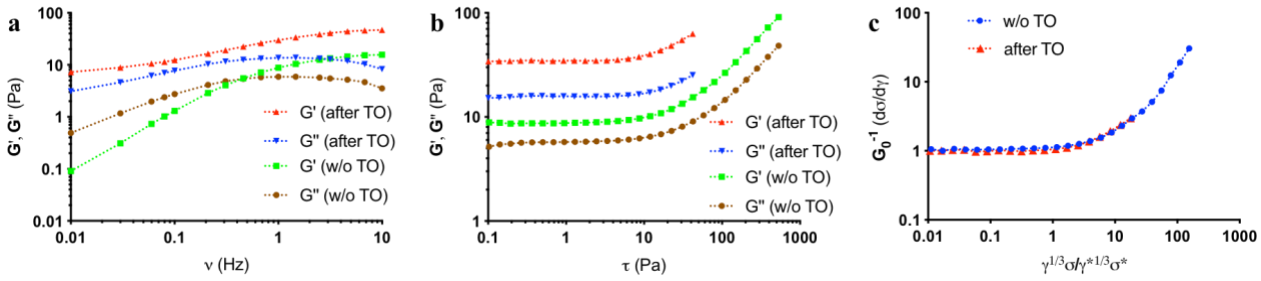

Figure 18. (a) Dependence of G' and G'' from frequency for CTL with boric acid 8 mM prior to (w/o TO) and after (after TO) continuous oscillatory shear. **(b)** Dependence of G' and G'' from stress for CTL with boric acid 8 mM prior to (w/o TO) and after (after TO) continuous oscillatory shear. **(c)** Reduced differential modulus for CTL with boric acid 8 mM prior to (w/o TO) and after (after TO) continuous oscillatory shear. Experimental conditions: [CTL] = 10 g/L, [B] = 8 mM, *T* = 25 °C, PBS 1X, pH 7.4.

After mechanical curing, the shear modulus increased (from 9.5 Pa to 35.3 Pa), but the chain extensibility decreased (Figure 18c). A similar behavior was previously reported also for transient networks based on actin.(Yao et al., 2013) Reorganization upon continuous compression was previously reported for dynamic covalently cross-linked synthetic polymer networks.(Chandran et al., 2015; Liu et al., 2012)

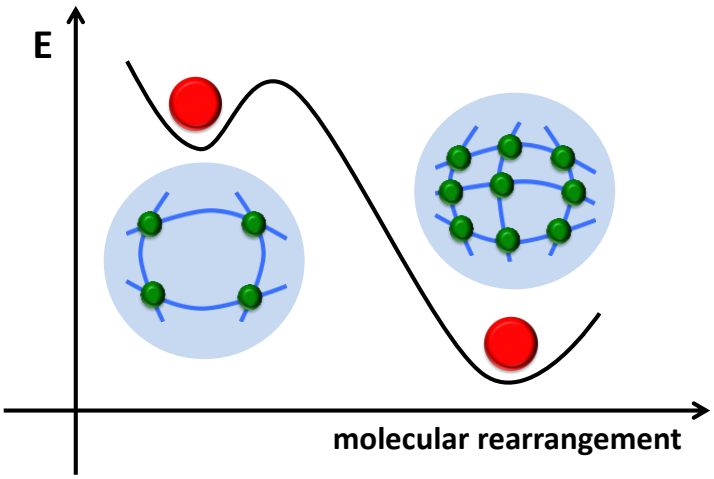

Scheme 4. Schematic representation of network rearrangement upon application of energy. Reprinted from Furlani *et al.*(Furlani, Sacco, Scognamiglio, et al., 2019)

Reorganization of the network upon thermal or mechanical curing was attributed to metastable properties of boric acid crosslinked networks, in which boric acid constantly break and reform linkages. The energy transferred guided the transition to a different potential energy well (Scheme 4). Thus, CTL based networks display a resemblance with the cell cytoskeleton,(Backouche, Haviv,

Groswasser, & Bernheim-Groswasser, 2006) and naturally occurring molecular motors, *e.g.* myosin II and actin filaments.(Backouche et al., 2006) Reorganization of networks upon curing was previously reported also for other synthetic and natural polymers.(Cooke et al., 2018; Danielsen et al., 2018; Robert, Rossow, Hookway, Adam, & Gelfand, 2015)

3.1.4 Main conclusions

In this section, an insight on the interactions between lactose modified chitosan (CTL) and boric acid in dilute and concentrated solutions was presented. When CTL and boric acid were mixed at pH 7.4 and in dilute conditions, polymer chains were found to associate for early additions of the cross-linker, thereby increasing the point-by-point connectivity and, at the same time, reducing the hydrodynamic volume as demonstrated by scattering and viscometric analyses. When further cross-linking agent is added to CTL solutions, a disruption of the chain−chain association was observed, likely ascribed to the increase of electrostatic repulsion of negative charges generated by boric acid binding to CTL diols. Switching from dilute to concentrated solutions, rheological analyses showed a strain-stiffening behavior as a consequence of the formation of chain−chain cross-links. The present non-linear response observed for CTL−boric acid system closely paralleled the one already known for proteins composing the natural ECM, *e.g.* collagen and neurofilaments.

It is interesting to note that the inorganic component can act like a motor for the formations of the network, thus providing nucleation, reorganization and disassembly depending on curing and concentration. In this sense, the CTL-boric acid network share resemblance with natural molecular motors. Yet, the possibility of using these tunable semi-synthetic networks opens up for novel potential interpretations for the mechanical behavior of the natural tissues. The elucidation of the specific aspects endowing CTL with these peculiar properties is still ongoing. Nevertheless, the peculiar biological and mechanical features of cross-linking molecules might pave the way to its use for novel and advanced applications in the field of mechano-responding biomaterials for soft tissue engineering.

3.2 CHAPTER II: Strategies for assisted gelation of lactose-modified chitosan

3.2.1 Aim of the work

This section is mainly focused on the development of methods amenable for forming homogeneous networks based on CTL and boric acid under physiological conditions avoiding syneresis. To this aim, different parameters were finely tuned to reduce the very fast kinetics of CTL/boron self-assembly. Two approaches were exploited, *i.e.* (*i*) a pH-assisted and (*ii*) a competitor-assisted gelation. The first one (*i*) envisages a two-step approach entailing the mixing of CTL and boric acid in acidic conditions followed by the addition of sodium bicarbonate to trigger gradually the increase of the pH of the system. The second one (*ii*) involves the use of mannitol - *i.e.* a polyol competitor for boron binding.

The main aims of this chapter are: (*i*) study the best conditions for obtaining homogenous networks by exploiting these two methods; (*ii*) investigate the physical-chemical and mechanical properties as well as responsiveness towards different stimuli (*e.g.* presence of small molecules or temperature) of resulting networks; (*iii*) evaluate the potential applications of resulting networks for regenerative medicine approaches.

3.2.2 Materials and methods

3.2.2.1 Materials.

Boric acid, sodium bicarbonate ($NaHCO_3$), sodium chloride (NaCl), Phosphate-buffered saline (PBS), ascorbic acid, AlamarBlue (*in vitro* Toxicology Assay Kit, Resazurin based, TOX-8) and sodium hydroxide (NaOH) were all purchased from Sigma-Aldrich Chemical Co. (U.S.A.). The composition of PBS is NaCl 137 mM, KCl 2.7 mM, and phosphate buffer 10 mM with final ionic strength (I) of 168 mM and pH 7.4. Sodium acetate (AcNa), acetic acid (AcOH) and hydrochloric acid were from Carlo Erba (Italy). Collagenase type II, from *Clostridium hystoliticum*, and hyaluronidase, from bovine testes, were from Worthington Biochemical Corporation (USA). DMEM (Dulbecco's Modified Eagle's Medium) High Glucose, DMEM Low Glucose and Fetal Bovine Serum (FBS), streptomycin, penicillin and trypsin were from EuroClone (Italy). All reagents and chemicals were of high purity grade.

Hydrochloride form of lactose-modified chitosan, CTL (previously termed also chitlac and CTL60), (CAS Registry Number 2173421-37-7) was provided by biopo*Life* s.r.l. (Trieste, Italy). It has been synthetized from a highly deacetylated chitosan (85/500, Chitoceuticals, HMC+, Germany)

following the procedure reported elsewhere with slight modifications.(I. Donati et al., 2005) The relative molecular weight of chitosan was 375 000 determined by viscometry,(F Furlani et al., 2017) using a CT 1150 Schott Geräte automatic measuring apparatus and a Schott capillary viscometer at 25 °C. The solvent was composed by 20 mM AcOH/AcNa and 100 mM NaCl buffer solution, pH 4.5.(Berth & Dautzenberg, 2002) Two different CTL batches were used:

(i) For CTL used for pH-assisted gelation the intrinsic viscosity, [η], of CTL was 511 mL/g. The CTL chemical composition was fraction of deacetylated units (F_D) 0.36, fraction of lactose-modified units (F_L) 0.56 and fraction of acetylated units (F_A) 0.08 as determined by $_1$H-NMR spectroscopy. The medium molecular weight of the repetitive unit (MW_{ru}) of CTL was 380. Given the chitosan molecular mass and CTL chemical composition, the estimated molecular weight of CTL was around 870 000.

(ii) For CTL used for competitor assisted gelation the intrinsic viscosity, [η] was found to be 480 mL/g and the weight average molecular weight, $\overline{M_W}$, was 770 000 with a polydispersity index (PDI) of 2.68 (SEC-MALLS, data not shown). The chemical composition of CTL was fraction of deacetylated units (F_D) 0.36, fraction of lactose-modified units (F_L) 0.57 and fraction of acetylated units (F_A) 0.07. The calculated molecular mass of CTL repeating unit (MW_{ru}) was then 383 g/mol.

Deionized Milli-Q water was used in all preparations.

3.2.2.2 Preparation of pH-assisted CTL-boric acid gels.

CTL (50 mg) was weighed in 5 mL beaker and solubilized using 3 mL of deionized water. After complete solubilization, 0.5 mL of NaCl 1.5 M were added. Then, the pH of solution was raised up to 5 using NaOH 1 M. Boric acid was prepared separately at a concentration of 80 mM and the pH adjusted to 5 using NaOH 0.1 M. Boric acid (0.5 mL) was then added to CTL solution under stirring. The pH of solution was constantly monitored using a digital XS pHmeter and kept equal to 5. Sodium bicarbonate 1 M was prepared into 1.5 mL Eppendorf tubes (the final volume of $NaHCO_3$ solution was 1.5 mL) just before the injection; vigorous stirring was used to completely solubilize NaHCO3. Hence, variable amounts of deionized water and finally $NaHCO_3$ were injected into CTL solution under stirring in order to reach a final volume of 5 mL. The final experimental conditions were: [CTL] = 1% w/v, [boric acid] = 8 mM, [NaCl] = 150 mM and [$NaHCO_3$] in the range 30 - 100 mM. After about 10 s of vigorous stirring, 2 mL of CTL-boric acid solutions were dispensed into a plate of a 6-well plates (Ø ~ 3.5 cm) by means of a syringe and left 24 h at rest. The whole procedure was performed at room temperature.

3.2.2.3 Preparation of solutions for competitor-assisted gelation of CTL.

CTL solutions were prepared in PBS buffer, pH 7.4. Briefly, 50 mg of polymer were solubilized in 3.5 mL of deionized water; the pH was then adjusted to 7.4 by adding aliquots of NaOH (1 M). Finally, 450 µL of PBS 10X and deionized water amounts were added to have a final volume of 4.5 mL.

Boric acid solutions were prepared in PBS buffer, pH 7.4. The final concentration of boric acid was 500 mM.

Mixtures of boric acid and mannitol were prepared in PBS buffer, pH 7.4. The final concentration of boric acid was 80 mM throughout all experiments. Briefly, the appropriate amount of mannitol was solubilized in 3.5 mL of deionized water; 800 µL of boric acid 500 mM (PBS 1X as solvent, pH 7.4) were added, followed by 420 µL of PBS 10X. Finally, the pH was adjusted to 7.4 using NaOH (5 M) and different amounts of deionized water were added to have a final volume of 5 mL.

3.2.2.4 Preparations of competitor-assisted CTL-based gels.

A typical synthesis was carried out as follows: 500 µL of boric acid (80 mM) / mannitol (from 0 to 640 mM, PBS 1X, pH 7.4) mixture were injected into 4.5 mL of CTL solution (PBS 1X, pH 7.4) under magnetic stirring. The final concentrations of boric acid and mannitol resulted 8 mM and 0 - 64 mM, respectively. The final concentration of CTL was 10 g/L, *i.e.* 1% w/v, throughout all experiments unless stated otherwise. After the addition of either boric acid or boric acid-mannitol mixture, the samples were mechanically stirred for a few seconds. Resulting samples were allowed to equilibrate for 20 min at room temperature prior to further analyses.

$R_{M/B}$ refers to the ratio [M]/[B], where [M] stands for the molar concentration of mannitol while [B] represents the molar concentration of added boric acid.

3.2.2.5 pH kinetics.

CTL solutions were prepared as described above, except for the fact that boric acid was omitted as to not promote CTL gelation. Upon $NaHCO_3$ addition, the pH of CTL solutions was constantly monitored over time using a pH electrode (XS pHmeter) and recorded at selected time points.

3.2.2.6 Rheological characterization.

Rheological measurements were performed using an HAAKE MARS III rheometer (Thermo Scientific) operating in oscillatory shear conditions.

The experimental settings used to characterize pH-assisted gels are the following: titanium shagreened plates with plate/plate geometry (Ø = 35 mm), gap 1 mm for frequency sweep and stress

sweep tests; titanium plates with 1° cone/plate geometry (Ø = 60 mm), gap 0.051 mm for time sweep tests. Time sweep experiments were carried in strain-controlled conditions, with deformation, γ, of 0.5% kept constant throughout the experiment, frequency, ν, of 1 Hz and time of 12 000 s. Upon addition of $NaHCO_3$, CTL-boric acid solutions were mixed under stirring for about 10 s to uniformly distribute $NaHCO_3$ and poured on the plate. The values of storage G' (elastic response) and loss G" (viscous response) moduli were recorded as a function of time. Frequency sweep and stress sweep experiments were conversely performed on CTL-boric gels after 24 h of gelation.

The experimental settings used to characterize competitor-assisted gels are the following: titanium plates with 1° cone/plate geometry (Ø = 60 mm) and gap 0.051 mm. Rheological tests were performed under steady shear conditions to determine dynamic viscosity values in the stress (τ) range 0.1 - 1000 Pa. In order to investigate the self-healing properties of the best performing sample ([CTL] = 1% w/v, [B] = 8 mM and [M] = 16 mM), sequential shear strain amplitudes of 1% (60 s) and 1200% (60 s) at a constant frequency of 1 Hz were applied. The same sample was analyzed also in the presence of 90% v/v FBS supplemented DMEM High and Low Glucose culture media.

Rheological tests for both type of gels were performed also under oscillatory shear conditions to determine the extension of the linear viscoelastic regime (stress sweep tests at ν = 1 Hz, stress range $1 < \tau < 10000$ Pa) and the mechanical spectra (frequency sweep, τ = 1 Pa, well within the linear viscoelasticity range). The complex viscosity (η^*), the storage (G') and loss (G") moduli of the systems were recorded in the frequency range 0.01 - 100 Hz. All tests were performed at T = 25 °C, except for the best performing sample with mannitol, for which also different temperatures (T = 31, 37 and 43 °C) were investigated. A glass bell covering the measuring device was used to improve thermal control and limit solvent evaporation.

3.2.2.7 Dynamic Light Scattering (DLS) measurements.

A Zetasizer Nano ZS with 173° detection optics and incident light at 633 nm (Malvern Instruments, Inc., Southborough, MA) was used.

Upon addition of $NaHCO_3$, CTL-boric acid solutions were placed in disposable plastic cuvettes with an optic length of 1 cm and were let gelling for 24 h. Measured count rates were normalized for the attenuation factor to yield derived count rates.

100 μL of boric acid, mixture of boric acid and mannitol or PBS 1X were added to 900 μL of CTL solutions (final polymer concentration 10 g/L) previously placed in disposable cuvette. Solutions were allowed to equilibrate for one minute prior to measurements. Data are reported as the relative

scattering intensity (*i.e.* derived count rate) of the resulting solutions and that of polymer without boric acid.

All measurements were performed at T = 25 °C.

3.2.2.8 *In vitro* biological tests.

Biological tests were performed using pig primary articular chondrocytes, human Dental Pulp Stem Cells (hDPSCs, Celprogen Inc.) and h-TERT immortalized human Adipocyte Derived Mesenchymal Stem Cells (hAD-MSCs, ATCC® SCRC-4000™, Manassas, USA) as cell models. hAD-MSCs were transfected with a YAP-TEAD reporter, which enable to display YAP-TEAD: (*i*) green (GFP) cytoplasmic and (*ii*) red (mCherry) nuclear (Oliver-De La Cruz et al., 2019)

3.2.2.8.1 Chondrocytes isolation.

Chondrocytes were isolated from the intact knee joint of mature pigs kindly provided by a local slaughterhouse. Articular cartilage was removed from the knee joint and then cells isolated by enzymatic digestion of the tissue. Collagenase type II was solubilized in PBS 1X (0.7 g/L final concentration). Hyaluronidase was solubilized in PBS 1X (0.62 g/L final concentration). Both enzyme solutions were sterilized by filtration using filters with a pore diameter equal to 0.22 µm. Penicillin/streptomycin solution was added to enzymes in order to have a final concentration of 2X in the case of collagenase and 3X for hyaluronidase.

The cartilaginous portion was aseptically removed from the knee joint. Articular cartilage was washed with PBS 1X, then thin slices of articular cartilage were cut by using a scalpel and incubated for 1 h in 15 mL of hyaluronidase solution, T = 37 °C and in humidified environment at 5% of CO_2. The medium was then removed, and slices of cartilage transferred in flasks (25 cm_2) containing 10 mL of collagenase solution. Tissue degradation was completed by an overnight incubation at 37 °C under shaking. The solution was filtered using a sieve to eliminate undigested tissue. Filtered solution was centrifuged at 250 x *g* for 10 min. The supernatant was discarded whereas the pellet was re-suspended in 10 mL of PBS 1X. Resulting solution was re-centrifuged at 250 x *g* for 10 min. The final pellet was re-suspended in 12 mL of FBS supplemented DMEM High Glucose. Cells were incubated at 37 °C in a humidified environment at 5% CO_2 for two days, then used for biological tests.

3.2.2.8.2 Cell cultures.

Chondrocytes and hAD-MSCs were cultured in Dulbecco's Modified Eagle Medium (DMEM) High Glucose supplemented with 10% v/v fetal bovine serum (FBS) (EuroClone, Italy), 100 U/mL penicillin, 100 µg/mL streptomycin, and 2 mM L-glutamine using 75 cm_2 flasks at 37 °C in

humidified environment at 5% of CO_2. hDPSCs were cultured in the same medium supplemented with ascorbic acid 100 µM. Chondrocytes and hDPSCs were detached with trypsin (EuroClone, Italy), whereas hAD-MSCs with TrypLE (Thermofisher). 200 µL of cells in the appropriate medium were plated in 96-well tissue culture plates. The initial concentration of chondrocytes was 6400 cells/well, and that of hDPSCs 2500 cells/well. For 2D-cultured cells tests, cells were left at rest for 1 day, then supernatants discarded and 200 µL of the corresponding treatment (CTL-based gel or its singular components) were added. Cells were incubated with the corresponding treatment for 3 days. All treatments were prepared in sterile conditions using a mixture of complete DMEM Low Glucose and PBS as medium. In the case of hDPSCs, ascorbic acid 100 µM was further added. The final composition of medium was 90:10 v/v medium/PBS for chondrocytes and hDPSCs. At least six independent replicates were performed for each treatment.

3.2.2.8.3 Biocompatibility tests on 2D-cultured cells.

The viability of adherent cells was assessed using the AlamarBlue assay according to the manufacturer's protocol. Briefly, the AlamarBlue was diluted 1:10 v/v with fresh medium. Treatments were discarded and 200 µL of the mixture AlamarBlue-medium were added to each well containing cells. Plates were incubated in dark conditions at 37 °C in a humidified environment at 5% CO_2. After 4 h of incubation, 100 µL of supernatants were transferred into a black 96-well microtiter plate. Fluorescence intensity was measured using a FLUOStar Omega by BMG-Labtech (Germany) spectrofluorometer, with excitation wavelength (λ_{ex}) of 544 nm and emission wavelength (λ_{em}) of 590 nm. The mixture AlamarBlue-DMEM was used as blank.

3.2.2.8.4 Setting of cell-laden gels.

hDPSCs were encapsulated into gels composed of [CTL] = 40 g/L, [B] = 8 mM and [M] = 16 mM. Briefly, 50 µL of hDPSCs in DMEM Low Glucose supplemented with ascorbic acid 100 µM were dispersed into 850 µL of a CTL solution (DMEM Low Glucose *plus* ascorbic acid 100 µM as medium, pH 7.4) and mixed through a 1 mL syringe into a 1.5 mL Eppendorf tube. Then, 100 µL of boric acid-mannitol mixture (boric acid 80 mM and mannitol 160 mM, PBS 1X, pH 7.4) were injected into CTL solution and extensively mixed by using a 1 mL syringe. Finally, resulting gels were dispensed into 24-well plates. The final concentration of cells was 42 000 cell/mL. All samples were prepared in sterile conditions. The final composition of medium was 90:10 v/v cell culture medium/PBS. At least six independent replicates were considered for each treatment.

hAD-MSCs were encapsulated into three gels with different composition: (*i*) [CTL] = 40 g/L, [B] = 8 mM and [M] = 16 mM, (*ii*) [CTL] = 40 g/L, [B] = 2 mM and [M] = 4 mM and (*iii*) [CTL] = 20 g/L, [B] = 8 mM and [M] = 16 mM. For cell encapsulation was used the same protocol reported

above. 200 µL of resulting gels were transferred in µ-Slide 8-well glass bottom plates (Ibidi, Germany). In this case the final composition of cells was 500 000 cell/mL. Plates were incubated at 37 °C in a humidified environment at 5% CO_2. After 24 h, 48h and 72h of incubation, confocal microscopy analyses were performed to evaluate YAP-TEAD localization.

3.2.2.8.4.1 Biocompatibility tests on 3D-cultured cells.

The metabolic activity of encapsulated cells was assessed using the AlamarBlue assay according to the manufacturer's protocol. Cells were loaded within CTL-boric acid gels and incubated for three days at 37 °C. Subsequently, 100 µL of cell-laden gels were transferred into a 96-well black microtiter plate by using a 1 mL syringe. The AlamarBlue was diluted 1:10 v/v with fresh medium (DMEM High Glucose). Then, 100 µL of the mixture AlamarBlue-DMEM were added to each well. Plates were incubated at 37 °C in a humidified environment at 5% CO_2. After 4 h of incubation, fluorescence intensity was measured as detailed in paragraph 2.7.3. The mixture AlamarBlue-empty gel was used as control.

3.2.2.8.4.2 Confocal laser scanning microscopy (CLSM).

Live/Dead assay (Sigma, USA) was performed according to the manufacturer's protocol to evaluate the viability of gel-embedded hDPSCs. Briefly, 2 µL of solution A (containing Calcein-AM) and 1 µL of solution B (containing Propidium Iodide) were added to 1 mL of PBS 1X. Then, 300 µL of resulting mixture were added to 300 µL of cell-laden gels 24 h after cell encapsulation. µ-Slide 4-well plates with ibiTreat Surface (Ibidi, Germany) were used as support. The final concentration of cells was 150 000 cells/mL. Plates were incubated in dark conditions at 37 °C in a humidified environment at 5% CO_2. After 4 h of incubation, CLSM analyses were performed to evaluate hDPSCs viability. CLSM images were acquired using a Nikon Eclipse C1si confocal laser scanning microscope with a Nikon Plan Apochromat 20× objective. Dead cells were red-stained (λ_{ex} = 564 nm; λ_{ex} = 590 nm) whereas live cells green-stained (λ_{ex} = 488 nm; λ_{ex} = 515 nm). Resulting Z-stacks were analyzed using ImageJ software.

hAD-MSCs embedded in 3D hydrogels were analyzed with Zeiss LSM 780 confocal microscope with either 10× (air) or 40× (oil-immersion) objectives. Live cells can display green cytoplasm (λ_{ex} = 488 nm; λ_{em} = 515 nm) or both green cytoplasm and red nuclei (λ_{ex} = 561 nm; λ_{em} = 590 nm), whereas dead cells display only red nuclei. 200 µm Z-stacks were acquired with the optimal interval suggested by the software, followed by the application of maximum intensity algorithm. YAP and TEAD nuclear to cytoplasmic ratios were calculated by evaluating the ratio between the cumulative number of red and green cells and only green cells.

3.2.2.9 Statistical analysis.

Statistical analysis and graph elaboration were performed using GraphPad Prism 8 (GraphPad Software, San Diego, CA). One-way ANOVA (analysis of variance) was performed following by Dunnett *post hoc* tests to evaluate differences among different groups and control. Unpaired Student's t-test was performed to evaluate differences between two groups. Differences were considered significant for *p*-values less than 0.05.

3.2.3 Results and discussion

Single injections of boric acid into CTL solutions at pH 7.4 without an extensive stirring promoted the instantaneous and inhomogeneous gelation of CTL due to fast kinetics of the crosslinking molecule.(Hall, 2011) Resulting samples consist of two phases, *i.e.* turbid macro-aggregates and a liquid polymer-poor phase. Such result could prevent the exploitation of the networks as biomaterials. Indeed, homogenous networks are preferred to uniformly distribute loads and to promote uniform cellular colonization. In order to achieve a slower and homogeneous gelation, two approaches were exploited, *i.e.* a pH-assisted and a competitor-assisted gelation.

3.2.3.1 pH-assisted gelation of CTL

In order to promote a homogeneous gelation of CTL in the presence of boric acid, a pH assisted gelation mechanism was developed. The proposed mechanism is reported in Scheme 5. This strategy involves a two-step approach requiring the preparation of acidic mixture of CTL and boric acid and then the addition of sodium bicarbonate to promote progressive pH increase. This system is based on the pH responsive behavior of boric acid: (*i*) in acid conditions it mainly exists as trigonal species and it is low reactive towards diols, (*ii*) at neutral and basic pH, it mainly exists in the tetracoordinate form, which is much more reactive towards diols.(Brooks & Sumerlin, 2016; Hall, 2011) Bicarbonate in acidic media is progressively converted in carbon dioxide and water. Simultaneously, the proton consumption leads to progressive formation of tetracoordinate borate anions, able to bind lactitol moieties of CTL (Scheme 5).

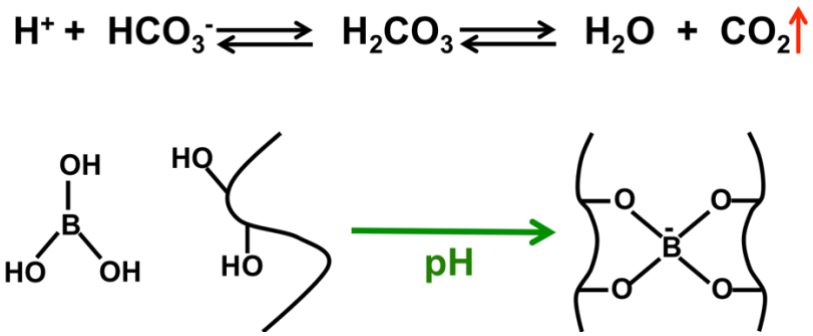

Scheme 5. Schematic representation of pH-assisted gelation mechanism. Reprinted with permission from Sacco *et al.*(Sacco, Furlani, Paoletti, & Donati, 2019) Copyright 2019 American Chemical Society.

3.2.3.1.1 pH kinetics

The evolution of pH upon bicarbonate trigger was evaluated in samples without any crosslinking agent, thus avoiding gelation. An immediate marked increase of pH was detected upon sodium bicarbonate addition (Figure 19). Then, a progressive pH increase was detected, until 24 hours. Experimental points were nicely fitted using eq. 10

$$pH(t) = pH_\infty - (pH_\infty - pH_0)e^{-k_1 t} \quad \text{(eq. 10)}$$

where pH_∞ is the pH of CTL solution at infinite times, pH_0 is the pH immediately after $NaHCO_3$ addition and k_1 is the rate constant. The sample with the higher concentration of $NaHCO_3$ displayed the higher pH_0, pH_∞ and also k_1 values. This data suggests a rate dependence of the pH increase from the concentration of sodium bicarbonate.

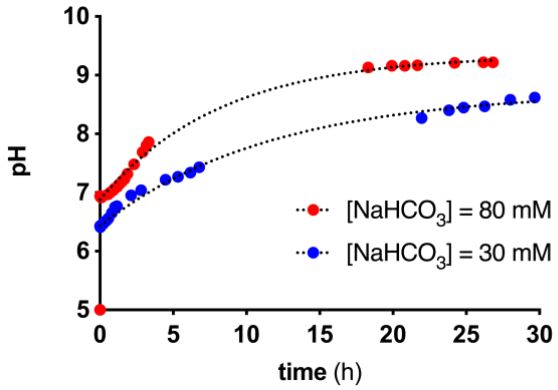

Figure 19. pH kinetics of CTL at different sodium bicarbonate ($NaHCO_3$) amount. $NaHCO_3$ was added to CTL solutions previously prepared at pH 5. Dotted lines represent the best fitting of experimental points using eq. 10. Experimental conditions are [CTL] = 1% w/v, [boric acid] = 8 mM, [NaCl] = 150 mM, T = 25 °C.

3.2.3.1.2 Responsiveness towards sodium bicarbonate

The evolution of boric acid binding to CTL upon $NaHCO_3$ addition was evaluated by time sweep rheological tests. Both storage (G′) and loss (G″) moduli changed with time (Figure 19a). Furthermore, their ratio increased, suggesting polymer structuring. The loss tangent, tan δ, *i.e.* G″/G′, was plotted as a function of time (Figure 19b).(Holly, Venkataraman, Chambon, & Henning Winter, 1988; Maleki, Kjøniksen, & Nyström, 2007) Experimental data were nicely fitted by eq. 11:

$$tan\delta\ (t) = (tan\delta_0 - tan\delta_\infty)e^{-k_2 t} + tan\delta_\infty \quad \text{(eq. 11)}$$

where $tan\delta_0$ is the value of loss tangent at time zero, $tan\delta_\infty$ is the loss tangent at infinite times and k_2 is the rate constant. A power-law dependence between the rate constant, and the sodium bicarbonate was detected (Figure 20c), *i.e.* $k_2 \propto [NaHCO_3]^{1.2}$. This indicate that gelation kinetics can be accelerated by using higher sodium bicarbonate amounts.

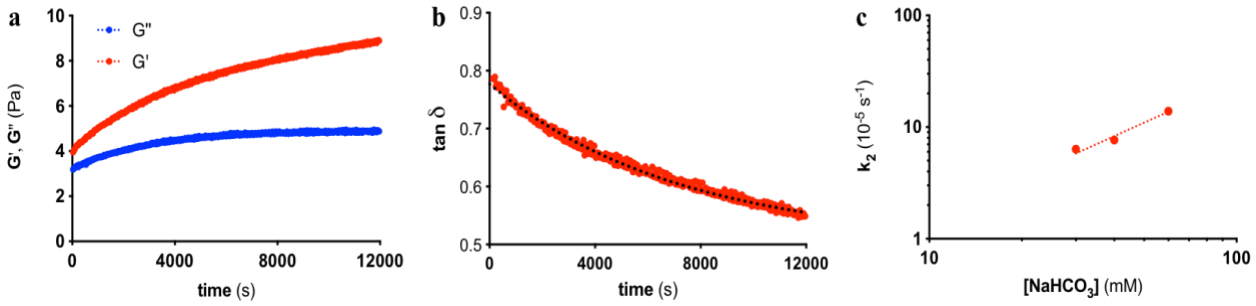

Figure 20. (a) Dependence of storage (G′) and loss (G″) moduli from time for CTL-boric acid system using 60 mM sodium bicarbonate ($NaHCO_3$) as trigger. **(b)** Dependence of the loss tangent, $tan\delta$, on time for CTL-boric acid systems using 60 mM sodium bicarbonate ($NaHCO_3$) as trigger; the black line represents the best fitting of experimental points using eq. 11. **(c)** Dependence of the rate constant, k_2, on $NaHCO_3$ concentration; the dotted line is the best-fit of the experimental data points according to equation $k_2 \propto [NaHCO_3]^{1.2}$. Experimental conditions are [CTL] = 1% w/v, [boric acid] = 8 mM, [NaCl] = 150 mM, T = 25 °C.

After 24 hours of gelation, mechanical performance of resulting samples was investigated by frequency and stress sweep tests. The dependence of elastic and viscous moduli on angular frequency shows the typical behavior of transient dynamic networks, with a crossover frequency, ω_{cross}, and two different viscoelastic regions, characterized by $G' > G''$ for $\omega > \omega_{cross}$ and $G' < G''$ for $\omega < \omega_{cross}$, respectively (Figure 21a).(Narita et al., 2013; Tang et al., 2018) At frequencies lower than ω_{cross}, the elastic and loss moduli were found to scale with the angular frequency according to the power laws: $G' \propto \omega^{0.5}$ and $G'' \propto \omega^{0.2}$, respectively. The crossover frequency, ω_{cross}, was around 0.15 rad/s, very close to the frequency where the viscous modulus shows a peak, ω_{max}. ω_{max} is an indication of the time in which an associated cross-linker reverts to its equilibrium position by one or more dissociation

steps.(Indei & Takimoto, 2010) This suggests that boric acid behaves as a weak transient crosslinker. Other authors reported similar profiles for borate-based gels.(Narita et al., 2013; Tang et al., 2018)

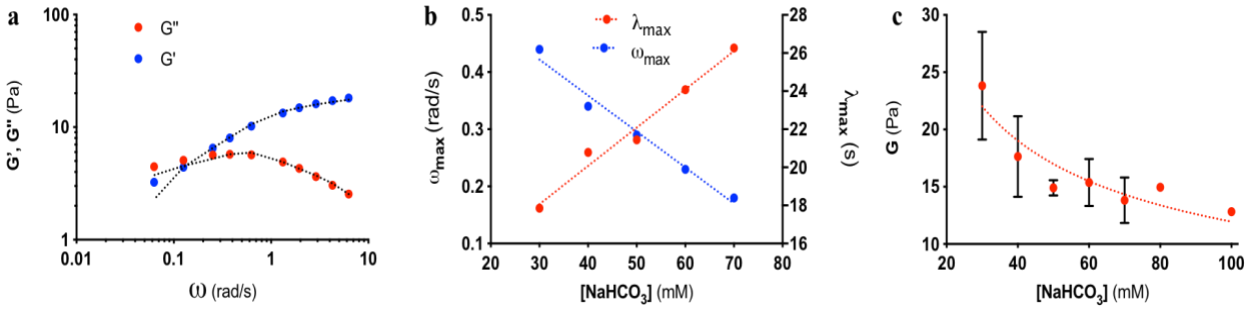

Figure 21. (a) Dependence of storage (G′) and loss (G″) moduli on frequency of CTL-boric acid gel obtained with 30 mM sodium bicarbonate ($NaHCO_3$); black dotted lines represent the best fitting of G' and G'' experimental points using the Maxwell model (eqs. 1 and 2). **(b)** Dependence of the angular frequency at which the viscous modulus shows a peak, ω_{max}, and that of boron association/dissociation time, λ_{max}, on $NaHCO_3$ concentration; dotted lines are drawn to guide the eye. **(c)** Dependence of shear modulus, *G*, on $NaHCO_3$ concentration; data are represented as mean (±SD, *n* = 3); the dotted line is drawn to guide the eye. Experimental conditions are [CTL] = 1% w/v, [boric acid] = 8 mM, [NaCl] = 150 mM, *T* = 25 °C.

Experimental data were nicely fitted by a combination of three Maxwell elements, composed by a sequence of springs and dashpots in parallel according to eqs. 1 and 2 (Figure 21a). The shear modulus of CTL-boric acid gels was determined according to eq. 12

$$G = \sum_{i=1}^{3} G_i \quad \text{(eq. 12)}$$

Furthermore, the association/dissociation time, λ_{max}, was determined as $\lambda_{max} = \frac{2\pi}{\omega_{max}}$. A linear correlation between the concentration of $NaHCO_3$ and both ω_{max} and λ_{max} was detected (Figure 21b). These results suggest that networks with a lower $NaHCO_3$ concentration display a faster association/dissociation time for boron. In general terms, lower association/dissociation times were reported by other authors for transient crosslinked gels; this indicates that CTL-boric acid gels display different dynamics with respect to similar systems already described in the literature.(Mayumi et al., 2013; Narita et al., 2013; Tang et al., 2018) Finally, a progressive reduction of the shear modulus was detected as function of sodium bicarbonate concentration (Figure 21c).

Frequency sweep data were also analyzed according to the Cole-Cole approach (eq. 13), where the dependence of the loss modulus, *i.e.* G″, on storage modulus, *i.e.* G′, is described by equation 13:

$$G''(\omega) = [G'(\omega)G_\infty - G'(\omega)^2]^m \quad \text{(eq. 13)}$$

where G_∞ is the plateau modulus (at infinite time) and m is the floating exponent.(Annable, Buscall, Ettelaie, & Whittlestone, 1993; Tam et al., 1998) Graphically, the mathematical model describes a semicircle (Figure 22a), in which the intersection with x-axis represents G_∞. An exponential decay of the plateau modulus as function of sodium bicarbonate was detected (Figure 22b).

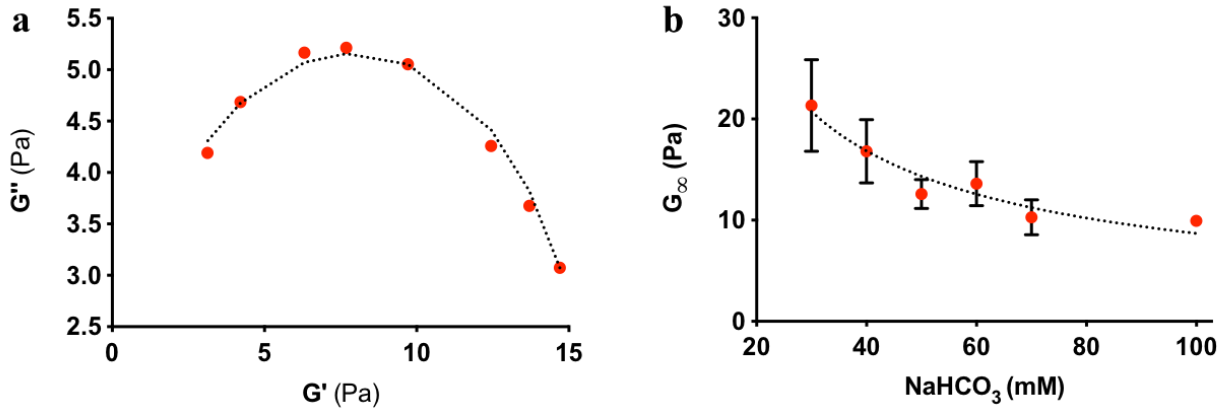

Figure 22. (a) Cole-Cole plot of sample-case CTL-boric acid gel obtained using 40 mM sodium bicarbonate ($NaHCO_3$). Solid red dots represent the experimental points whereas the black dotted line is the best fitting using eq. 13. **(b)** Dependence of the plateau modulus, G_∞, on sodium bicarbonate ($NaHCO_3$) content for CTL-boric gels obtained with different $NaHCO_3$ amount. The black dotted line is the best fit according to an exponential decay. Data are means ± standard deviation (SD) of at least two measurements. Experimental conditions are [CTL] = 1% w/v, [boric acid] = 8 mM, [NaCl] = 150 mM, T = 25 °C.

The mechanical performance at large deformations was then investigated by long stress sweep tests. In the stress-strain plot, two regions were detected, namely (*i*) a linear behavior for about three orders of magnitude of strain, and (*ii*) a marked strain hardening at large deformations (Figure 23a). Strain hardening was reported also for other hydrogels based on boron and was traced back to the strain induced formation of an higher number of elastically active chains.(He, Zhang, Zhang, & Guan, 2011; Wang, 1992) Experimental points were efficiently fitted using eq. 4.(Erk et al., 2010) The dependence of γ^* on $NaHCO_3$ concentration shows that the critical deformation necessary to promote a deviation from the linear regime was directly proportional to sodium bicarbonate amount up to 60 mM; for higher $NaHCO_3$ concentration, the critical strain was almost constant. This peculiar behavior can be traced back to the final pH of networks after 24 hours. More in detail, at higher pH the amount of bound negatively charged boric acid increases, thus a higher strain is needed for the onset of strain hardening. This process could then be partially prevented by a large amount of close negatively charges accompanying the binding of boron.

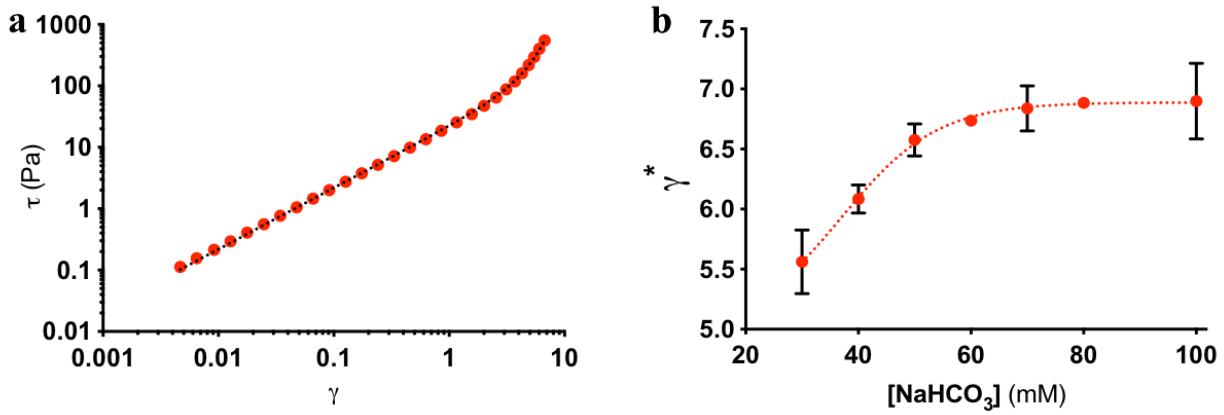

Figure 23. (a) Stress-strain plot for CTL-boric acid gel obtained with 30 mM of sodium bicarbonate ($NaHCO_3$). The dotted line represents the best fitting of experimental points using eq. 4. **(b)** Dependence of the critical deformation at which stiffening emerges , γ^*, on $NaHCO_3$ concentration; the dotted line is drawn to guide the eye. Experimental conditions are [CTL] = 1% w/v, [boric acid] = 8 mM, [NaCl] = 150 mM, T = 25 °C.

3.2.3.1.3 Macromolecular structuring of networks

Structuring of CTL based gels with different amounts of sodium bicarbonate was then evaluated by DLS analyses after 24 hours. The sample with the lowest sodium bicarbonate amount, *i.e.* 30 mM, displayed a scattering of the visible light significantly higher than the homologous sample with the highest amount of $NaHCO_3$, *i.e.* 100 mM (Figure 24). Thus, the polymer mass per unit volume is higher for lower $NaHCO_3$ concentrations. This result suggests an enlargement of polymer mesh upon increasing $NaHCO_3$ amount and it is in line with the decrease of elastically active chains density (see Paragraph 3.2.3.1.2). Again, this result was attributed to the final pH of resulting samples. More in detail, the final pH of the sample was equal to 8.40 with $NaHCO_3$ 30 mM, whereas a value of 8.93 was obtained with $NaHCO_3$ 100 mM. The pH increase entail (*i*) a 3.4-fold increase of OH^- groups competing with the diol ones and (*ii*) a higher number of negatively charges bore by borate esters. These processes lead to repulsion between negatively charged borate esters, unzipping some of the junctions. This means a progressive shift from intermolecular complex (green circles) to intramolecular junctions (blue circles) (Scheme 6). These phenomena are associated with the weakening of the network, and thus reduction of mechanical performance.

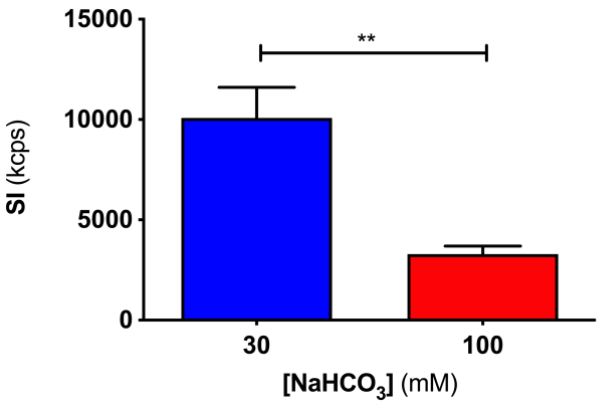

Figure 24. Total scattering intensity, *i.e.* derived count rate, for CTL-boric acid gels prepared using different sodium bicarbonate ($NaHCO_3$) amount after 24 hours upon mixing. Unpaired Student's t-test was performed to compare scattering intensities (**: p value < 0.01). Data are means ± standard deviation (SD) of at least three measurements. Experimental conditions are [CTL] = 1% w/v, [boric acid] = 8 mM, [NaCl] = 150 mM, T = 25 °C.

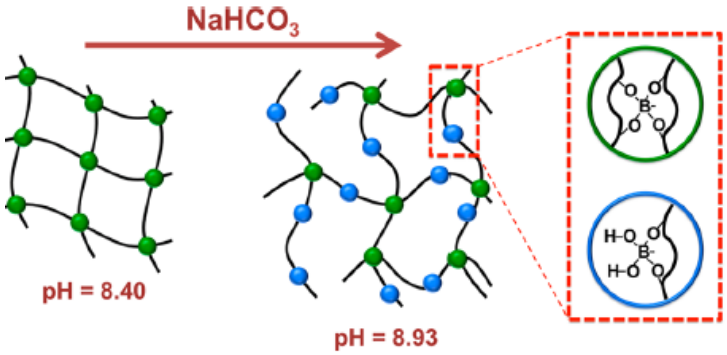

Scheme 6. Schematic representation of polymer mesh within networks with different sodium bicarbonate ($NaHCO_3$) concentrations, *i.e.* 30 mM (left) and 100 mM (right), and thus also different final pH values after 24 hours. Reprinted with permission from Sacco *et al.*(Sacco et al., 2019) Copyright 2019 American Chemical Society.

3.2.3.2 Competitor assisted gelation of CTL

In order to promote the homogeneous gelation of CTL, a competitor-assisted gelation mechanism was developed. As competitor was selected a diol-rich molecule, *i.e.* mannitol, which is able to partially bind boric acid with high affinity.(Springsteen & Wang, 2002) Thus, the proposed strategy is a two-phase approach entailing: (*i*) mixing of boric acid and mannitol and (*ii*) addition of the mixture to CTL, in order to support a gradual availability of boric acid, able to bind the polymer and promote gelation. Both these phases can be performed at physiological pH, *i.e.* 7.4.

3.2.3.2.1 Homogeneity of resulting networks

By using the competitor-assisted gelation in the presence of mannitol it was possible to obtain homogeneous and colorless networks, without appreciable syneresis (Figure 25a).

Homogeneity of resulting networks was evaluated by semi-quantitative analyses exploiting DLS. In the presence of the sole crosslinking agent, *i.e.* boric acid, a significant increase of visible light scattered by networks was detected, suggesting an increment of polymer mass per unit volume due to large (and visible) aggregates (Figure 25b). By exploiting the competitor assisted gelation only a limited increase of the amount of scattered light was detected. This result point to an excellent improvement of homogeneity of resulting networks in the presence of competitor.

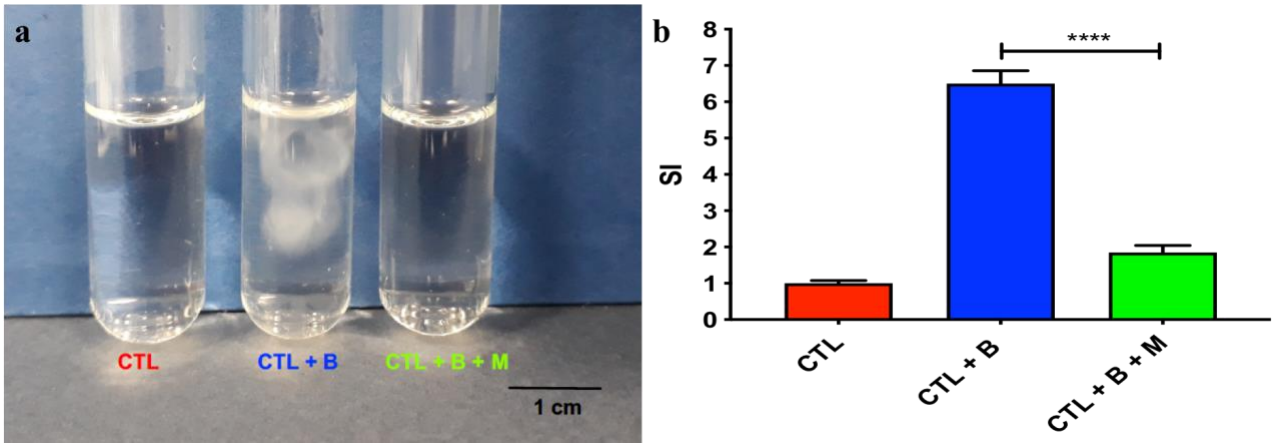

Figure 25. (a) Visual analysis of CTL control sample (without boric acid), CTL treated with boric acid (8 mM final concentration) and CTL with a mixture of boric acid and mannitol (boric acid 8 mM and mannitol 16 mM final concentrations, $R_{M/B}$ = 2). **(b)** Normalized scattering intensity (SI) of the same samples as in (a). Data are means ± standard deviation (SD) of three measurements. Unpaired Student's t-test was performed to compare scattering intensities (****: *p* value < 0.0001). Experimental conditions: *T* = 25 °C, PBS 1X, pH 7.4. In all cases, the concentration of CTL was 10 g/L. Adapted with permission from Furlani *et al.*(Furlani, Sacco, Cok, et al., 2019) Copyright 2019 American Chemical Society.

3.2.3.2.2 Response to competitor

The responsiveness of CTL based hydrogels towards competitor was investigated by rheological measurements performed with constant concentration of both CTL and boric acid and in the presence of different amounts of mannitol. The molar ratio between mannitol and boric acid was indicated as $R_{M/B}$. Samples without competitor were not considered due to their heterogeneity under the same preparation conditions.

The mechanical performance was investigated by long stress sweep tests in order to study the extent of linear viscoelastic regime for homogeneous samples. Likewise, in the pH assisted approach

(Figure 23a), in the stress-strain plot of the sample with $R_{M/B}$ = 2, two regions were detected, namely (*i*) a linear behavior extending for about three orders of magnitude of strain, and (*ii*) a marked strain hardening at large deformations (Figure 26a). The onset of strain-hardening was prevented only in the case of high concentration of mannitol (*i.e.* $R_{M/B}$ = 8) (Figure 26b), suggesting that a mannitol overload hinders network structuring. The experimental data were nicely fitted using eq. 4:

$$\tau = G_0\, \gamma\, e^{\left(\left(\frac{\gamma}{\gamma^*}\right)^2\right)} \quad \text{(eq. 4)}$$

where τ is the applied stress, G_0 is the shear modulus at zero strain, γ is the experimental deformation and γ^* is the critical strain at which the deviation from linearity becomes dominant.(Erk et al., 2010)

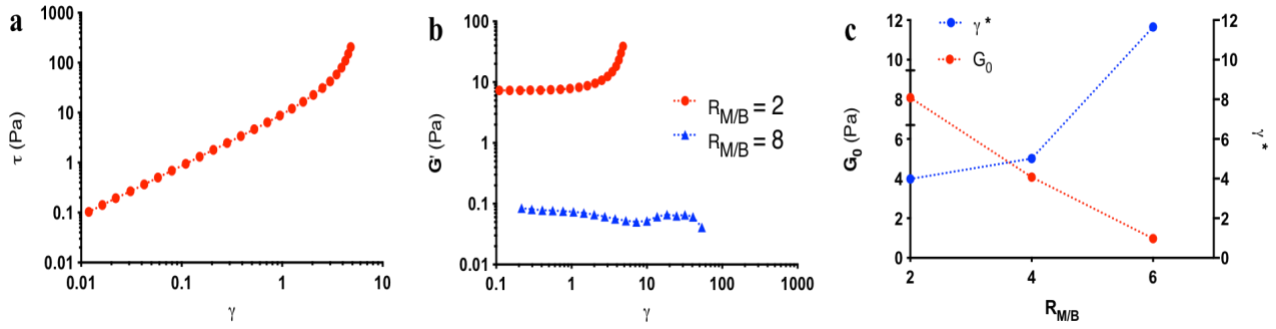

Figure 26. (a) Dependence of stress-strain response for CTL gel showing mannitol to boric acid molar ratio, $R_{M/B}$, = 2 (boric acid 8 mM and mannitol 16 mM final concentrations); dotted line represents the best fit of experimental points according to eq. 4. **(b)** Dependence of storage modulus (G') on applied deformation for the sample with $R_{M/B}$ = 2 (boric acid 8 mM and mannitol 16 mM final concentrations) and that with $R_{M/B}$ = 8 (boric acid 8 mM and mannitol 64 mM final concentrations); dotted lines are drawn to guide the eye. **(c)** Dependence of the shear modulus at zero strain (G_0) and that of critical strain (γ^*) on $R_{M/B}$; dotted lines are drawn to guide the eye. Experimental conditions: [CTL] = 10 g/L, *T* = 25 °C, PBS 1X, pH 7.4. Adapted with permission from Furlani *et al.*(Furlani, Sacco, Cok, et al., 2019) Copyright 2019 American Chemical Society.

Homogeneous CTL-based networks were studied also in steady state conditions. In this case experimental data in the linear part of the flow curve were modeled by eq. 9.(Cross, 1965; Marsich et al., 2013) Results closely resemble those of the stress sweep tests (Figure 27). Upon increasing $R_{M/B}$, a progressive decrease in the mechanical response was detected, as evidenced by G_0 trends (Figure 26c and 27b). Simultaneously, an increase of γ^* was detected. This behavior closely resemble that reported above upon decreasing the cross-linker concentration.(Paragraph 3.1.3.3)

The dependence of elastic and viscous moduli on angular frequency displays a similar trend to that previously detected for pH assisted hydrogels (Figure 21a) and it is typical of transient dynamic networks.(Narita et al., 2013; Tang et al., 2018) Furthermore, the G" profile, showing a maximum

(associated to a value of ω_{max}), recalls physically associated networks and gels based on synthetic polymers and boron compounds.(Indei & Takimoto, 2010; Tang, Habicht, Li, Seiffert, & Olsen, 2016; Tang et al., 2018) At frequencies lower than ω_{cross}, a power law dependence of elastic and loss moduli as function of angular frequency was detected, *i.e.* $G' \propto \omega^{1.3}$ and $G'' \propto \omega^{0.7}$, respectively. Narita and collaborators detected similar profiles for networks based on poly(vinyl alcohol) (PVA) and borax, *i.e.* $G' \propto \omega^{1}$ and $G'' \propto \omega^{0.5}$, respectively.(Narita et al., 2013)

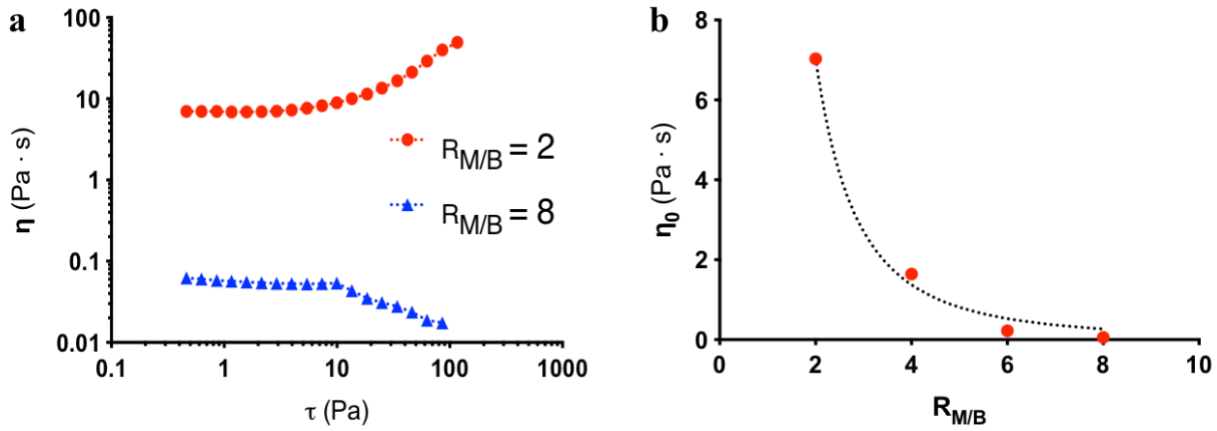

Figure 27. (a) Dependence of the shear viscosity, η, on applied stress, τ; dotted lines are drawn to guide the eye. **(b)** Dependence of the zero-shear viscosity, η_0, on $R_{M/B}$; dotted line is drawn to guide the eye. Experimental conditions: [CTL] = 10 g/L, T = 25 °C, PBS 1X, pH 7.4. $R_{M/B}$ refers to the ratio [M]/[B], where [B] represents the total molar concentration of boric acid while [M] stands for the molar concentration of mannitol. Adapted with permission from Furlani *et al.*(Furlani, Sacco, Cok, et al., 2019) Copyright 2019 American Chemical Society.

Experimental data of frequency sweep tests were also nicely fitted by exploiting the Cole-Cole approach (eq. 13). Mathematically, the non-zero intersection of the semicircle with the x-axis identifies the plateau modulus (at infinite time), *i.e.* G_∞ (Figure 28b). A power law dependence between G_∞ and $R_{M/B}$ was detected, *i.e.* $G_\infty \propto R_{M/B}^{-1.4}$ (Figure 28c). This result parallels the stress sweep analyses, suggesting that a high competitor concentration is detrimental to mechanical response of networks.

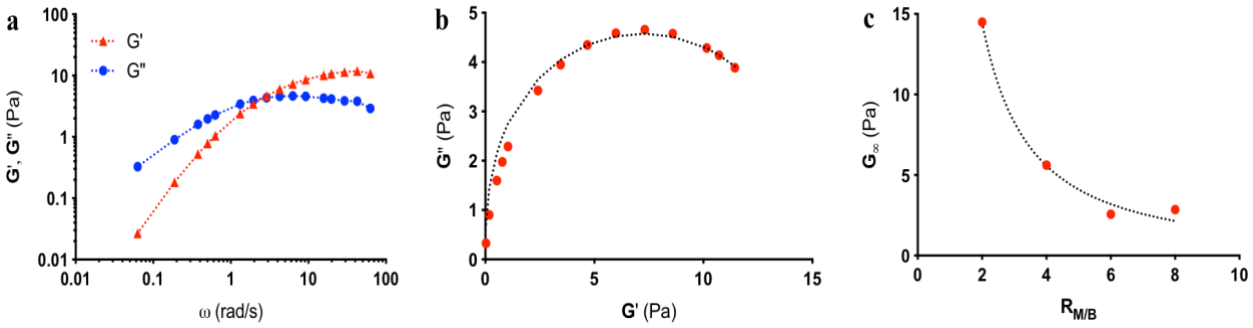

Figure 28. (a) Dependence of storage (G') and loss moduli (G") on angular frequency, ω, for CTL gels with boric acid 8 mM and mannitol 16 mM ($R_{M/B}$ = 2); dotted lines are drawn to guide the eye. **(b)** Cole-Cole plot for the same sample as in (a); the dotted line is the best fit of experimental points according to eq. 2. **(c)** Dependence of the plateau modulus, G_∞, on $R_{M/B}$; the dotted line is drawn to guide the eye. Experimental conditions: [CTL] = 10 g/L, T = 25 °C, PBS 1X, pH 7.4. $R_{M/B}$ refers to the ratio [M]/[B], where [B] represents the total molar concentration of boric acid while [M] stands for the molar concentration of mannitol. Adapted with permission from Furlani *et al.*(Furlani, Sacco, Cok, et al., 2019) Copyright 2019 American Chemical Society.

3.2.3.2.3 Response to temperature

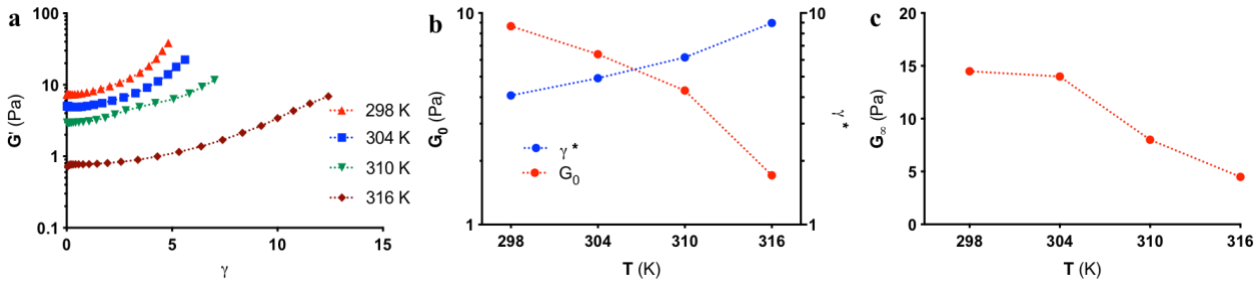

Figure 29. (a) Dependence of the elastic modulus, G', on applied deformation, γ, at different T. **(b)** Dependence of the shear modulus at zero strain, G_0, and that of critical strain, γ^*, on T. **(c)** Dependence of the plateau modulus, G_∞, on T. All dotted lines are drawn to guide the eye. In all cases the concentration of CTL was 10 g/L, that of boric acid 8 mM and that of mannitol 16 mM ($R_{M/B}$ = 2). All measurements were performed in PBS, pH 7.4. Reprinted with permission from Furlani *et al.*(Furlani, Sacco, Cok, et al., 2019) Copyright 2019 American Chemical Society.

The influence of temperature on mechanical performance for hydrogel samples presenting $R_{M/B}$ = 2 was investigated. More in detail, different rheological test (*i.e.* flow curves, frequency sweep and stress sweep tests) were performed in a temperature range from 25 to 43 °C. Flow curves and stress sweep data were nicely fitted according to eq. 4 and eq. 9, whereas frequency sweep data according to eq. 13 and eq. 14. A nonlinear response to stress and strain-hardening were detected for all investigated temperatures (Figure 29a). An exponential decay in shear modulus, and a simultaneous

increase of γ^*, as function of temperature, was detected (Figure 29b). A similar trend was detected for the plateau modulus (Figure 29c). These results suggest that mechanical performance of resulting gels is affected by temperature.

3.2.3.2.4 Response to glucose

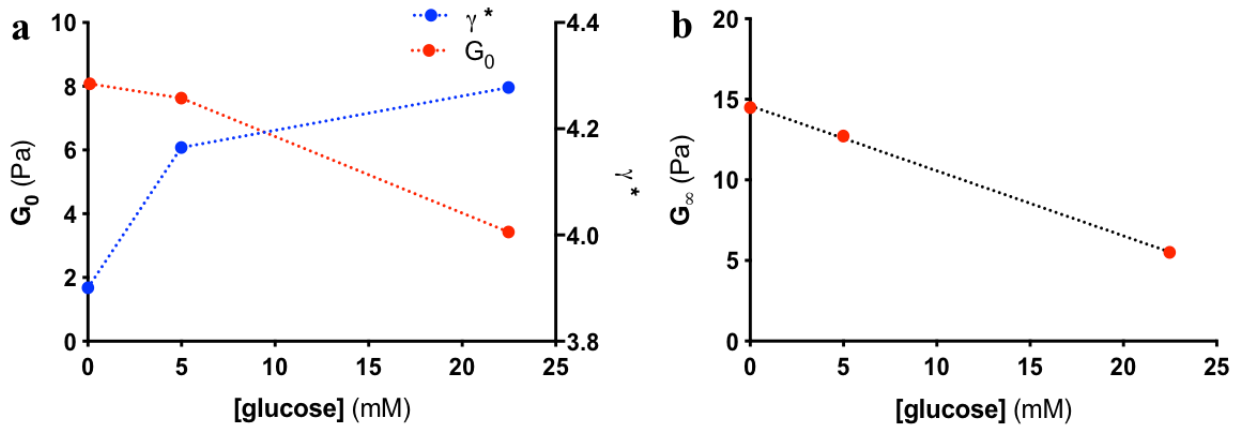

Figure 30. (a) Dependence of the shear modulus at zero strain, G_0, and that of critical strain, γ^*, on glucose concentration. **(b)** Linear dependence of the plateau modulus, G_∞, on glucose concentration. All curves have been drawn to guide the eye. Experimental conditions: medium, [CTL] = 10 g/L, [boric acid] = 8 mM, [mannitol] = 16 mM, pH 7.4, T = 25 °C. The medium composition was: PBS 1X for the samples at [glucose] = 0; FBS-supplemented DMEM:PBS 90:10 v/v for samples containing glucose. The concentration of glucose in the media used in experiments with cells was 5.6 mM in the case of Low Glucose DMEM and 25 mM for High Glucose DMEM. Reprinted with permission from Furlani *et al.*(Furlani, Sacco, Cok, et al., 2019) Copyright 2019 American Chemical Society.

The influence of the presence of glucose on CTL based networks was studied by using as "solvent" a cell culture media, *i.e.* DMEM, commonly used for *in vitro* biological tests. The presence of the cell culture media did not affect the possibility to fabricate networks. Rheological analyses were performed by exploiting DMEM with two different glucose concentration, namely DMEM Low Glucose (5.6 mM) and DMEM High Glucose (25 mM). Experimental results of flow curves, stress sweep and frequency sweep were respectively fitted by eq. 9, eq. 4, and eq. 13 and eq. 14. A progressive decrease in mechanical performance upon increasing glucose was detected (Figure 30). These results suggest that glucose partially seize boric acid, preventing its binding to CTL. As a matter of fact, boron compounds are able to bind glucose with high affinity and this process is reversible.(Kotsuchibashi, Agustin, Lu, Hall, & Narain, 2013; Springsteen & Wang, 2002; Yesilyurt et al., 2016) In avascular tissues, *e.g.* cartilage, the glucose concentration is comparable to that of media with low glucose,(Mobasheri, Shakibaei, Mobasheri, Richardson, & Hoyland, 2006) thus CTL

based networks can be suitable for tissue engineering and regenerative medicine applications, in particular for cartilage.

3.2.3.2.5 Self-healing properties of CTL-boric acid gels

The self-healing properties of resulting hydrogels were studied by both visual examinations and rheological measurements. After breakage, the sample spontaneously self-heal after some minutes. Furthermore, the healed network could extensively stretch (Figure 31a).

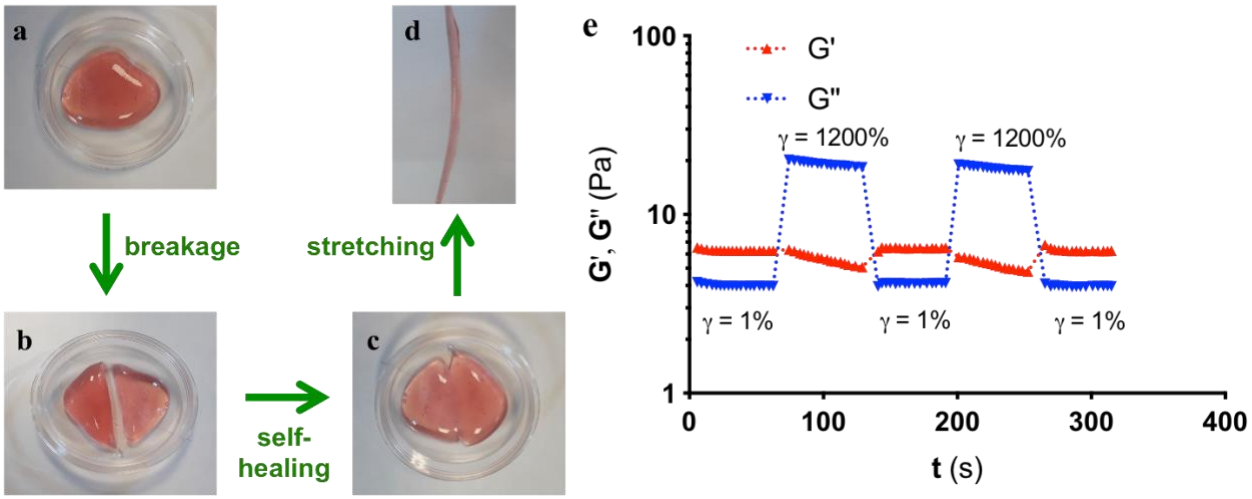

Figure 31. Self-healing properties of CTL-boric acid gels: **(a)** a freshly prepared sample was **(b)** cut into two separate pieces; **(c)** the sample spontaneously rejoined after 5 minutes and **(d)** restored its viscoelastic properties if stretched. Experimental conditions: [CTL] = 40 g/L, [boric acid] = 8 mM and [mannitol] = 16 mM, ($R_{M/B}$ = 2); DMEM low glucose:PBS 90/10 v/v as medium, pH 7.4. **(e)** Dependence of storage (G') and loss (G") moduli as a function of time; consecutive deformation steps were applied, namely 1% and 1200%. Experimental conditions: [CTL] = 10 g/L, [boric acid] = 8 mM and [mannitol] = 16 mM, ($R_{M/B}$ = 2), PBS 1X, pH 7.4. Adapted with permission from Furlani *et al.*(Furlani, Sacco, Cok, et al., 2019) Copyright 2019 American Chemical Society.

The self-healing ability was confirmed by rheological step-strain tests, consisting of alternating cyclic phases: (*i*) a small strain amplitude, *i.e.* 1%, within the linear viscoelastic regime and (*ii*) a large strain amplitude, *i.e.* 1200%, to promote network break. For small deformations G' was higher than G", whereas for large deformations an opposite trend (*i.e.* G">> G') was detected, suggesting network break. When a small deformation was applied again, networks were able to recover their original mechanical features (Figure 31b). The self-healing ability was traced back to the efficient rearrangement of network mesh due to boric acid association/dissociation dynamics. These results

are in line with previous data on boronic esters based gels and also on gels based on chitosan, although strain-hardening behavior was not reported in those cases.(Pettignano et al., 2017; Smithmyer et al., 2018; Tarus et al., 2014; Y. Zhang, Tao, Li, & Wei, 2011)

3.2.3.2.6 *In vitro* 2D-cell response toward CTL-boric acid gels

Cell viability and proliferation in the presence of CTL based gels was investigated in order to assess suitability of CTL based gels for regenerative medicine applications.

Primary pig chondrocytes and human dental pulp stem cells (hDPSCs) proliferation was not affected by the presence of networks (Figure 32). Also, singular components of gels (*i.e.* CTL and the mixture boric acid and mannitol) were used for these tests. Only the mixture boric acid-mannitol significantly affect the proliferation of cells. The toxicity was attributed to the inorganic crosslinker, since the sole mannitol played an inert role (data not shown).

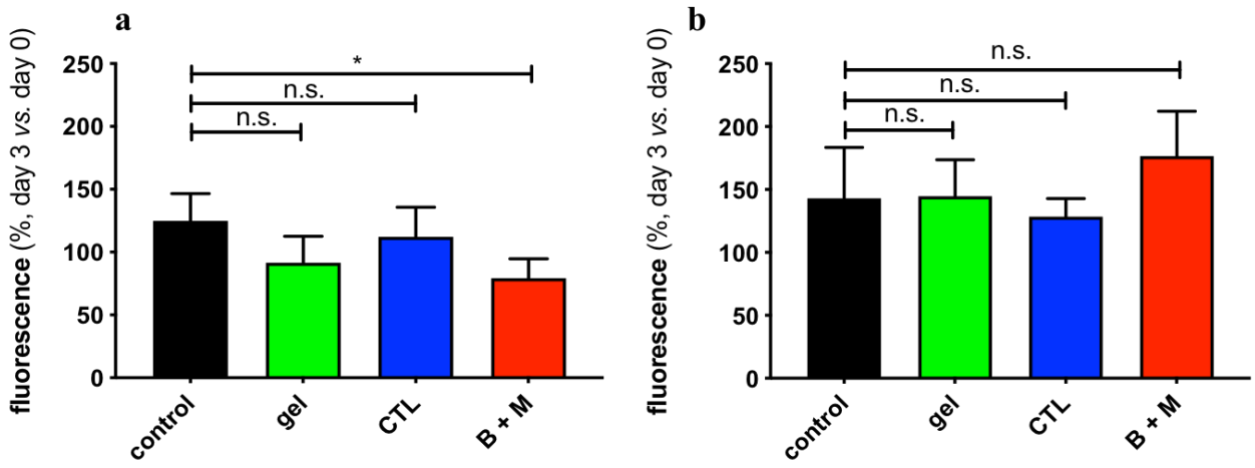

Figure 32. AlamarBlue Assay on primary pig chondrocytes **(a)** and human Dental Pulp Stem Cells (hDPSCs) **(b)**. Cells were treated with the sample-case gel ([CTL] = 10 g/L, [B] = 8 mM, [M] = 16 mM, $R_{M/B}$ = 2) and its singular components. One-way ANOVA followed by Dunnett *post-hoc* test was performed to compare groups (n.s.: not significant; *: *p* value < 0.05). In all cases data are reported as means ± standard deviations (SD) of at least six measurements. Adapted with permission from Furlani *et al.*(Furlani, Sacco, Cok, et al., 2019) Copyright 2019 American Chemical Society.

3.2.3.2.7 *In vitro* 3D-cell response toward CTL-boric acid gels

Attention then moved to the possibility of encapsulating cells in 3D networks. Thus, hDPSCs were loaded into CTL based hydrogels and Live/Dead assay was performed to verify cell viability in 3D conditions (Figure 33a). Almost all cells resulted to be alive, *i.e.* green-stained, whereas only a limited number of cells were dead, *i.e.* red-stained. This means that hydrogels are suitable media for

cells. These results are in line with what observed by other authors for cells encapsulated within dynamic networks based on boron.(Chen et al., 2018; Smithmyer et al., 2018) On the other hand, other authors reported a slight toxicity for cells encapsulated in networks displaying similar mechanics.(Chen et al., 2018; McKinnon, Domaille, Cha, & Anseth, 2014)

The AlamarBlue assay was finally performed to confirm the metabolic activity of cells embedded in CTL based hydrogels. A marked fluorescence signal was detected for cell-laden hydrogels (Figure 33b), proving safety of CTL based gels for stem cells biology.

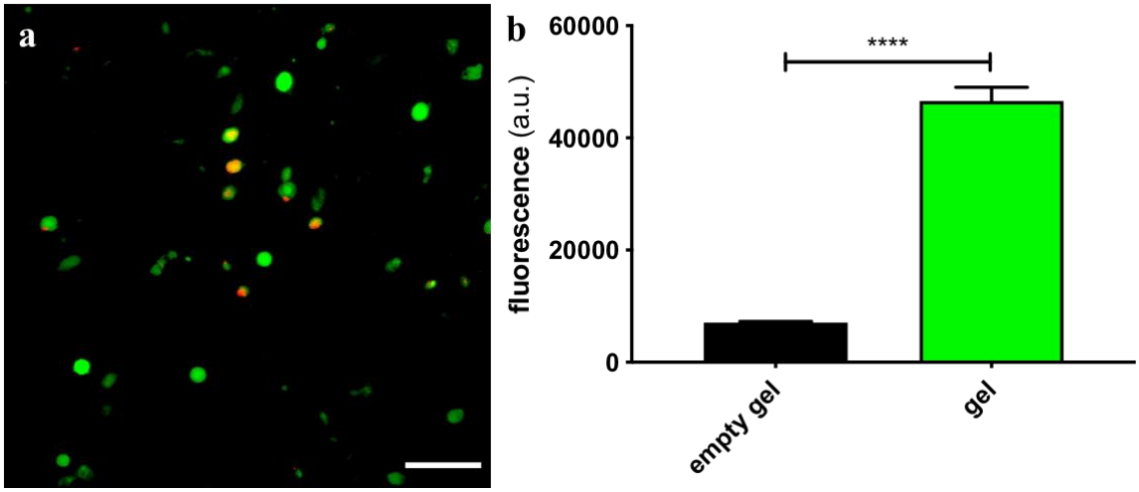

Figure 33. (a) Live/Dead assay on hDPSCs-laden within CTL-based gels ([CTL] = 40 g/L, [B] = 8 mM, [M] = 16 mM, $R_{M/B}$ = 2); scale bar is 100 µm. **(b)** AlamarBlue Assay on hDPSCs-laden within CTL-based gels ([CTL] = 40 g/L, [B] = 8 mM, [M] = 16, $R_{M/B}$ = 2) after 3 days of incubation. Student's t-test, ****: *p* value < 0.0001. In all cases data are reported as means ± standard deviations (SD) of at least six measurements. Adapted with permission from Furlani *et al.*(Furlani, Sacco, Cok, et al., 2019) Copyright 2019 American Chemical Society.

AD-MSCs were finally loaded into CTL-boric acid gels with different stiffness, by tuning polymer and boric acid concentrations. The activation of the Hippo pathway, governed by YAP and TAZ (and consequently TEAD), and governed by mechanical properties of materials,(Dupont et al., 2011; Oliver-De La Cruz et al., 2019) was investigated by confocal microscopy. In Figure 34a and 34b images of cells are reported embedded in gels with different polymer concentration but constant crosslinker concentration. Similar images were acquired also by using constant crosslinker concentration and different polymer concentration (image not shown for the sample [CTL] = 40 g/L, [B] = 2 mM, [M] = 4 mM, $R_{M/B}$ = 2). Only sparse red-labeled AD-MSCs, *i.e.* dead cells, were detected, confirming again that CTL-based networks represent safe materials for stem cells. The percentage of cell positive to the presence of nuclear YAP-TEAD was approximately 30% and no difference was

detected in gels with different composition (Figure 34c). The localization of YAP-TEAD was not affected by different polymer and crosslinker concentrations. Furthermore, the activation of Hippo pathway was not affected by the investigated range of gel stiffness. Possible explanations of this response could be that (*i*) in gels displaying strain hardening Hippo pathway activation is not affected by stiffness or (*ii*) the investigated range of stiffness was not sufficient to detect differences. Currently, these hypothesis cannot be tested since (*i*) softer gels are not suitable for 3D cell encapsulation (cells would fall down) and (*ii*) it is not possible to develop stiffer CTL-based gels by using only boric acid as crosslinking agent since higher polymer concentration cannot be handled and higher crosslinker concentrations would induce network disassembly (and therefore a decrease of mechanical properties would be detected, according to paragraph 3.1.3.2). Similar results, *i.e.* mainly localization of YAP in the nucleus, was reported also by Yang and collaborators for mesenchymal stem cells cultured on polyacrylamide gels with low ligand density.(Stanton, Tong, Lee, & Yang, 2019) Anyway, Zheng and collaborators reported that the main localization of YAP in the cytoplasm is beneficial for maintenance of chondrogenic phenotype.(Zhong et al., 2013)

Other authors reported different behavior of mesenchymal stem cells on 2D substrate with different stiffness. For instance, Yang and co-workers reported that most of cells on matrigel with different stiffness were positive to the nuclear presence of YAP.(Lee, Stanton, Tong, & Yang, 2019)

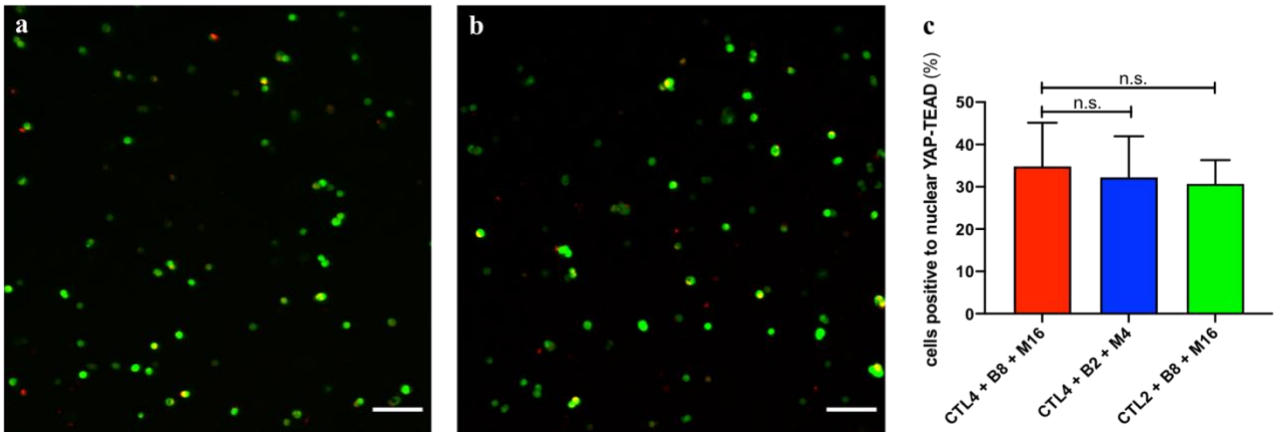

Figure 34. Confocal microscopy images after 3 days on AD-MSCs-laden within CTL-based gels with different stiffness: **(a)** [CTL] = 40 g/L, [B] = 8 mM, [M] = 16 mM, $R_{M/B}$ = 2 and **(b)** [CTL] = 20 g/L, [B] = 8 mM, [M] = 16 mM, $R_{M/B}$ = 2; scale bar is 100 µm. **(c)** Cell positive to nuclear presence of YAP-TEAD after 3 days within 3 hydrogels with different composition ([CTL] = 40 g/L, [B] = 8 mM, [M] = 16 mM, $R_{M/B}$ = 2; [CTL] = 40 g/L, [B] = 2 mM, [M] = 4 mM, $R_{M/B}$ = 2; [CTL] = 20 g/L, [B] = 8 mM, [M] = 16 mM, $R_{M/B}$ = 2), and different stiffness. One-way ANOVA followed by Dunnett *post-hoc* test was performed to compare cell viability (n.s.: p value < 0.05). Data are reported as means ± standard deviations (SD) of three measurements.

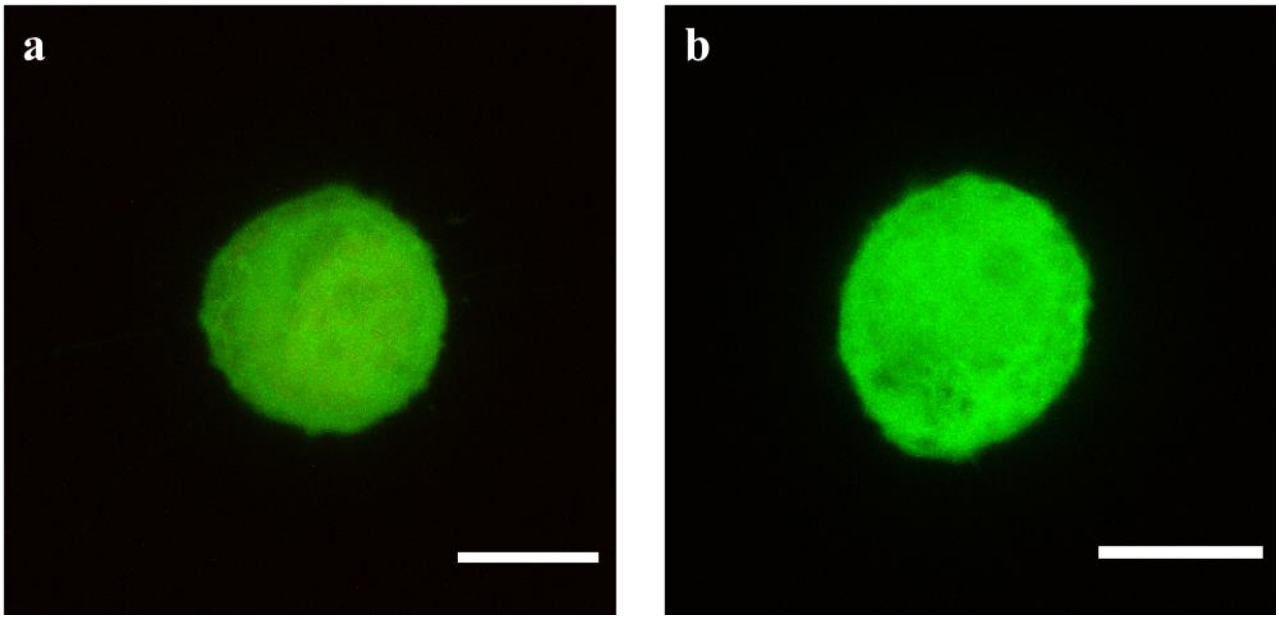

Figure 35. Confocal microscopy images after one day on AD-MSCs-laden within CTL-based gels with different stiffness: **(a)** [CTL] = 40 g/L, [B] = 8 mM, [M] = 16 mM, $R_{M/B}$ = 2 and **(b)** [CTL] = 20 g/L, [B] = 8 mM, [M] = 16 mM, $R_{M/B}$ = 2; scale bar is 10 μm.

In Figure 35 high magnification images are reported after one day of cells embedded in gels with different polymer concentration but constant crosslinker concentration. Almost all cells displayed a similar round shape. Similar images were acquired also by using constant crosslinker concentration and different polymer concentration (image not shown for the sample [CTL] = 40 g/L, [B] = 2 mM, [M] = 4 mM, $R_{M/B}$ = 2). The same results were detected also at longer timeframes (2, 3 and 4 days after cell embedding, images not shown). This indicate that these cells were not able to spread in CTL-based gels. This behavior could be governed by gels mechanical (*e.g.* a too low stiffness) or chemical (*e.g.* semi-synthetic nature of the polymer or low ligand density) properties.

Similar shapes of cells on or within 3D hydrogels were reported also by other authors.(Branco da Cunha et al., 2014; Lee, Gu, Mooney, Levenston, & Chaudhuri, 2017; Stanton et al., 2019; Tang et al., 2018) Yang and collaborators reported a round shape of mesenchymal stem cells (MSCs) cultured on polyacrylamide gels with low ligand density.(Stanton et al., 2019) Similar cell shapes were reported also by Anseth and co-workers for MSCs encapsulated in boronate-based hydrogels.(Tang et al., 2018) Chauhduri and collaborators detected similar round shape of MSCs embedded in alginate-based hydrogels.(Chaudhuri et al., 2016) By using the same cell line, AD-MSCs, within different gels Forte and collaborators detected interesting results.(Oliver-De La Cruz et al., 2019) AD-MSCs embedded in synthetic hydrogels (consisting of PEG) with the same ligand density, but different stiffness, displayed a similar round shape. On the other hand, AD-MSCs

encapsulated in natural occurring gels (consisting of fibrin) displayed a round shape in stiff gels, whereas were able to spread in soft gels.

Results for CTL-based gels are partially in contrast with other reports.(Liu, Mihaila, Rowan, Oosterwijk, & Kouwer, 2019; Lou, Stowers, Nam, Xia, & Chaudhuri, 2018) Kouwer and collaborators encapsulated AD-MSCs in synthetic hydrogels displaying a non-linear response to stress and strain hardening.(Liu et al., 2019) They reported an high ability of cell to spread, which was directly proportional to the stiffening response.

3.2.4 Main conclusions

To summarize, in this section were developed two simple approaches allowing for the controlled gelation of CTL in the presence of boric acid as a cross-linker.

For the first one – *i.e.* pH assisted gelation – the pivotal prerequisite is that boric acid is mixed with CTL in acidic conditions, where the less reactive trivalent neutral form of boric acid prevails over the more reactive anionic tetrahedral species. Upon addition of $NaHCO_3$, the time-dependent pH increase triggered CTL gelation due to the progressive formation of reactive tetrahedral borate anions. Interestingly, the gel strength was found to depend inversely on $NaHCO_3$ concentration. This trend was traced back to a progressive shift from interchain to intrachain complexes due to an increase of negative charges introduced in the network upon borate binding.

For the second one – *i.e.* competitor assisted gelation – the pivotal prerequisite is that the latter is mixed with the competitor, *e.g.* mannitol, where they can form soluble complexes. Then the mixture can be added to a CTL solution in physiological conditions and progressively make available the crosslinking agent. Suitable mannitol concentrations were able to control CTL reticulation thus allowing for the formation of homogeneous networks. Notably, CTL-boric acid gels displayed both a non-linear response to applied stress and a strain-hardening behavior, confirming their potential role as biomimetics of ECM. Exploiting the dynamically transient nature of borate esters, it was demonstrated the multi-responsiveness of CTL-boric acid gels toward different stimuli, *e.g.* temperature and glucose. Furthermore, gels self-healed after breakage. In the last part of this chapter the good biocompatibility of CTL-boric acid gels was demonstrated toward primary chondrocytes and human stem cells.

To summarize, it was possible to find two new alternative approaches to finely tune gelation of CTL.(Patent No. 102019000006448, 2019) CTL-boric acid gels preserved the characteristic strain-hardening behavior, confirming an interesting role for the present systems as *in vitro* mimics of

natural tissues. The use of CTL-boric gels can be proposed as multi-responsive biomaterials for tissue engineering and regenerative medicine, especially for articular cartilage regeneration.

3.3 CHAPTER III: Stable covalent gelation of lactose-modified chitosan

3.3.1 Aim of the work

In this chapter the main aims are (*i*) evaluate the possibility to use genipin as crosslinker for CTL in physiological conditions of pH and osmolarity, (*ii*) evaluate the possibility to have a dual crosslinking of CTL in the presence of boric acid and genipin, (*iii*) evaluate mechanical properties of resulting networks as function of crosslinker concentration in order to find samples displaying mechanical properties similar to those of natural tissues.

3.3.2 Materials and methods

3.3.2.1 Materials.

Chitin (from crab shells, practical grade), boric acid, sodium chloride (NaCl), Phosphate-buffered saline (PBS), glucosamine, N-acetil-glucosamine, lactose, ascorbic acid, AlamarBlue (*in vitro* Toxicology Assay Kit, Resazurin based, TOX-8), D_2O deuterium chloride (DCl), sodium nitrite ($NaNO_2$) and sodium hydroxide (NaOH) were all purchased from Sigma-Aldrich Chemical Co. (U.S.A.). The composition of PBS is NaCl 137 mM, KCl 2.7 mM, and phosphate buffer 10 mM with final ionic strength (I) of 168 mM and pH 7.4. Acetic acid (AcOH) and hydrochloric acid were from Carlo Erba (Italy). Genipin was from Challenge Bioproducts Co., Ltd. (Taiwan). DMEM (Dulbecco's Modified Eagle's Medium) High Glucose and Fetal Bovine Serum (FBS), streptomycin, penicillin and trypsin were from EuroClone (Italy). All reagents and chemicals were of high purity grade.

Hydrochloride form of lactose-modified chitosan, CTL (previously termed also chitlac and CTL60), (CAS Registry Number 2173421-37-7) was provided by biopo*Life* s.r.l. (Trieste, Italy). It has been synthetized from a highly deacetylated chitosan (ChitiNor, Norway) following the procedure reported elsewhere with slight modifications.(Donati et al., 2005) The relative molecular mass, *i.e.* molecular weight, of chitosan was estimated by capillary viscosity measurements and resulted to be 325 000; the dynamic viscosity of 1 % chitosan (1% acetic acid as solvent) resulted to be equal to 387 mPas. The chemical composition of CTL was determined by ^{1}H-NMR spectroscopy and resulted to be: fraction of deacetylated units (F_D) 0.21, fraction of lactose-modified units (F_L) 0.63 and fraction of acetylated units (F_A) 0.16. The calculated molecular mass of CTL repeating unit is 403.3 (MW_{ru}). The physical properties were determined by viscometry: the intrinsic viscosity, [η], of CTL was measured at 25 °C by means of a CT 1150 Schott Geräte automatic measuring apparatus and a Schott capillary viscometer. A buffer solution composed by 20 mM AcOH/AcNa, pH 4.5, and 100 mM NaCl

was used as solvent.(Berth & Dautzenberg, 2002) The resulting [η] was found to be 344 mL/g. The estimated molecular weight of CTL was around 780 000.

Deionized Milli-Q water was used in all preparations.

3.3.2.2 Preparation of genipin-assisted and dual crosslinked CTL-based gels.

CTL solutions were prepared in PBS buffer, pH 7.4, according to Paragraph 3.2.2 with slight modifications. Briefly, 50 mg of polymer were solubilized in 3.5 mL of deionized water; the pH was then adjusted to 7.4 by adding aliquots of NaOH (1 M). Finally, 400 µL of PBS 10X and deionized water amounts were added to have a final volume of 4.0 mL.

Mixtures of boric acid (80 mM) and mannitol (160 mM) were prepared in PBS 2X buffer, pH 7.4. Briefly, 145.7 mg of mannitol were solubilized in 3.5 mL of deionized water; 800 µL of boric acid 500 mM (PBS 1X as solvent, pH 7.4) were added, followed by 920 µL of PBS 10X. Finally, the pH was adjusted to 7.4 using NaOH (5 M) and different amounts of deionized water were added to have a final volume of 5 mL.

Genipin was solubilized in deionized water at concentration equal to 5.2 mM. This solution was then diluted in water in order to have a concentration equal to 2.6 and 1.3 mM.

Mixtures of genipin, boric acid and mannitol were prepared by mixing an equal volume of genipin (water as solvent) and mixture of boric acid and mannitol (PBS 2X as solvent), in order to have a solution with PBS 1X as solvent and pH 7.4.

A typical gel preparation was carried out as follows: 1 mL mixture of genipin, boric acid and mannitol (PBS 1X, pH 7.4) was injected into 4.0 mL of CTL solution (PBS 1X, pH 7.4) under magnetic stirring. The final concentrations of genipin, boric acid and mannitol resulted 0.52-0.13 mM, 8 mM and 16 mM, respectively. In the case of gels crosslinked without boric acid 1 mL of genipin (PBS 1X, pH 7.4) was injected into 4.0 mL of CTL solution (PBS 1X, pH 7.4) under magnetic stirring. The final concentration of CTL was 10 g/L, *i.e.* 1% w/v, throughout all experiments. After the addition of crosslinking agents, samples were mechanically stirred for a few seconds.

$R_{G/N}$ refers to the ratio [G]/[N], where [G] stands for the molar concentration of genipin while [N] represents the molar concentration of primary amine groups, *i.e.* F_D, in CTL.

3.3.2.3 Rheological characterization.

Rheological measurements were performed using an HAAKE MARS III rheometer (Thermo Scientific) operating in oscillatory shear conditions. The experimental settings used to characterize genipin-crosslinked and dual crosslinked gels are the following: titanium plates with 2° cone/plate

geometry (Ø = 35 mm) and gap 0.105 mm. Time sweep experiments were carried in strain-controlled conditions, with deformation, γ, of 0.03 for chitosan and 0.01 for CTL, kept constant throughout the experiment, frequency, ν, of 1 Hz and time of 10 800 s. Upon addition of crosslinking agents (genipin or mixture of genipin, boric acid and mannitol), solutions were mixed under stirring for about 10 s to uniform samples and poured on the plate. The values of storage G' (elastic response) and loss G" (viscous response) moduli were recorded as a function of time. Time sweep experiments were performed at different temperatures, *i.e.* 37, 45, 50 and 60°C.

Rheological tests were then performed at T = 37 °C on crosslinked gels (after time sweep experiments at 60°C for three hours) under oscillatory shear conditions to determine the mechanical spectra (frequency sweep, τ = 1 Pa, well within the linear viscoelasticity range and in the frequency range 0.01 - 100 Hz) and the extension of the linear viscoelastic regime (stress sweep tests at ν = 1 Hz, stress range $1 < \tau < 10000$ Pa).

Oil was used to seal the interface between the two plates in order to improve thermal control and limit solvent evaporation.

3.3.2.4 UV-visible analyses.

UV-Visible spectroscopy measurements were performed on CTL-based gels by means of Cary 400 spectrophotometer in the λ range 350 – 800 nm. Samples were prepared according to Paragraph 3.3.2.4. The final genipin concentration was fixed to 0.26 mM in order to avoid exceeding of linear dependence of absorbance (A<1). After mixing of crosslinking agents, samples were dispensed in 1 mL disposable plastic cuvette by using a 1 mL syringe. Disposable cuvettes were incubated at 37°C, then at appropriate timeframes samples were analyzed. Each formulation was analyzed at least in triplicate after different timeframes, *i.e.* 0, 3, 6, 24, 48 and 120 hours. Solvent (PBS 1X) was used as blank solution and subtracted to all spectra recorded.

3.3.2.5 Cell cultures and biocompatibility tests.

human Dental Pulp Stem Cells (hDPSCs, Celprogen Inc.) were used as cell models in order to test the biocompatibility of different concentrations of free genipin. hDPSCs were cultured in Dulbecco's Modified Eagle Medium (DMEM) High Glucose supplemented with 10% v/v fetal bovine serum (FBS) (EuroClone, Italy), 100 U/mL penicillin, 100 µg/mL streptomycin, 2 mM L-glutamine, and ascorbic acid 100 µM using 75 cm_2 flasks at 37 °C in humidified environment at 5% of CO_2. 200 µL of cells were plated in 96-well tissue culture plates. The initial concentration of hDPSCs was 2000 cells/well. Cells were left at rest for 1 day, then supernatants discarded and 200 µL of the corresponding treatment (genipin or control) were added. Each treatment consist of 90%

V/V DMEM and 10% genipin (water as solvent). Three concentrations of genipin were used, *i.e.* 0.52, 0.26 and 0.13 mM. At least four independent replicates were performed for each treatment.

The viability of adherent cells was assessed after different timeframes (1 and 3 days) using the AlamarBlue assay according to the protocol reported in the Paragraph 3.2.2.8.3 with slight modifications. In the present case, AlamarBlue was diluted 1:20 v/v with fresh medium.

3.3.3 Results and discussion

3.3.3.1 Genipin crosslinked CTL-based gels

Samples with constant CTL concentration and different amounts of genipin were prepared, transferred in glass tubes, and incubated at 37°C for 24 hours. Resulting samples turned into blue gels, with color intensity proportional to genipin concentration (Figure 36). Similar results were reported also by other authors for genipin crosslinked gels.(Fessel, Cadby, Wunderli, Van Weeren, & Snedeker, 2014; Muzzarelli, El Mehtedi, Bottegoni, Aquili, & Gigante, 2015) All samples (except the control) were positive to gelation according to inverted test tube.(Bhattarai et al., 2005; Jeong, Bae, & Kim, 1999)

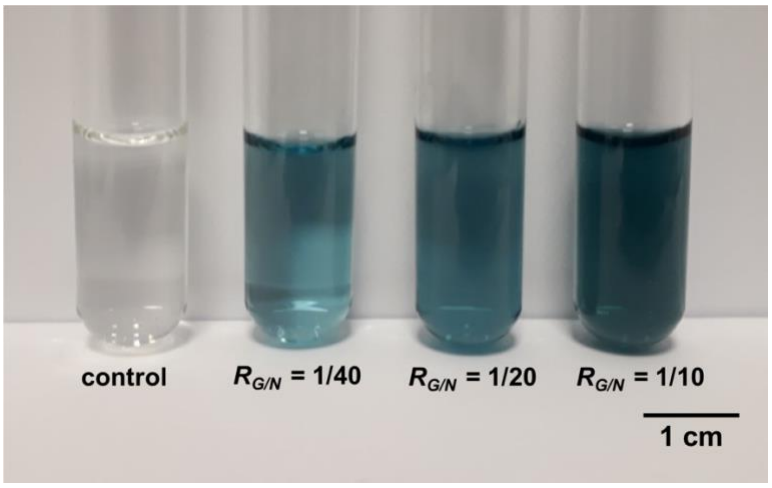

Figure 36. Visual analysis after 24 hours at 37°C of CTL control sample (without any crosslinking agent) and samples with different genipin concentrations, *i.e.* 0.13 mM ($R_{G/N}$ = 1/40), 0.26 mM ($R_{G/N}$ = 1/20), and 0.52 mM ($R_{G/N}$ = 1/10). Experimental conditions are [CTL] = 1% w/v, PBS 1X, pH 7.4.

Time sweep analyses were performed on samples with CTL 1% w/v and [genipin] = 0.52 mM ($R_{G/N}$ = 1/10) incubated at 60°C for three hours. A progressive decrease of the loss tangent values was detected as function of time (data not shown), suggesting gelation of CTL. By evaluating mechanical properties of resulting samples after time sweep, non-linear response to stress and a strain-hardening

behavior were detected (Figure 37a). In addition, focusing on the mechanical spectrum, both elastic and viscous moduli were almost constant and parallel in the frequencies range investigated (Figure 37b).

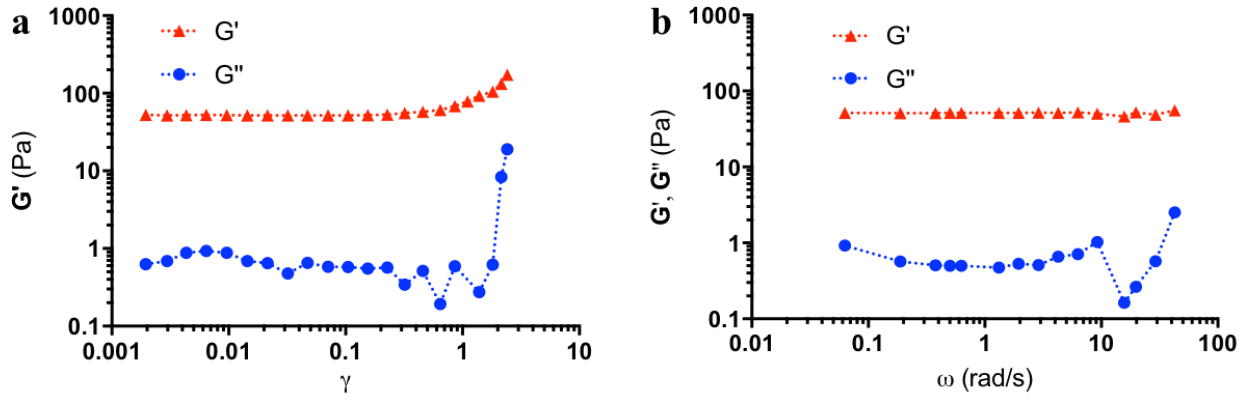

Figure 37. (a) Dependence of storage (G') and loss moduli (G") on strain, γ, for CTL in the presence of genipin. **(b)** Dependence of storage (G') and loss moduli (G") on angular frequency, ω, for CTL samples in the presence of genipin. Dotted lines are drawn to guide the eye. Experimental conditions are [CTL] = 1% w/v, [genipin] = 0.52 mM ($R_{G/N}$ = 1/10), PBS 1X, pH 7.4, T = 37°C. Experiments were performed after time sweep analysis at 60°C for three hours.

Strain-hardening behavior was attributed to the formation of non-covalent (and also covalent, for the presence of genipin) bounds, *e.g.* hydrophobic interactions and hydrogen bounds, which could be able to rearrange upon application of stress. None author reported such phenomena for hydrogels based on commercial chitosan crosslinked with genipin.(Muzzarelli, 2009; Muzzarelli et al., 2015; Pandit et al., 2013) On the other hand, a similar mechanical behavior (*i.e.* with strain hardening) was reported for PEG-grafted chitosan gels, crosslinked with genipin in physiological conditions.(Chang et al., 2018)

It is important to note that only a limited amount of genipin (0.52 mM) was needed for gelation of CTL. Other authors reported protocols which usually needed at least ten fold higher genipin concentrations.(Barbosa et al., 2010; Bi et al., 2011; Mi, Sung, Shyu, Su, & Peng, 2003; Muzzarelli et al., 2015; Mwale et al., 2005) To have such high genipin concentrations, they used organic solvents (*e.g.* DMSO and ethanol) to solubilize the crosslinking agent and fabricated gels mainly in acidic conditions.(Jinke Xu, Strandman, Zhu, Barralet, & Cerruti, 2015)

Furthermore, it is noteworthy that a three-fold higher shear modulus was detected for CTL based gels, compared to the one obtained for chitosan with F_A = 0.55 ones, by using the same polymer and crosslinker concentrations (polymer 1% w/V and [genipin] = 0.52 mM) (data not shown). More

in detail, by exploiting eq. 4, for chitosan-based gels shear modulus at zero strain, *i.e.* G_0, was ~ 17 Pa, whereas for CTL-based ones G_0 was ~ 52 Pa. This result seems quite unexpected, since (*i*) lactose moieties in CTL should partially prevent ammine binding to due to steric hindrance and (*ii*) chitosan have more ammine groups available for genipin binding. Although, these results could stem from the higher molecular weight of CTL (*i.e.* 780 000) with respect to chitosan (*i.e.* 90 000), an alternative explanation could involve the formation of a higher number of low energy bonds (*e.g.* hydrophobic interactions and/or hydrogen bonds) in CTL, fostered by its branched lactitol moieties. Another mechanism could involve other types of bonds, beyond ammine crosslink, between genipin and CTL; to test this hypothesis the interaction between genipin and singular components of CTL will be investigated.

3.3.3.2 Dual crosslinked CTL-based gels

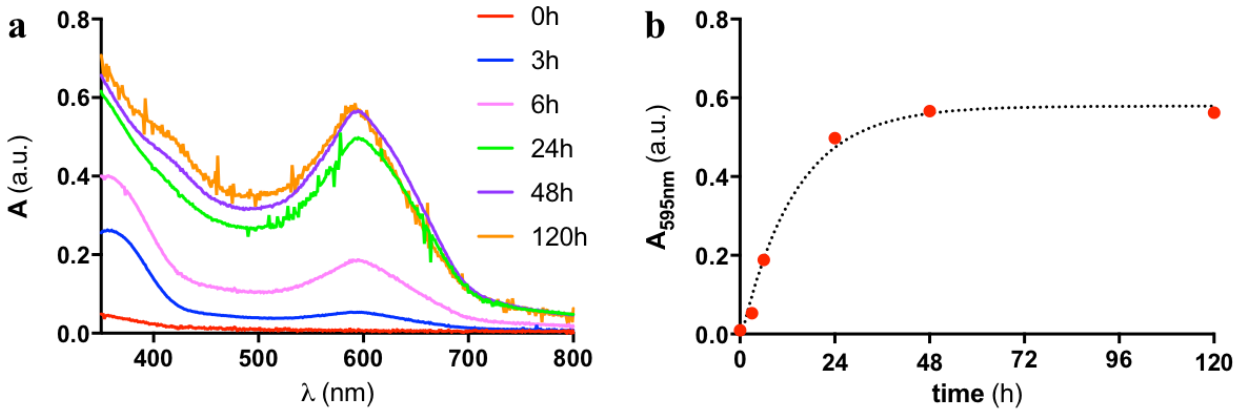

Figure 38. (a) Dependence of absorbance (A) on wavelength for CTL in the presence of boric acid and genipin at different timeframes after incubation at 37°C. **(b)** Dependence of absorbance at 595 nm on time for CTL in the presence of boric acid and genipin at different timeframes after incubation at 37°C. The black dotted line is drawn to guide the eye. Experimental conditions are [CTL] = 1% w/v, [genipin] = 0.26 mM ($R_{G/N}$ = 1/20), [boric acid] = 8 mM, [mannitol] = 160 mM PBS 1X, pH 7.4.

The interaction between CTL and genipin, in the presence of boric acid as transient crosslinking agent, was investigated by UV-visible spectrophotometric analyses. CTL was mixed with a mixture of both crosslinking agents, *i.e.* genipin and boric acid, then samples were incubated at 37°C and analyzed after different timeframes. A progressive increase of absorbance, in the whole wavelength range, was detected (Figure 38a) with a peak at 595 nm. The same absorbance peak was detected for glucosamine (not reported), therefore the primary ammine groups of CTL can be safely considered as the interaction sites with genipin. A marked increase in absorbance at λ = 595 nm was detected for

the first 48 hours followed by a plateau (Figure 38b). These results indicate that genipin was able to complete crosslinking of CTL within two days, thus with a speed was lower than that for free glucosamine (data not shown). The slower binding activity detected for CTL can be easily explained considering that in the presence of the transient crosslinking agent, *i.e.* boric acid, the high viscosity and the possible steric hindrance could partially prevent or delay interaction between CTL and genipin.

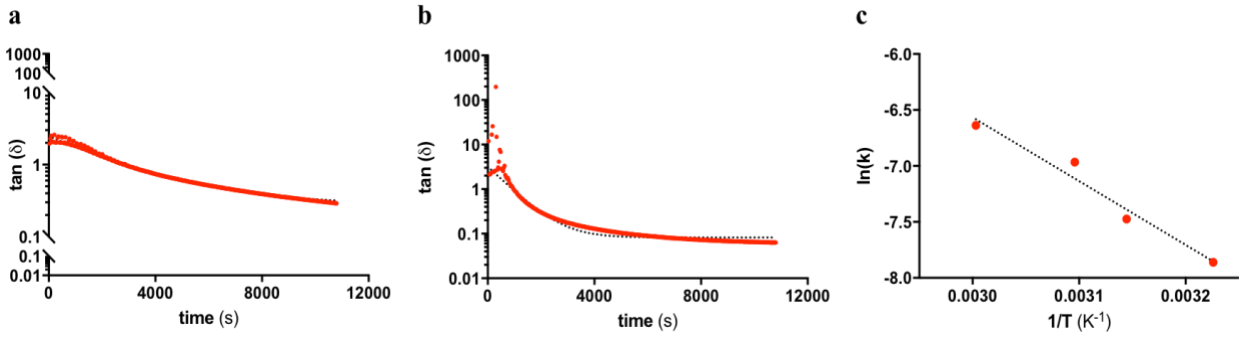

Figure 39. Dependence of the loss tangent, $tan\delta$, on time of dual crosslinked (with genipin and boric acid) CTL system at 37°C **(a)** and 60°C **(b)**. Black dotted lines represent the best fitting of experimental points using eq. 11. **(c)** Arrhenius plot, *i.e.* dependence of the natural logarithm of the rate constant (k_2) on the inverse of temperature; the black dotted line represents the best fitting of experimental points according to a linear dependence ($R_2 > 0.95$). Experimental conditions are [CTL] = 1% w/v, [genipin] = 0.52 mM ($R_{G/N}$ = 1/10), [boric acid] = 8 mM, [mannitol] = 160 mM, PBS 1X, pH 7.4.

Time sweep rheological analyses were performed on hydrogel samples with constant polymer and crosslinker concentrations – CTL 1% w/v, [genipin] = 0.52 mM ($R_{G/N}$ = 1/10), [boric acid] = 8 mM, [mannitol] = 160 mM – at different temperatures, *i.e.* 37, 45, 50 and 60°C, for three hours. Figure 39 reports the loss tangent values, tan δ, *i.e.* G''/G', as a function of time at two temperatures, *i.e.* 37 and 60 °C. In both cases, a progressive decrease in loss tangent values was detected, indicating polymer structuring. At 37°C the loss tangent continues to decrease during the whole test, indicating that three hours were not sufficient to complete gelation. Otherwise, at 60°C the values of the loss tangent were almost constant after one hour. Experimental data were nicely fitted by using equation 11:

$$tan\delta\ (t) = (tan\delta_0 - tan\delta_\infty)e^{-k_2 t} + tan\delta_\infty \quad \text{(eq. 11)}$$

where $tan\delta_0$ is the value of loss tangent at time zero, $tan\delta_\infty$ is the loss tangent at infinite times and k_2 is the rate constant. A correlation between the kinetic of the process and the temperature was found from an Arrhenius plot. This finding clearly unveils that gelation can be accelerated by increasing the temperature. A similar dependence of mechanical performance of genipin crosslinked in different

conditions, *e.g.* temperature and time, was reported also by other authors.(Bi et al., 2011; Fessel et al., 2014)

The activation energy of the process resulted to be equal to 5.7 ± 0.8 kJ/mol. This value is at least one order of magnitude lower than that reported for other chitosan-based networks.(Félix, Hernández, Argüelles, & Goycoolea, 2005; Moore & Roberts, 1980)

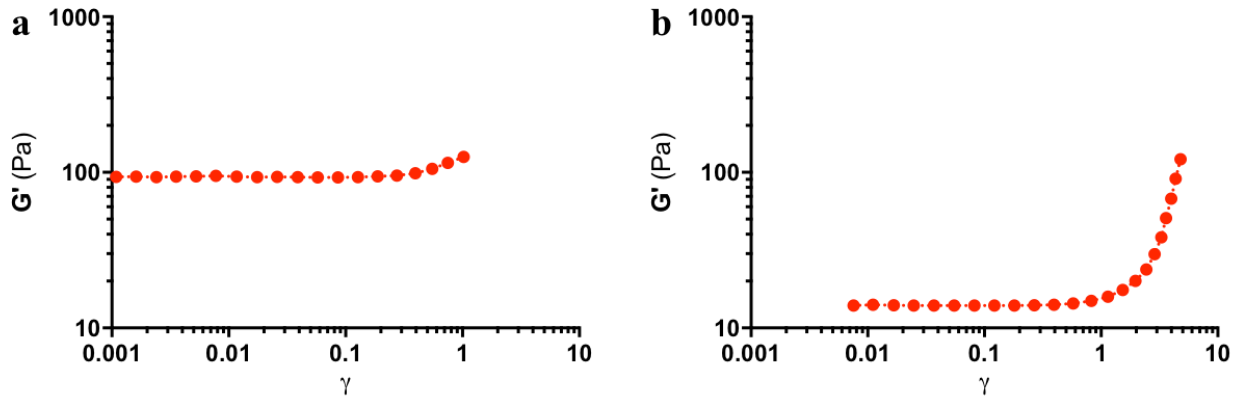

Figure 40. (a) Dependence of storage modulus (G') on strain, γ, for CTL in the presence of boric acid ([B] = 8 mM) and genipin ([genipin] = 0.52 mM ($R_{G/N}$ = 1/10)). **(b)** Dependence of storage modulus (G') on strain, γ, for CTL in the presence of boric acid ([B] = 8 mM) and genipin ([genipin] = 0.13 mM ($R_{G/N}$ = 1/40)). Dotted lines are drawn to guide the eye. Experimental conditions are [CTL] = 1% w/v, [genipin] = 0.52 mM ($R_{G/N}$ = 1/10), [boric acid] = 8 mM, [mannitol] = 160 mM, PBS 1X, pH 7.4, T = 37°C. Experiments were performed after time sweep analysis at 60°C for three hours.

The mechanical performance of gels with different genipin amounts was determined after thermal curing by performing stress sweep and frequency sweep analyses. In the presence of the highest genipin concentration ([genipin] = 0.52 mM; $R_{G/N}$ = 1/10) only a slight deviation from linear stress-strain response was a detected (Figure 40a). This result is quite unexpected since CTL in the presence of singular crosslinkers (with only genipin or with only boric acid) display a non-linear response to stress and strain hardening. This is probably caused by the high overall concentration of crosslinkers, that probably partially prevented the sliding of polymer chains upon application of shear. By using lower genipin concentrations, a marked non-linear behavior with strain hardening was detected (Figure 40b, [genipin] = 0.26 mM, $R_{G/N}$ = 1/20; data not shown for [genipin] = 0.13 mM, $R_{G/N}$ = 1/40).

Frequency sweep analyses were performed on samples with different genipin concentrations. By using the highest genipin concentration, *i.e.* [genipin] = 0.52 mM ($R_{G/N}$ = 1/10), storage modulus was almost constant in the whole range of frequency, whereas loss modulus was dependent on applied

frequency (Figure 41a). In the case of the lowest genipin concentration, *i.e.* [genipin] = 0.13 mM ($R_{G/N}$ = 1/40), both moduli were dependent on applied frequency, as previously detected for samples crosslinked only with boric acid (Figure 11a). A similar trend was reported by Narita and co-authors for networks consisting of PVA (poly(vinyl alcohol)) simultaneously crosslinked with borate and a stable covalent crosslinking agent.(Narita et al., 2013)

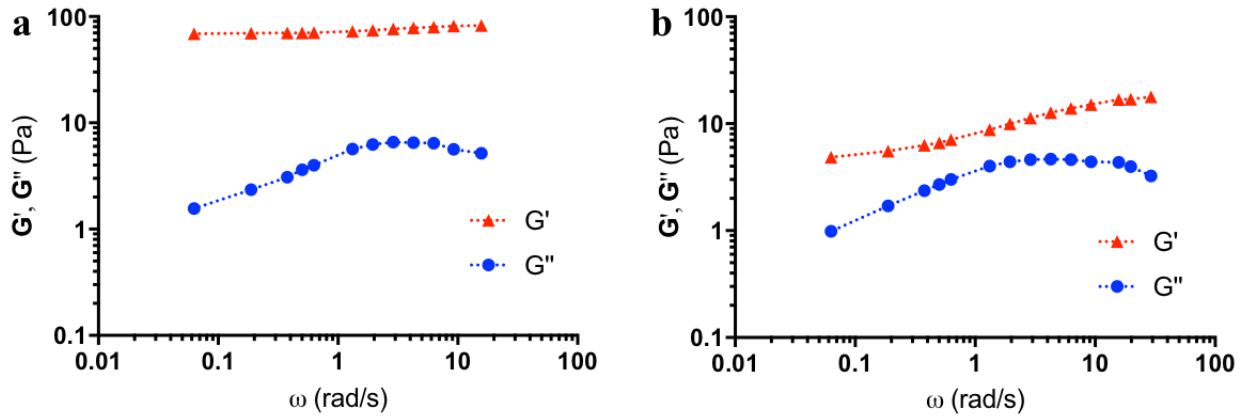

Figure 41. (a) Dependence of storage (G') and loss moduli (G'') on angular frequency, ω, for CTL in the presence of boric acid ([B] = 8 mM) and genipin ([genipin] = 0.52 mM ($R_{G/N}$ = 1/10)). **(b)** Dependence of storage (G') and loss moduli (G'') on angular frequency, ω, for CTL in the presence of boric acid ([B] = 8 mM) and genipin ([genipin] = 0.13 mM ($R_{G/N}$ = 1/40)). Dotted lines are drawn to guide the eye. Experimental conditions are [CTL] = 1% w/v, [genipin] = 0.52 mM ($R_{G/N}$ = 1/10), [boric acid] = 8 mM, [mannitol] = 160 mM, PBS 1X, pH 7.4, T = 37°C. Experiments were performed after time sweep analysis at 60°C for three hours.

All investigated samples, with different genipin concentration, displayed the same ω_{max}, equal to 0.46 Hz. This suggests that, in resulting networks, the transient cross-linker behaves as a weak sticker. The correlated association/dissociation time, λ_{max}, was equal to 2.1 s. This value is quite lower than the one detected for boric acid crosslinked samples in the presence of sodium bicarbonate (Figure 21b) and about twenty fold higher than that reported for PVA dual crosslinked with borate and permanent bounds,(Narita et al., 2013) indicating that CTL gels exhibit different dynamics.

All samples displayed the same trend of loss moduli from frequencies lower than ω_{max}, *i.e.* $G'' \propto \omega^{0.4}$. For the sample with the lowest genipin concentration, *i.e.* [genipin] = 0.13 mM, $R_{G/N}$ = 1/40 (Figure 41b), at frequencies lower than ω_{max}, the elastic and loss moduli were found to scale with the angular frequency according to the power laws: $G' \propto \omega^{0.2}$ and $G'' \propto \omega^{0.4}$, respectively. Narita and co-workers reported a different trend for networks consisting of PVA and borax, with $G' \propto \omega^{1}$ and $G'' \propto \omega^{0.5}$, respectively.(Narita et al., 2013)

3.3.3.3 Genipin biocompatibility

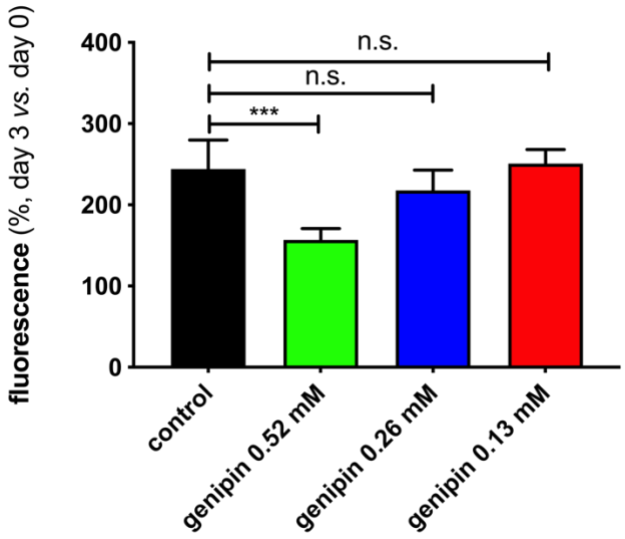

Figure 42. Alamar Blue Assay on primary human Dental Pulp Stem Cells (hDPSCs). Cells were treated with different concentration of genipin. One-way ANOVA followed by Dunnett *post-hoc* test was performed to compare groups (n.s.: not significant; *: p value < 0.05). In all cases data are reported as means ± standard deviations (SD) of at least six measurements.

To consider gels as potential candidates for regenerative medicine applications, the effect on cell viability and proliferation was verified using free genipin in 2D condition. Only the highest genipin concentration, *i.e.* 0.52 mM, significantly impaired cell proliferation (Figure 42). It should be considered that when CTL-based gels are used, only a limited amount of genipin should be able to interact with cells, therefore resulting gel could be safe for hDPSCs. On the other hand, lower genipin concentrations (*e.g.* 0.26 and 0.13 mM) represent a non-hazardous environment for hDPSCs biology. Nevertheless, these results are only preliminary data on a model stem cell line. Thus, the same set of experiments should be performed on cells plated on or embedded in the resulting hydrogels; it should be considered that genipin could be able to crosslink also cell membrane, so attention should be focused on cells plated on crosslinked hydrogels (at the end of gelation). These results are in line with results from other authors on other cell types. Snedeker and collaborators reported a similar trend with genipin for cells harvested from horse tendon.(Fessel et al., 2014) A slight decrease in cell viability was also reported for mesenchymal stem cells on genipin-crosslinked chitosan/collagen scaffolds for cartilage tissue engineering.(Bi et al., 2011) Also Wang and collaborators indicated genipin concentrations within 0.5 mM as safe for primary chondrocytes and human osteoblasts.(Wang, Lau, Loh, Su, & Wang, 2011)

3.3.4 Main conclusions

In this section, an insight on the interaction between genipin and lactose derivative of chitosan (CTL) was presented. Genipin, even at very low concentrations, was able to efficiently crosslink CTL in physiological conditions. Resulting blue gels displayed a nonlinear response to stress and strain hardening. Such behavior was attributed to the formation and reorganization of intermolecular low-energy bounds (*e.g.* hydrogen bounds and hydrophobic interactions).

Genipin was used also as second crosslinking agent for boric acid-CTL gels. Resulting gels displayed common features of both transient and permanent crosslinked networks. It is interesting to note that by using a high overall crosslinkers concentration, the onset of strain hardening was partially prevented.

The possibility to use these semi-synthetic networks could help unveiling the peculiar mechanical properties of the natural tissues. Furthermore, due to the peculiar rheological properties of polymers in the presence of cross-linking molecules, networks might be used for tissue engineering and regenerative medicine, in particular for cartilage regeneration.

3.4 CHAPTER IV: Synthesis and characterization of nanoparticles based on chitosan and hyaluronan

3.4.1 Aim of the work

In this chapter, a protocol requiring mild conditions was used to fabricate a library of chitosan/hyaluronan nanoparticles. The main aims are: (*i*) evaluate the influence of chitosan molecular properties (*i.e.* fraction of acetylation and molecular weight) on stability and physical-chemical properties of resulting nanoparticles; (*ii*) study the influence of physical-chemical properties of resulting nanoparticles on interaction and response of innate immune systems cells; (*iii*) investigate the possibility to use nanoparticles as drug delivery system for anti-inflammatory drugs; (*iv*) evaluate the suitability of nanocomposite networks consisting of nanoparticles and CTL-based networks for drug delivery purposes.

3.4.2 Materials and methods

3.4.2.1 Materials.

Hydrochloride chitosans (CH) with different molecular weights (viscosity average molecular weight, $\overline{M_v}$, in the range 10 000 - 400 000, calculated using the following Mark-Houwink-Sakurada parameters, *i.e.* K = 8.43 x 10^{-3} mL/g and a = 0.92 according to Berth and Dautzenberg.(Berth & Dautzenberg, 2002)) and different fraction of acetylated units, F_A, (determined by ^{1}H-NMR) were kindly provided by Novamatrix/FMC Biopolymer (Sandvika, Norway) and by the late Prof. Kjell Morten Vårum (NTNU, Trondheim, Norway). The characteristics of CH are presented in Table 1. Hydrochloride chitosan sample with F_A = 0.02 was obtained *via* heterogeneous deacetylation (K M Vårum et al., 1991) starting from a chitosan template with an original F_A = 0.14. Hydrochloride chitosan sample with F_A = 0.25 was obtained *via* re-*N*-acetylation (Sacco, Cok, et al., 2018) starting from a chitosan template with an original F_A = 0.16. The characteristics of CH are presented in Table 1. The endotoxin content in chitosan samples was determined by the kinetic turbidimetric limulus amebocyte lysate (LAL) test according to Ph. Eur. 7.0, 2.6.14, Method C. Sodium hyaluronate (HA), ($[\eta]$ = 270 mL/g; $\overline{M_v}$ = 90 000, Bioibérica S.A.) was kindly provided by Sigea Srl (Trieste, Italy). Sodium tripolyphosphate pentabasic (TPP ≥ 98%), *N*-(3-dimethylaminopropyl)-*N'*-ethylcarbodiimide hydrochloride (EDC), *N*-hydroxysuccinimide (NHS), fluorescinamine isomer I, aceclofenac, Phosphate Buffered Saline (PBS), Percoll, bovine serum albumin (Cohn fraction V BSA, ≥ 96% cell culture-tested), dihydrorhodamine 123 (DHR), horseradish peroxidase (HRP), type VI,

fibrinogen (FBG), from human plasma, phorbol-12-myristate-13-acetate (PMA), lipopolysaccharide (LPS), $NaHCO_3$, 4-(2-hydroxyethyl)-1-piperazineethanesulfonic acid (HEPES), ethanol, mucin (from porcine stomach, type III, bound sialic acid 0.5-1.5%, partially purified), penicillin, dexamethasone, streptomycin and glutamine were from Sigma-Aldrich Co. (St.Louis, MO). RPMI (Roswell Park Memorial Institute) 1640 and Fetal Bovin Serum (FBS) were from EuroClone (Italy). High-purity Trypan Blue (TB, Color Index 23850) - obtained from Merck KgaA (Darmstadt, Germany) - was dissolved in distilled water at 5 mg/mL and filtered through a Millipore filter to remove non-solubilized material. All other reagents were from Sigma-Aldrich. All reagents and chemicals were of high purity grade. Deionized (Milli-Q) water was used in all experiments, except for the solutions used in the biological assays, which were prepared in endotoxin-free water or physiologic saline (0.9% w/v NaCl) for clinical use.

Table 1. Fraction of acetylated units (F_A), intrinsic viscosity, $[\eta]$, viscosity average molecular weight, $\overline{M_v}$, molecular weight of chitosan repetitive unit, $MW_{r.u.}$, viscosity average degree of polymerization, $\overline{DP_v}$, and endotoxins content of hydrochloride chitosans used for the synthesis of nanoparticles. ND: not determined. Adapted with permission from Furlani *et al.*(Furlani, Sacco, Decleva, et al., 2019) Copyright 2019 American Chemical Society.

F_A	$[\eta]$ (mL/g)	$\overline{M_v}$	$MW_{r.u.}$	$\overline{DP_v}$	Endotoxins (EU/g)
0.63	300	90 000	201	448	ND
	550	170 000		846	81
	950	310 000		1542	ND
0.46	340	100 000	200	500	ND
	650	210 000		1050	ND
	920	300 000		1500	ND
0.25	600	190 000	199	955	309
0.16	110	30 000	199	152	ND
	681	220 000		1111	64
	1026	340 000		1717	ND
0.02	690	220 000	198	1112	24

3.4.2.2 Preparation of nanoparticles (NPs).

The synthesis of NPs was performed according to a previously reported procedure.(Sacco, Decleva, et al., 2017) Briefly, polymers and TPP were solubilized in deionized water at a concentration equal to 0.6 mg/mL for chitosan, 1.25 mg/mL for sodium hyaluronate and 0.5 mg/mL for TPP. After complete solubilization, 150 µL of TPP solution were then added dropwise to 3 mL of

hyaluronate solution under stirring. Solutions were filtered through 0.22 μm filters (Biosigma, Italy) and stored at room temperature until use. In a 5 mL beaker 500 μL of the HA-TPP solution were added to 0.5 of chitosan solutions under stirring to allow the formation of nanoparticles with CH/HA weight ratio equal to 1:1. Solutions were kept under stirring for 10 minutes and left at rest for 20 minutes. All the relevant concentrations pertaining to the different (final) NPs components in the cases of chitosans having different values of F_A have been reported in Table 2.

Table 2. Molecular features of chitosan/hyaluronan nanoparticles (NPs). Fraction of acetylated units (F_A) of chitosan, molecular weight of the repetitive unit (MW_{ru}) of the respective molecule, concentration (mg/mL), molarity, charges, total of negative charges and ratio between positive and negative charges in NPs are reported. Adapted with permission from Furlani *et al.*(Furlani, Sacco, Decleva, et al., 2019) Copyright 2019 American Chemical Society.

F_A	**Molecule**	**MW_{ru}**	**C (mg/mL)**	**M**	**Charges (eq/L)**	**Σ negative charges**	***Posit.charges/ negat.charges***
0.02	Chitosan	197.78	0.40	2.02E-03	1.98E-03		1.84
	Hyaluronan	401.35	0.40	9.89E-04	9.89E-04	1.10E-03	
	TPP	367.86	0.00794	2.16E-05	1.08E-04		
0.16	Chitosan	198.56	0.40	2.01E-03	1.69E-03		1.54
	Hyaluronan	401.35	0.40	9.89E-04	9.89E-04	1.10E-03	
	TPP	367.86	0.00794	2.16E-05	1.08E-04		
0.25	Chitosan	200.22	0.40	2.00E-03	1.51E-03		1.40
	Hyaluronan	401.35	0.40	9.89E-04	9.89E-04	1.10E-03	
	TPP	367.86	0.00794	2.16E-05	1.08E-04		
0.46	Chitosan	200.22	0.40	2.00E-03	1.08E-03		0.98
	Hyaluronan	401.35	0.40	9.89E-04	9.89E-04	1.10E-03	
	TPP	367.86	0.00794	2.16E-05	1.08E-04		
0.63	Chitosan	201.16	0.40	1.99E-03	7.36E-04		0.67
	Hyaluronan	401.35	0.40	9.89E-04	9.89E-04	1.10E-03	
	TPP	367.86	0.00794	2.16E-05	1.08E-04		

3.4.2.3 Physical-chemical characterization of nanoparticles.

3.4.2.3.1 NPs size, surface charge and homogeneity.

Formulations were analyzed by means of Dynamic Light Scattering (DLS) on a Zetasizer Nano ZS with 173° detection optics (Malvern Instruments) to evaluate their size (hydrodynamic diameter), PolyDispersity Index (PDI) and surface charge (ζ-potential). Each formulation was analyzed using disposable cuvettes at least in triplicate at T = 25 °C after dilution 1:10 v/v in deionized filtered water. The size was expressed as the hydrodynamic diameter, obtained by a cumulative analysis of the correlation function using the viscosity and refractive index of water in the calculations. ζ-potential was determined *via* Laser Doppler velocimetry (LDV) technique.

3.4.2.3.2 Stability of nanoparticles.

The stability of NPs was evaluated by DLS using PBS as buffer.(Parajó et al., 2010) The composition of PBS is: NaCl 137 mM, KCl 2.7 mM, phosphate buffer 10 mM with final ionic strength (I) of 168 mM and pH 7.4. Simulated Body Fluid (SBF) was used as additional medium to study NPs stability. The composition of SBF was: NaCl 136.8 mM, $NaHCO_3$ 4.2 mM, KCl 3 mM, K_2HPO_4 1 mM, $MgCl_2.6H_2O$ 1.5 mM, $CaCl_2.2H_2O$ 2.5 mM, Na_2SO_4 0.5 mM, Tris-base 50 mM with final ionic strength (I) of 184 mM and pH 7.4.

Resulting formulations were analyzed in triplicate by means of DLS after dilution 1:10 v/v in the appropriate media. The considered parameters to assess the stability of NPs were: (*i*) DLS size quality report, (*ii*) size and volume distribution curves and (*iii*) PDI values.

3.4.2.3.3 Small Angle X-Ray Scattering (SAXS) measurements.

Small-Angle X-ray Scattering (SAXS) measurements were performed at the Austrian SAXS beamline of the electron storage ring ELETTRA-Sincrotrone Trieste (Amenitsch et al., 1998) using a photon energy of 8 keV and a beamsize of 0.5 × 2.5 mm. The beamline setup was adjusted to a sample to detector distance of 1.00916 m to provide an accessible q-range of 0.086-7.26 nm^{-1}. All images were recorded using the Pilatus3 1 M (Dectris, Switzerland) with at least 3 exposures of 10 s each per sample to check for radiation damage. Reference patterns to calibrate the q-scale were collected of silver-behenate (d-spacings of 5.838 nm). All measurements were performed using a custom-made flow through cell with 1.5 mm X-ray capillary (Hilgenberg, Germany). Radial averaging and image calibration were conducted using the FIT2D software.(Hammersley, Svensson, Hanfland, Fitch, & Hausermann, 1996) All presented data were corrected for fluctuations of the primary intensity and, transmission; the corresponding background has been subtracted from each solution scattering pattern. Nanoparticles composed by F_A = 0.16 and $\overline{M_v}$ = 220 000 chitosan were fabricated and diluted in deionized filtered water or PBS buffer. As reference, singular polymers (CH

and HA), after dilution in the appropriate media (water or PBS) were analyzed as well.

3.4.2.4 *In vitro* assays with macrophages.

Macrophage-like cells obtained from the differentiation of the human pro-monocytic cell line U937 (Sigma) were used as the cellular model.(Sundström & Nilsson, 1976) Undifferentiated U937 were cultured in suspension in RPMI-1640, supplemented with 10% v/v fetal bovine serum (FBS), 100 U/mL penicillin, 100 μg/mL streptomycin, and 2 mM L-glutamine in an atmosphere with 5% CO_2 at 37 °C. To induce differentiation in adherent macrophages, 150 000 cells/well in 400 μL of RPMI were plated in 24-well tissue culture plates, and 100 μL/well of PMA diluted in RPMI (15 ng/mL final concentration) were added. After three days of incubation at 37 °C, supernatants were removed and replaced with the same volume of fresh medium. Macrophages were let to restore for two days. Cell medium was then discarded, replaced with 450 μL/well of fresh medium and finally 50 μL of water (in the case of control), NPs and polymer solutions added to each well. In each experiment, macrophages exposed to 1 ng/mL LPS were considered as positive controls. After three hours of incubation, supernatants were recovered and centrifuged at 13 000 x *g* for 10 min to remove any cellular debris.

NPs used in these experiments were prepared using sterile glassware and instruments. All solutions were prepared using water for injection (Eurospital SpA-Trieste). Solutions were further sterilized by filtration using filters with a pore diameter equal to 0.22 μm.

3.4.2.4.1 Viability test.

The viability of differentiated adherent U937 macrophages was assessed using the Neutral red assay.(Repetto, del Peso, & Zurita, 2008) Briefly, neutral red powder was dissolved in water (5 mg/mL final concentration), centrifuged at 16 000 x *g* for 10 min to remove any insoluble residue, and stored in dark conditions until use. Neutral red was diluted in "warm" PBS (37 °C) to obtain a final concentration of 100 μg/mL. 400 μL of the dye were added to each well. The plate was incubated at 37 °C for 20-30 min, then the dye was removed; each well was washed once with 500 μL of warm PBS and 400 μL of a 50% v/v ethanol/water *plus* 1% v/v acetic acid solution were then added to each well. Finally, a 150 μL-volume was transferred from each well into a 96 multi-well plate and the absorbance measured at 540 nm using a plate reader spectrophotometer (Infinite 200Pro NanoQuant, Tecan Trading AG, Switzerland).

3.4.2.4.2 Cytokine production.

ELISA tests (Invitrogen Corporation, Thermo Fischer, USA) were carried out according to manufacturer's protocol for the quantification of TNF-α (tumor necrosis factor-α) secreted by U937 macrophages upon NPs treatment.

3.4.2.4.3 Membrane association and internalization.

To evaluate membrane association and cellular internalization of the NPs, fluoresceinamine isomer I-labeled-HA was used for the synthesis of NPs. HA was labeled according to a procedure reported elsewhere.(Sacco, Decleva, et al., 2017) The association of fluorescence-labeled NPs with macrophage membrane and their internalization were determined by means of flow cytometry according to the method described by Busetto *et al.*,(Busetto, Trevisan, Patriarca, & Menegazzi, 2004) with minor modifications. Cells were differentiated as described in paragraph 2.4. and, after 3 or 24 h of incubation with the NPs, the supernatants were discarded and the cells washed with PBS. Cells were then gently scraped using a plastic spatula, re-suspended in ice-cold PBS supplemented with $CaCl_2$ 1 mM and centrifuged for 5 min at 125 x *g*. Supernatants were discarded and pellets re-suspended in ice-cold PBS supplemented with $CaCl_2$ 1 mM, yielding a final concentration of 2 x 10_6 cells/mL. Cells were put on ice prior analyses. Flow cytometry was performed with a FACSCalibur (BectonDickinson) equipped with an air-cooled 15 mW argon-ion laser, operating at 488 nm. Immediately before the analysis, 250 µL of each sample were diluted with an equal volume of ice-cold 0.1 M citrate buffer, pH 4. Control cells were analyzed as they were to determine the autofluorescence, and after addition of 50 µL of NPs to determine NPs association. To distinguish between cell association and internalization, each sample was analyzed after 1 min from the addition of TB (75 µg/mL final concentration). Fluoresceinamine isomer I fluorescence (FL1, green) was collected using a 530 (± 30) nm bandpass filter, instead red fluorescence emitted after quenching by TB (FL3) was collected by using a 650 (± 13) nm bandpass filter. Data were collected using a linear amplification for FSC and SSC, and a logarithmic amplification for FL1 and FL3. For each sample 10 000 events were collected and analyzed using the CellQuest software from Becton Dickinson. Macrophages population was identified by combined measurement of FSC and SSC and gated in R1 region. The percentage distribution of macrophage subsets was calculated from dot plot analyses (FL-1 *vs.* FL-3) of R1-gated events.

3.4.2.5 *In Vitro* Assays with Neutrophils.

3.4.2.5.1 Neutrophil Isolation.

Institutional ethics committee approval was obtained and written informed consent was signed by healthy volunteers from which venous blood was withdrawn. Neutrophils were isolated by a discontinuous Percoll gradient centrifugation, as previously described,(Menegazzi, Busetto, Dri, Cramer, & Patriarca, 1996) and suspended in PBS solution, pH 7.4, containing 5 mM glucose and 0.2% w/v BSA (PBS-BSA).

3.4.2.5.2 Preparation of FBG-Coated Surfaces.

Flat-bottom poly(styrene) wells (F16 MaxiSorp Nunc-Immuno Modules or F16 Black MaxiSorp Fluoronunc Cert, Thermo Fisher Scientific, Roskilde, Denmark) were coated with FBG as described elsewhere.(Dri, Cramer, Spessotto, Romano, & Patriarca, 1991) Briefly, 50 µL of FBG solution (400 µg/mL in PBS) were put in each well, and the plate was left at 37 °C for 1-2 h in a humidified chamber. Just before use, the wells were rinsed three times with PBS.

3.4.2.5.3 Evaluation of H_2O_2 production.

Neutrophils H_2O_2 generation was assessed using the conversion of non-fluorescent DHR into fluorescent rhodamine-123 in the presence of HRP.(Henderson & Chappell, 1993; Mauch et al., 2007; Rinaldi, Moroni, Paape, & Bannerman, 2007) Neutrophils (1.25×10^6 cells/mL in PBS-BSA) were incubated with 40 µM DHR for 30 min at 37 °C in a shaking water bath, in the dark. Five to ten min before starting the assay, the cell suspension was supplemented with 1 mM $CaCl_2$ and 1 mM $MgCl_2$. Then, 60 µL aliquots of this suspension were dispensed into FBG-coated black wells containing or not the NPs (chitosan with F_A = 0.16, 80 µg/mL final concentration), and HRP (1 µg/mL final concentration), in a total volume of 0.15 mL PBS-BSA supplemented with 1 mM $CaCl_2$ and 1 mM $MgCl_2$ (Ca^{2+}/Mg^{2+} PBS-BSA). The plate was incubated at 37 °C in the dark and at the desired times readings were taken with a microplate fluorescence reader (Tecan Infinite F200; Tecan Austria GmbH, Grödig, Austria) at 485 nm (λ_{ex}) and 535 nm (λ_{em}).

3.4.2.5.4 Evaluation of granular component release.

The effect of NPs on neutrophil degranulation was assayed following the release of myeloperoxidase (MPO), a widely used marker of neutrophil primary granules.(Bainton, 1973; Ferrante, Nandoskar, Walz, Goh, & Kowanko, 1988; Menegazzi, Zabucchi, Knowles, Cramer, & Patriarca, 1992) Neutrophils (1.0×10^6 cells/mL in PBS-BSA) were pre-warmed in suspension for 10 min at 37 °C. Five min before starting the assay, the cell suspension was supplemented with 1 mM $CaCl_2$ and 1 mM $MgCl_2$. Then, 150 µL aliquots of this suspension were dispensed into quadruplicate FBG-coated wells containing or not the NPs (chitosan with F_A = 0.16, 80 µg/mL final concentration) in a total volume of 200 µL. After 60 or 90 min of incubation at 37 °C, the plates were centrifuged at 200 x *g* and the supernatants were collected. As a positive control, the MPO released in the supernatant of neutrophils stimulated with the known secretagogue N-Formyl-L-methionyl-L-leucyl-L-phenylalanine (fMLP) (Sigma-Aldrich) in the presence of cytochalasin D (Sigma-Aldrich) (final concentrations, 5 x 10^{-7} M and 2.5 µg/mL, respectively) was assayed in a separate plate after 20 min of incubation at 37 °C. Released MPO was measured by using 3,3,5,5-tetramethylbenzidine (TMB) (Sigma-Aldrich) as substrate following the method described by Menegazzi *et al.* with some

modifications.(Menegazzi et al., 1992) Briefly, 75 µL of 20 mM acetate buffer (pH 5.5) containing 2 mM TMB and 0.1% (w/v) cetyltrimethylammonium bromide (Sigma-Aldrich) were deposited into wells of a separate plate. Then, 75 µL of either supernatant fluid or 20-fold diluted neutrophil lysate were added to each well. The peroxidatic reaction was started with H_2O_2 (0.3 mM final concentration) and blocked after 3-5 min with 100 µL of 2 N H_2SO_4. Absorbance was then read at 405 nm. The amount of released MPO was expressed as percentage of the total MPO activity as measured in neutrophil lysates.

3.4.2.5.5 Measurement of neutrophil adhesion.

The number of neutrophils adherent to FBG was assessed by quantifying myeloperoxidase (MPO) activity as described in the paper by Menegazzi *et al.*(Menegazzi et al., 1996) Adhesion tests were conducted in FBG-coated transparent wells to monitor cell morphology by light microscopy. They were run in parallel to those evaluating H_2O_2 production, and in the same experimental conditions except for the omission of DHR and HRP.

3.4.2.6 Evaluation of NPs muco-adhesiveness.

The muco-adhesive properties of NPs were evaluated *in vitro* by assessing the interaction between NPs and mucin.(Yin et al., 2009) Mucin was purified *via* dialysis against deionized water prior to use. The solution was thereafter filtered through 8 µm Millipore filters and freeze-dried. Freeze-dried mucin was solubilized in deionized water at 2 mg/mL prior to use. NPs (80 µg/mL final concentration) were added (1:10 v/v, 1 mL final volume) to solutions of mucin at different concentrations (0.1, 0.2, and 0.5 mg/mL). Resulting mixtures, which had a final pH ~ 5.5, were re-suspended under vigorous stirring and analyzed by DLS. The change in NPs size distribution was used as a parameter to evaluate aggregation phenomena.

3.4.2.7 Evaluation of NPs as drug delivery system.

3.4.2.7.1 Encapsulation of a model molecule and anti-inflammatory drugs.

Best performing NPs were used to encapsulate a model molecule, *i.e.* fluorescinamine isomer I, a molecule able to simulate a drug, and two anti-inflammatory drugs, *i.e.* dexamethasone and aceclofenac.

Fluorescinamine isomer I was selected as model molecule to study the ability of formulations to encapsulate payloads. This fluorophore was solubilized in methanol (5 mg/mL final concentration), and used to prepare serial dilutions using water as solvent. The linear range of fluorescence intensity *vs.* concentration (buffer without fluorophore was used as blank) was recorded using a BMG LABTECH 96 spectrofluorometer, with λ_{ex} = 485 nm and λ_{em} = 520 nm. 100 µL of fluorophore were

added to 1 mL of chitosan under stirring. As the control, the same volume of water was added to chitosan. Solutions were left five minutes under stirring and finally HA-TPP mixture was added. Resulting mixtures were kept under stirring for 10 minutes.

Centrifugation was used for the determination of encapsulation efficiency. 1.5 mL of each formulation were placed in 1.5 mL Eppendorf tubes and centrifuged at 12 000 x *g* for 1 h. At the end of centrifugation, supernatants were collected and analyzed using the same parameters above described. Supernatants derived from samples without the fluorophore were used as blank. Calibration curve (with $R^2 > 0.99$) was exploited to determine the fluorophore concentration in the supernatants. Encapsulation efficiency (%) was determined using the following formula (eq. 16):

$$EE = \frac{C_i - C_x}{C_i} \times 100 \text{ (eq. 16)}$$

where C_i corresponds to the initial concentration of the fluorophore, C_x is the fluorophore concentration in the supernatant after sample centrifugation.(H. Li et al., 2009)

Dexamethasone and aceclofenac were selected as anti-inflammatory drugs to study the ability of NPs to encapsulate commonly used drugs. These drugs were respectively solubilized in methanol and dimethyl sulfoxide (final concentration equal to 2 mM), and used to prepare serial dilutions using water as solvent. The linear range of absorbance *vs.* concentration (water was used as blank) was recorded using an Amersham Biosciences UV−vis spectrometer Ultraspec 2100 pro. by using quarts cuvettes with λ = 242 nm for dexamethasone and λ = 274 nm for aceclofenac. 100 µL of drugs were added to 1 mL of chitosan under stirring. As the control, the same volume of water was added to chitosan. Solutions were left five minutes under stirring and finally HA-TPP mixture was added. Resulting mixtures were kept under stirring for 10 minutes.

Centrifugation was used for the determination of encapsulation efficiency. 1.5 mL of each formulation were placed in 1.5 mL Eppendorf tubes and centrifuged at 12 000 x *g* for 1 h. At the end of centrifugation, supernatants were collected and analyzed using the same parameters above described. Supernatants derived from samples without the drug were used as blank. Calibration curve (with $R^2 > 0.99$) was exploited to determine the drug concentration in the supernatants. Encapsulation efficiency (%) was determined according to eq. 16.

3.4.2.7.2 Investigation of NPs precipitation efficiency.

Turbidimetric analyses by DLS after centrifugation were used to evaluate the precipitation efficiency (*i.e.* the percentage of NPs in the pellet after centrifugation) of NPs. 1.5 mL of each formulation were placed in 1.5 mL Eppendorf tubes and were centrifugated for different timeframes,

i.e. 15 – 60 minutes, and at different speed, *i.e.* 2 000 – 12 000 g, in order to separate NPs from free drugs (or free model molecules). Then 1 mL of each samples were placed in disposable cuvettes and the relative scattering intensity (*i.e.* derived count rate) was analyzed by Dynamic Light Scattering (DLS). A calibration curve scattering intensity *vs.* NPs concentration (with $R^2 > 0.99$) was plotted by analyzing non-centrifugated formulations at different concentration (after dilution in water). The precipitation efficiency was determined by exploiting the calibration curve.

3.4.2.7.3 Preparation of nanocomposite networks for drug delivery purposes.

Nanoparticles encapsulating payloads were embedded in CTL-based networks in order to evaluate the possibility to use nanocomposite networks for drug delivery purposes. CTL-based networks were prepared according to chapter 3.2.2.4 with slight modifications. A network consisting of [CTL] = 10 g/L, [B] = 8 mM and [M] = 16 mM (PBS 1X as solvent, pH 7.4) was used for this purpose. Briefly, 500 µL of NPs encapsulating aceclofenac were added to 4 mL of CTL solution ([CTL] = 10 g/L, PBS 1X as solvent, pH 7.4) and resulting sample was mechanically stirred for a few seconds. Then 500 µL of a mixture of boric acid and mannitol ([B] = 80 mM and [M] = 160 mM, PBS 1X as solvent, pH 7.4) were injected in the NPs-CTL mixture and the resulting sample was stirred for a few seconds. The final concentration of aceclofenac in the resulting mixture was equal to 44.3 µg/mL.

3.4.2.7.3.1 Drug release from nanocomposite networks.

Dialysis was exploited as technique to evaluate drug release from nanocomposite network. 1 mL of nanocomposite network was transferred in a dialysis tube (average flat width 25 mm, cutoff 12 000; Sigma Aldrich, Chemical Co., U.S.A.). Dialysis tube was sealed and put in a 50 mL Falcon tube containing 20 mL of PBS 1X. Falcon tube was transferred in a thermostatic bath at 37 °C under shaking. At selected timeframes (1 and 4 hours, 1, 3, 12 and 40 days) dialysis media was collected and analyzed (in quartz cuvettes) by UV-Vis spectroscopy (λ = 274 nm) in order to detect the cumulative release of aceclofenac. Each analysis was performed at least in triplicate. The cumulative release of aceclofenac was determined exploiting the calibration curve. After analysis, release media was transferred again in the falcon tube.

3.4.2.8 Statistical analysis.

Statistical analysis was performed using the unpaired Student's *t*-test, using GraphPad Prism 7.0 (GraphPad Software, San Diego, CA). *p*-values less than 0.05 were considered statistically significant.

3.4.3 Results and discussion

3.4.3.1 Physical-chemical characterization of nanoparticles (NPs) and stability studies

The influence of chitosan molecular properties, *i.e.* FA and molecular weight, on physical properties of nanoparticles (*i.e.* size, polydispersity, surface charge and porosity) was investigated by Dynamic Light Scattering (DLS) and Small Angle X-ray Scattering (SAXS) analyses.

3.4.3.1.1 Effect of molecular properties of chitosan on nanoparticles formation and physical properties

Table 3. Characterization of CH/HA nanoparticles after dilution 1:10 (v/v) in water. Nanoparticles were fabricated using chitosans at different fraction of acetylated units (FA) and viscosity average molecular weight ($\overline{M_v}$). Hydrodynamic diameter, aggregation at time zero, polydispersity index (PDI) and surface charge, *i.e.* ζ-potential, (all of them ±SD) of the resulting formulations are reported. ND: non determined. Adapted with permission from Furlani *et al.*(Furlani, Sacco, Decleva, et al., 2019) Copyright 2019 American Chemical Society.

FA	$\overline{M_v}$	pH	hydrodynamic diameter (nm)	PDI	ζ-potential (mV)	Notes
0.02	220 000	4.6	513 ± 13	0.24 ± 0.02	37 ± 5	no aggregation
0.16	30 000	ND	180 ± 1	0.12 ± 0.01	29 ± 2	no aggregation
	220 000	5.6	200 ± 4	0.21 ± 0.01	32 ± 1	no aggregation
	340 000	ND	215 ± 3	0.21 ± 0.01	37 ± 1	no aggregation
0.25	190 000	5.8	348 ± 11	0.24 ± 0.02	27 ± 4	no aggregation
0.46	100 000	ND	254 ± 27	0.20 ± 0.07	-19 ± 2	no aggregation
	210 000	6.0	219 ± 4	0.20 ± 0.01	-14 ± 1	limited aggregation
	300 000	ND	253 ± 6	0.18 ± 0.16	-28 ± 3	no aggregation
0.63	90 000	ND	227 ± 1	0.17 ± 0.02	-28 ± 2	no aggregation
	170 000	6.3	238 ± 1	0.19 ± 0.02	-25 ± 3	no aggregation
	310 000	ND	253 ± 3	0.20 ± 0.03	-23 ± 1	limited aggregation

A large library of NPs formulations was prepared by exploiting complex coacervation between hyaluronan, in the presence of TPP, and chitosans with molecular weights in the range 30 000 -

340 000. Physical properties (*i.e.* size, polydispersity and surface charge) of resulting formulations were at first investigated by DLS analyses in water. In general term, whatever the FA, all formulations displayed good homogeneity showing PDI ≤ 0.24, in line with similar NPs.(Almalik, Day, et al., 2013; de la Fuente et al., 2008a) More in detail, formulations fabricated with medium molecular weights chitosans (*i.e.* ~ 200 000) showed good homogeneity (PDI ~ 0.2), with hydrodynamic diameters around 200 nm for NPs prepared with chitosans with FA = 0.16, 0.46 and 0.63. Conversely, NPs fabricated with chitosans with FA = 0.02 and 0.25 displayed larger dimensions. Some visible aggregates were detected only in the case of NPs synthetized with chitosans with FA = 0.46, $\overline{M_v}$ = 210 000 and FA = 0.63, $\overline{M_v}$ = 310 000 (Table 3).

In the case of FA = 0.16 and FA = 0.63 chitosans, a linear dependence of the hydrodynamic diameter on the degree of polymerization, $\overline{DP_v}$, was detected (Figure 43a and 43c). These results are in line with findings of Wu and Delair.(Wu & Delair, 2015) On the other hand, in the case of FA = 0.46 chitosans, no correlation between hydrodynamic diameter and $\overline{DP_v}$ was detected (Figure 43b); this finding could be due to the presence of large aggregates for the medium molecular weight chitosan ($\overline{DP_v}$ = 1050) and to the high experimental data dispersion.

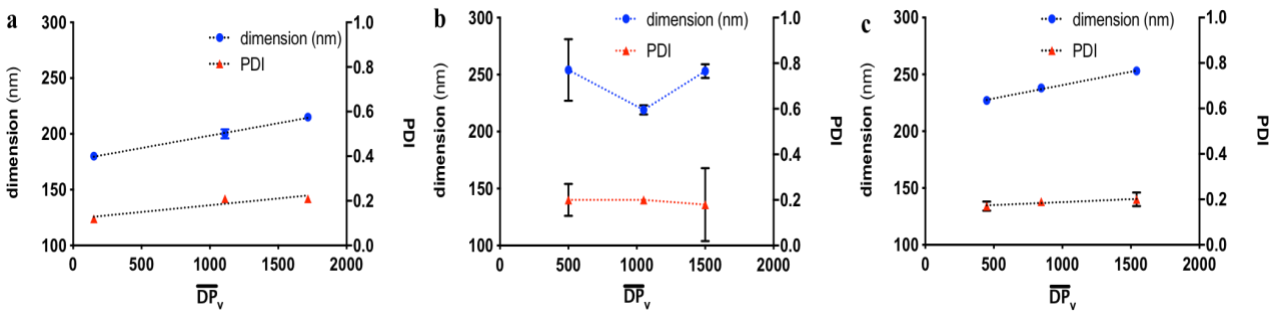

Figure 43. Dependence of nanoparticles hydrodynamic diameter and polydispersity index (PDI) on chitosan degree of polymerization ($\overline{DP_v}$) for formulations at different fraction of acetylated units, *i.e.* FA = 0.16 **(a)**, FA = 0.46 **(b)** and FA = 0.63 **(c)**. Dotted lines are drawn to guide the eye.

Surface charge of NPs was strictly dependent on FA of chitosans. More in detail, a negative surface was detected both for NPs made of chitosan with FA = 0.46 and for chitosan with FA = 0.63 (Figure 44). On the other hand, a positive surface charge was observed for NPs fabricated with chitosan with FA = 0.02, 0.16 and 0.25. Given the constant amount of TPP and HA in the different NPs, this behavior depends on the molecular properties of chitosans, since the lower the value of FA, the higher the (positive) polymer charge density. Similar results were reported by Goycoolea and collaborators.(Goycoolea et al., 2016)

This finding indicate that chitosan with higher molecular weight is more prone to be present at NPs surface than to the core. A similar linear trend was detected for NPs fabricated with F_A = 0.63 chitosans. Conversely, no correlation between ζ-potential on $\overline{DP_v}$ was observed F_A = 0.46 chitosans, likely ascribed to the presence of large aggregates.

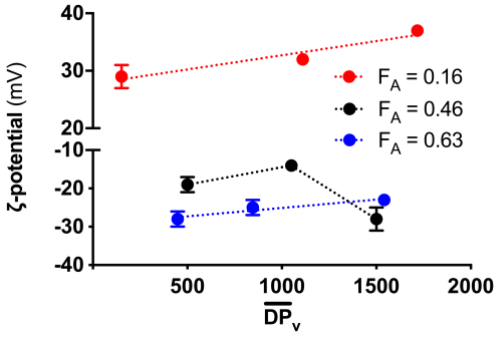

Figure 44. Dependence of nanoparticles surface charge (ζ-potential) on chitosan degree of polymerization ($\overline{DP_v}$) for formulations at different fraction of acetylated units, F_A: F_A = 0.16, F_A = 0.46 and F_A = 0.63. Dotted lines are drawn to guide the eye.

3.4.3.1.2 Stability of nanoparticles as function of chitosan molecular properties

Nanoparticles stability was then evaluated by DLS after dilution in PBS buffer, characterized by an ionic strength of 168 mM, [phosphate] = 10 mM and pH = 7.4. All NPs fabricated with F_A = 0.46 and F_A = 0.63 chitosans were not stable upon dilution in PBS (Table 4). More in detail, NPs displayed high dimensional heterogeneity (PDI $\geq$ 0.3) and with dissolution and/or aggregation phenomena.

Taking into account NPs formed of F_A = 0.16 chitosans, only the formulation fabricated with medium molecular weight chitosan, *i.e.* $\overline{M_v}$ = 220 000, resulted stable in PBS. These NPs displayed a single narrow monomodal size distribution curve, albeit shifted toward larger size than that in water, and a PDI value ~ 0.1 (red curve of Figure 46a and Table 3), *i.e.* even smaller than that in water (blue curve of Figure 45b, Figure 46a and Table 4). Such low values of PDI (and thus high dimensional homogeneity) are difficult to observe in most of the polysaccharide-based NPs; indeed, the PDI values of chitosan/hyaluronan NPs are usually higher than 0.2.(Almalik, Day, et al., 2013; Almalik, Karimi, et al., 2013; de la Fuente et al., 2008b; Parajó et al., 2010) The dimensional shift is in line with that reported in literature for similar NPs based on chitosan.(de la Fuente et al., 2008a; López-león, Carvalho, Seijo, Ortega-vinuesa, & Bastos-gonzález, 2005; Oyarzun-Ampuero et al., 2009; Parajó et al., 2010) Conversely, Tirelli and collaborators reported only a limited increase in size in PBS buffer for CH/HA nanoparticles formed by using similar polymers.(Deng et al., 2014)

Table 4. Characterization of CH/HA nanoparticles after dilution 1:10 (v/v) in PBS buffer. Nanoparticles were fabricated using chitosans at different fraction of acetylated units (F_A) and different viscosimetric molecular weight ($\overline{M_v}$). pH, hydrodynamic diameter, aggregation at time zero and polydispersity index (PDI), (all of them ±SD) of the resulting formulations are reported. (*) stands for formulations where significant signal errors in the size quality report were detected by DLS analyses; (§) stands for formulations with visible flocculated suspensions after 24 h of incubation. Adapted with permission from Furlani *et al.*(Furlani, Sacco, Decleva, et al., 2019) Copyright 2019 American Chemical Society.

F_A	$\overline{M_v}$	hydrodynamic diameter (nm)	PDI	Notes
0.02	220 000	[1797 ± 840] (*,§)	[0.17 ± 0.12] (*,§)	unstable
0.16	30 000	[270 ± 42] (*)	[0.40 ± 0.03] (*)	unstable
	220 000	773 ± 21	0.08 ± 0.07	stable
	340 000	[1307 ± 461] (*)	[0.35 ± 0.36] (*)	unstable
0.25	190 000	[1666 ± 357] (*)	[0.78 ± 0.39] (*)	unstable
0.46	100 000	[194 ± 38] (*)	[0.49 ± 0.23] (*)	unstable
	210 000	[982 ± 743] (*)	[0.76 ± 0.28] (*)	unstable
	300 000	[213 ± 49] (*)	[0.32 ± 0.06] (*)	unstable
0.63	90 000	[1060 ± 823] (*)	[0.82 ± 0.20] (*)	unstable
	170 000	[1037 ± 21] (*)	[0.38 ± 0.04] (*)	unstable
	310 000	[103 ± 24] (*)	[0.66 ± 0.02] (*)	unstable

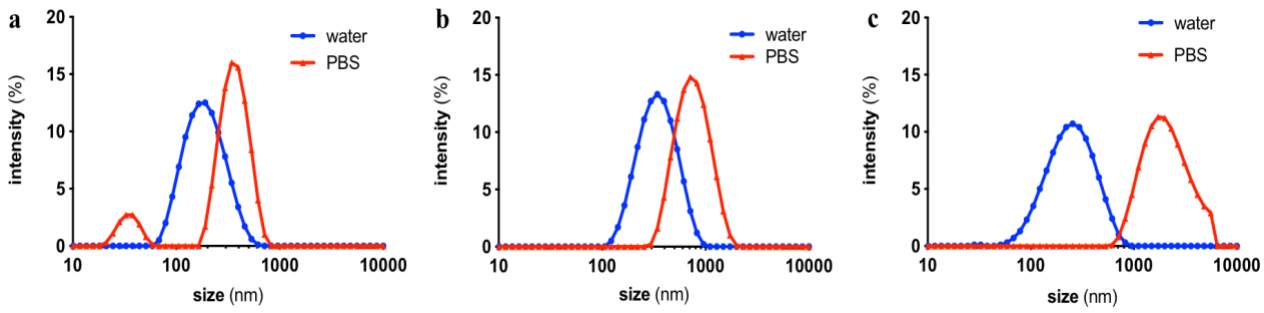

Figure 45. DLS intensity size distribution curves of nanoparticles composed by F_A = 0.16 chitosans at different molecular weight: $\overline{M_v}$ = 30 000 **(a)**, 220 000 **(b)** and 340 000 **(c)**. Nanoparticles were diluted 1:10 (v/v) in two different media prior measurements, namely deionized water and PBS (Phosphate Buffered Saline).

On the other hand, by using higher and lower chitosan molecular weight, a marked instability was detected. For NPs with chitosan the lowest molecular weight (*i.e.* $\overline{M_v}$ = 30 000), a second peak appeared at lower size, suggesting dissolution (Figure 45a). Conversely, for NPs with the highest molecular weight (*i.e.* $\overline{M_v}$ = 340 000), a second peak appeared at larger size, suggesting aggregation (Figure 45c). Similar phenomena, with broadening of dimensions and heterogeneity of the system, were detected by using a constant molecular weight, *i.e.* ~ 220 000, but different fraction of acetylation (Figure 46b and 46c).

These findings suggest a correlation between chitosan molecular properties and NPs stability. More in detail, a limited acetylation, *i.e.* F_A ~ 16%, together with a medium molecular weight chitosan, *i.e.* $\overline{M_v}$ ~ 220 000, seem able to promote formation of NPs, in combination with HA and TPP, stable in physiological-mimicking conditions without dissolution or severe aggregation. Other molecular properties of chitosan seem detrimental for NPs stability, leading to the limit (or just beyond it) of the possibility of still describing those systems as homogeneous samples of spheroidal NPs.

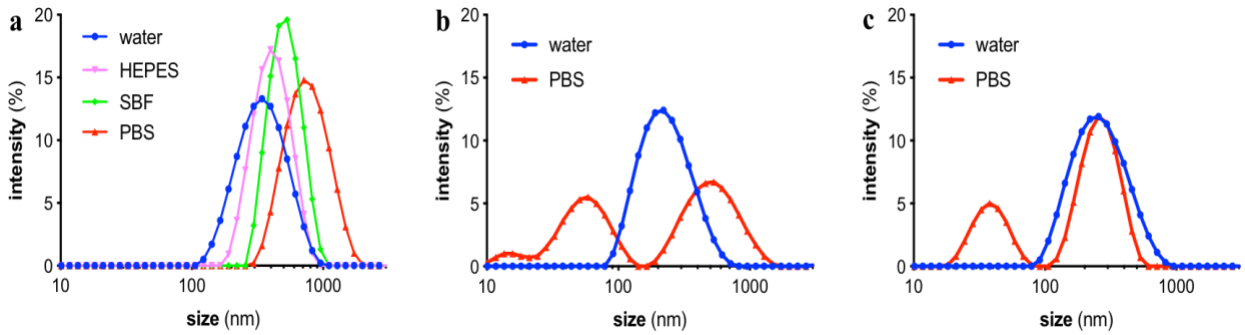

Figure 46. (a) Intensity size distribution of NPs synthetized using chitosan with F_A = 0.16 and CH/HA 1:1 w/w after dilution 1:10 (v/v) at pH 5.6 (in water, blue curve), and at pH = 7.4 and I = 0.160 M in HEPES (violet curve), 0.168 M in PBS (red curve) and 0.184 M in SBF (Simulated Body Fluid) (green curve), respectively. **(b)** Intensity size distribution of NPs synthetized using chitosan with F_A = 0.46 and CH/HA 1:1 w/w after dilution 1:10 (v/v) at pH = 6.0 (in water, blue curve) and at pH = 7.4 and I = 0.168 M (in PBS, red curve). **(c)** Intensity size distribution of NPs synthetized using chitosan with F_A = 0.63 and CH/HA 1:1 w/w after dilution 1:10 (v/v) at pH = 6.0 (in water) and at pH = 7.4 and I = 0.168 M (in PBS). Adapted with permission from Furlani *et al.*(Furlani, Sacco, Decleva, et al., 2019) Copyright 2019 American Chemical Society.

3.4.3.1.3 DLS characterization of NPs as a function of various physical-chemical parameters

Stability studies were deepened on the only case resistant to physiological pH and ionic strength, namely that of NPs prepared with chitosan with F_A = 0.16 and $\overline{M_v}$ = 220 000, in order to assess the role of different conditions on NPs stability. More in detail, the influence of pH, ionic

strength and phosphate concentration was investigated.

At constant pH (water and HEPES/NaCl at pH 5.6), the increase in ionic strength promoted a limited dimensional shift (Table 5). A limited increase of size was detected at physiological ionic strength and by increasing pH (HEPES/NaCl at pH 5.6 and 7.4). It stems from the partial screening of the attractive interactions between oppositely charged chitosan and hyaluronan. Conversely, by using a constant pH and similar ionic strength (HEPES/NaCl pH 7.4, SBF and PBS), a marked dimensional shift, proportional to phosphate concentration, was detected (Figure 46a and Table 5). Thus, the marked increase in dimension detected in PBS was mainly attributed to the presence of phosphate. Indeed, the negatively charged phosphate ions are able to bind chitosan with high affinity. The binding of phosphate can thus promote NPs swelling. It is conceivable that the cross-link elements holding together the NPs are of two types: (*i*) interpolyelectrolyte interactions between chitosan and hyaluronan and (*ii*) point interactions between TPP and chitosan.

Table 5. Characterization of CH/HA nanoparticles prepared using chitosan with F_A = 0.16, M_v = 220 000 and CH/HA 1:1 w/w after dilution 1:10 (v/v) at different values of pH, ionic strength and phosphate concentration; hydrodynamic diameter and polydispersity index (PDI) of resulting formulations are reported. Adapted with permission from Furlani *et al.*(Furlani, Sacco, Decleva, et al., 2019) Copyright 2019 American Chemical Society.

Solvent	pH	Ionic strength (mM)	[phosphate] (mM)	Hydrodynamic diameter (nm)	PDI
Water	5.6	~ 1	0	207 ± 12	0.21 ± 0.01
HEPES/NaCl	5.6	160	0	321 ± 6	0.21 ± 0.01
HEPES/NaCl	7.4	160	0	384 ± 18	0.28 ± 0.05
SBF	7.4	184	1	569 ± 18	0.11 ± 0.02
PBS	7.4	168	10	786 ± 26	0.07 ± 0.06

Furthermore, these NPs were able to maintain good features after storage at physiological temperature, *i.e.* 37°C (Figure 47a); a limited reduction of dimensions was detected after 3 months, but NPs maintained a good homogeneity, confirming the possibility to store (and to use) them also for long timeframes.

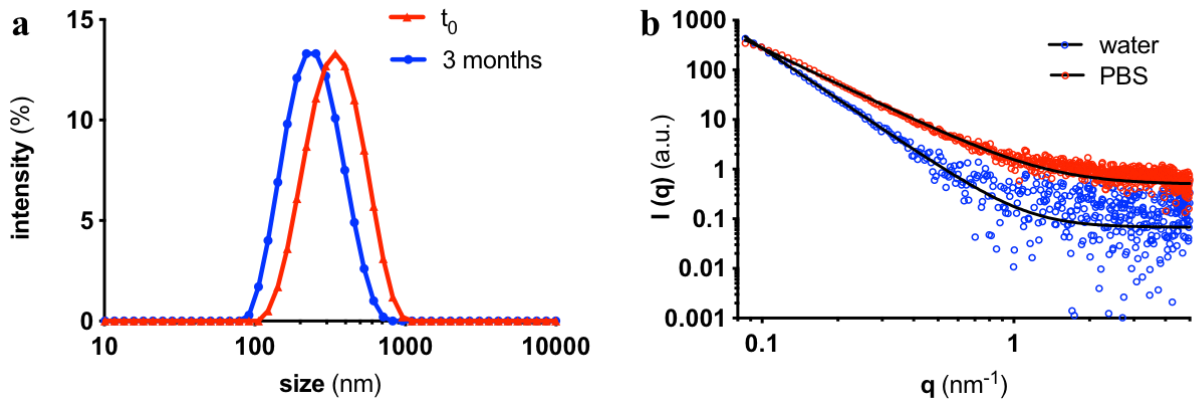

Figure 47. (a) DLS intensity size distribution curves of nanoparticles composed by F_A = 0.16, $\overline{M_v}$ = 220 000 chitosans at 37°C after 3 months. **(b)** SAXS pattern profiles of nanoparticles composed by F_A = 0.16 and $\overline{M_v}$ = 220 000 chitosan. Nanoparticles are dispersed in deionized water and PBS. The final medium composition is the following: 90% v/v nanoparticles in deionized water + 10% v/v water or 10X PBS. Black solid lines represent the best fit of experimental data according to eq. 14.

3.4.3.1.4 SAXS characterization

Small-Angle X-ray Scattering (SAXS) analyses were then performed to evaluate macromolecular rearrangement upon dilution in PBS. Scattering profiles in both water and PBS did not show any polyelectrolyte peak in the high *q* range (Figure 47b), as previously reported by Delair and co-workers.(Crépet et al., 2016) Experimental data were nicely fitted according to a generalized Porod law by using eq. 14:

$$I(q) = k + {c_p}/{q^\alpha} \quad \text{(eq. 14)}$$

where *I(q)* represents the scattering intensity, *q* is the scattering vector, *k* is a constant, c_p is a pre-factor and α is the Porod exponent, indicating structure compactness. More in detail, a Porod exponent of 4 indicates a compact structure, whereas an exponent between 3 and 4 indicates a porous structure.(Beaucage, 1996; Tallian et al., 2018) SAXS profiles for single NPs components showed a Porod exponent of 1.3 - 2, suggesting a rod-like structure, typical of long polymer chains.(Ben Messaoud et al., 2018) For NPs in water the Porod exponent was equal to 3.4, whereas in PBS was equal to 2.4. The decrease in the Porod exponent suggest a macromolecular reorganization, with enlargement of polymer mesh due to swelling after dilution in PBS.

3.4.3.2 Biological characterization

The influence of physical properties of nanoparticles (*i.e.* size, polydispersity, surface charge and porosity) on innate immune system cells was then investigated. Nanoparticles (and their singular

components) formed using chitosans with different F_A, with M_v ~ 220 000 and CH/HA 1:1 w/w, were used for such characterization.

3.4.3.2.1 Effect of NPs on macrophage viability

Neutral Red assay was performed to investigate the biocompatibility of NPs toward cultured human macrophages. No significant difference in cell viability of NPs treated cells was detected (Figure 48). The biocompatibility of NPs is in line with data reported by other authors which used polymers with similar molecular properties (*i.e.* degree of acetylation and/or molecular weight).(Almalik, Day, et al., 2013; de la Fuente et al., 2008a, 2008c; Parajó et al., 2010; Rios de la Rosa, Tirella, Gennari, Stratford, & Tirelli, 2017) Furthermore, all NPs components tested separately (*i.e.* CH and HA/TPP) were biocompatible (data not shown).

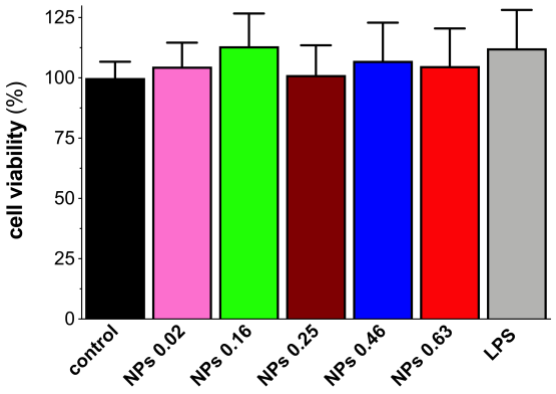

Figure 48. Neutral Red assay (cell viability, %) on U937 cells after 3 h of incubation as function of the respective treatment (NPs synthetized with chitosans at different F_A). Final concentrations were 80 μg/mL for NPs, and 1 ng/mL for LPS). Error bars indicate the standard deviation (SD) of at least 4 measurements. Reprinted with permission from Furlani *et al.*(Furlani, Sacco, Decleva, et al., 2019) Copyright 2019 American Chemical Society.

3.4.3.2.2 Effect of NPs on TNF-α production by macrophages

To evaluate the influence of NPs and of their components on the production of pro-inflammatory cytokines by human macrophages, the release of TNF-α by macrophages was quantified after 3 h of incubation. Macrophages displayed a low basal level of TNF-α production (black column of Figure 49) that significantly increased in the presence of LPS (grey column of Figure 49). HA/TPP and chitosans with F_A = 0.02 and 0.25 mildly elicited TNF-α production, whereas other chitosans with different F_A did not significantly affect the TNF-α production (Figure 49a). This effect can be explained for F_A = 0.25 chitosan by the limited presence of endotoxins (Table

1), whereas for F_A = 0.02 chitosan by a physical effect since this type of chitosan is insoluble at physiological pH and tends to precipitate. By taking into account cell response to NPs, only those made of F_A = 0.16 chitosan did not elicit TNF-α production both in basal (Figure 49b) and in LPS-stimulated conditions (Figure 50). Conversely, NPs synthetized with other chitosans significantly stimulated the production of TNF-α.

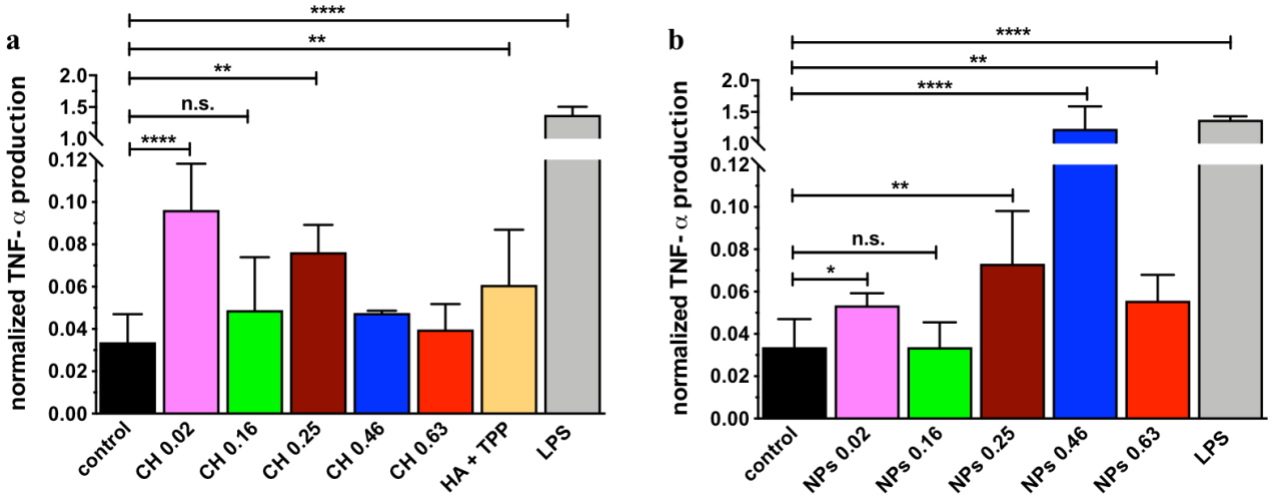

Figure 49. (a, b) TNF-α production by U937 macrophages treated with the indicated substances (final concentrations were 80 μg/mL for NPs, 40 μg/mL for CH and HA and 1 ng/mL for LPS) for 3 h. All NPs (and CH) were from chitosans with M_v ~ 220 000 and CH/HA 1:1 w/w. Results were normalized for the number of viable cells. Data are means (±SD) of 3 to 10 measurements. Student's *t*-test: n.s., not significant; *, $p < 0.05$; **, $p < 0.01$; ****, $p < 0.0005$. Adapted with permission from Furlani *et al.*(Furlani, Sacco, Decleva, et al., 2019) Copyright 2019 American Chemical Society.

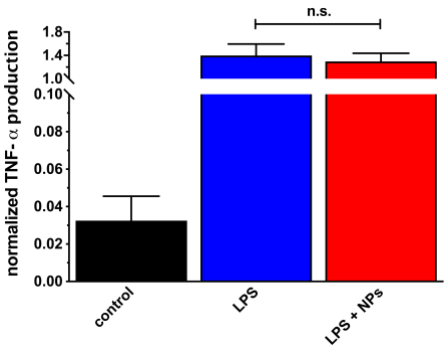

Figure 50. TNF-α production normalized for viable cell number by macrophages (U937 cells) treated for 3 h with LPS or LPS in combination with NPs (chitosan with F_A = 0.16, M_v = 220 000 and CH/HA 1:1 w/w). Error bars indicate standard deviation (SD) of two measurements. Student's *t*-test: n.s., not significant. Reprinted with permission from Furlani *et al.*(Furlani, Sacco, Decleva, et al., 2019) Copyright 2019 American Chemical Society.

By taking into account the above reported stability investigations, the production of TNF-α of NPs fabricated with chitosans with F_A = 0.02, 0.25, 0.46 and 0.63 can be traced back to their physical structure and partial instability. This proof is supported by the pro-inflammatory activity of singular HA/TPP mixture and of some chitosans. More in detail, with NPs fabricated with F_A = 0.46 chitosan the pro-inflammatory activity was comparable to LPS treated cells due to marked instability, heterogeneity and presence of large aggregates in such sample (Figure 46b). The finding that NPs prepared with F_A = 0.16 chitosan did not affect the TNF-α production is in contrast with the data reported by Tirelli and collaborators, where a significant TNF-α production was detected using similar NPs (obtained by using chitosan with F_A = 0.15).(Almalik, Day, et al., 2013)

Given the excellent performance of NPs prepared with F_A = 0.16 chitosan in terms of both macrophage biocompatibility and absence of pro-inflammatory stimulus, all the subsequent experiments were performed with the aforementioned chitosan.

3.4.3.2.3 Membrane association and internalization of NPs by macrophages

The interaction between macrophages and fluorescence-labeled NPs was then investigated by means of flow-cytometry (Figure 51). Upon NPs addition, a significant shift of the green fluorescence signal was detected (Figure 51b), indicating that almost all cells (96.8%) interacted with NPs. This suggest a very fast interaction, paralleling what previously reported between similar NPs and neutrophils.(Sacco, Decleva, et al., 2017) This rapid interaction can be due to receptor-mediated association (*e.g.* CD44) for both the polysaccharides,(Almalik, Karimi, et al., 2013; Rao et al., 2015) or to electrostatic interactions between positively charged NPs and negatively charged cells. After three hours of incubation only a limited number of cells were positive to internalization (Figure 51d). At this incubation stage, the interaction between cells and NPs was weak; indeed low centrifugation speed was sufficient to promote almost complete NPs detachment, as previously reported for human neutrophils.(Sacco, Decleva, et al., 2017) After 24 hours of incubation most cells (~60%) were positive to internalization (Figure 51e), suggesting NPs internalization as a slow-paced process.(de la Rosa et al., 2017) The slow internalization of NPs by macrophages could be an advantage for the delivery of bioactive molecules that need to be released in the extracellular space. Indeed, an excessively rapid carrier seize would impair the therapy.

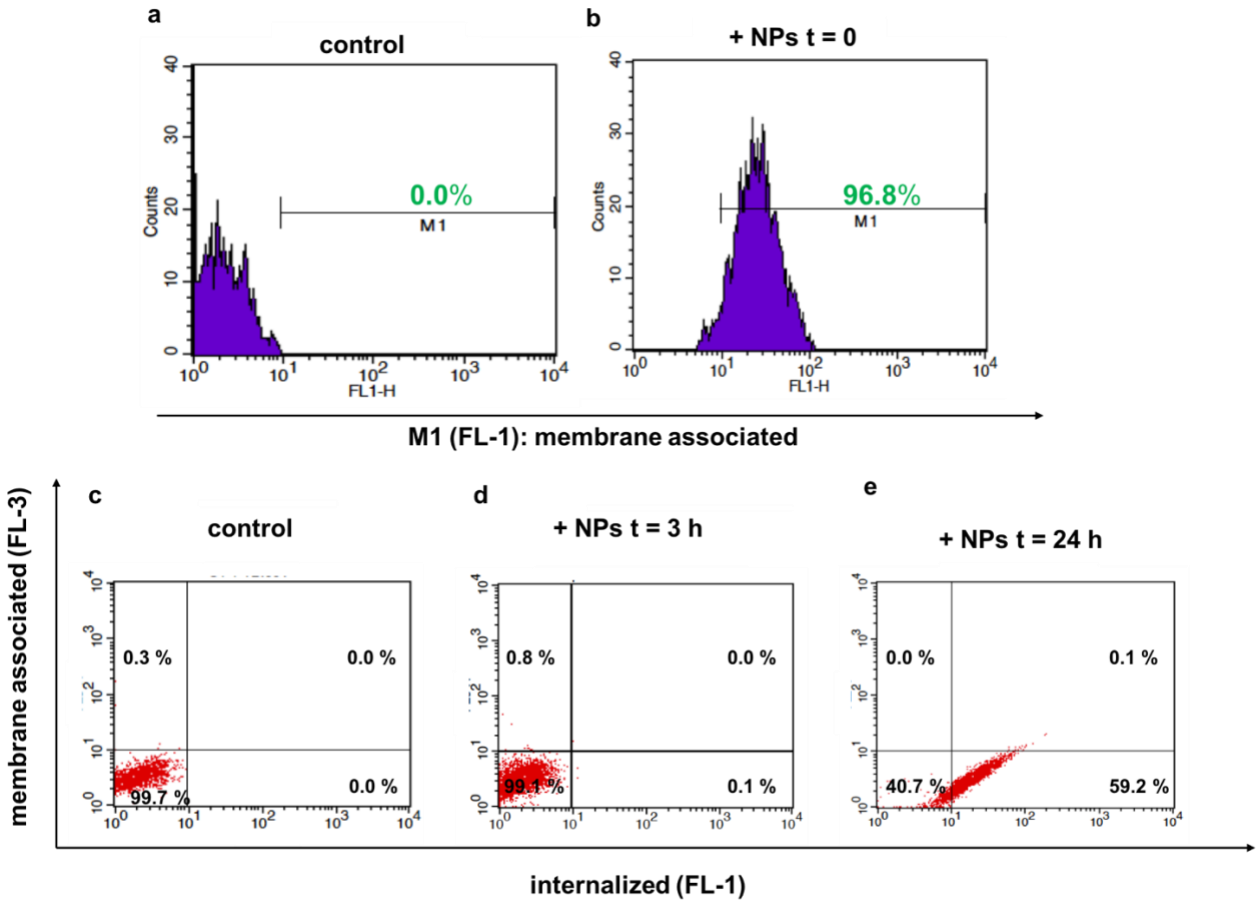

Figure 51. Membrane association and internalization of fluoresceinamine isomer I-labeled NPs (chitosan with F_A = 0.16, M_v = 220 000 and CH/HA 1:1 w/w) by U937 macrophages. **(a, b)**: Green fluorescence (FL-1) for control cells (**a**) and for NPs-treated cells immediately before the cytometric analysis **(b)**. **(c, d, e)**: Dot plot of green (FL-1) and red (*i.e.*, TB-quenched) fluorescence (FL-3) of control cells **(c)**, cells incubated with NPs for 3 h (**d**) and for 24 h (**e**). Four cell subsets are identifiable: lower left quadrant, no interaction; upper left quadrant, association; upper right quadrant, association and internalization; lower right quadrant, internalization. The number of events falling in each quadrant is expressed as a percentage of total gated events. Macrophages were incubated at 37 °C with NPs (chitosan with F_A = 0.16, M_v = 220 000 and CH/HA 1:1 w/w; 80 µg/mL final concentration) or not (control). Before being analyzed, samples were diluted with a TB (Trypan Blue) solution to quench the green fluorescence. Samples were washed after the incubation with NPs. Reprinted with permission from Furlani *et al.*(Furlani, Sacco, Decleva, et al., 2019) Copyright 2019 American Chemical Society.

3.4.3.2.4 Effect of NPs on neutrophil activation

The neutrophil functional response in the presence of NPs fabricated with F_A = 0.16 was then evaluated. More in detail, the ability of neutrophils to adhere to fibronectin, *i.e.* one of the first steps of cell recruitment during inflammation, and to produce two pro-inflammatory mediators usually secreted during inflammation, *i.e.* H_2O_2 and MPO, were investigated. NPs did not affect neither adhesion to FBG-coated surfaces nor H_2O_2 production (Figure 52a and 52b, respectively). Furthermore, NPs did not affect the amount of MPO released from the cells (Figure 52c). These

results suggest that NPs do not alter the neutrophil recruitment to the inflamed sites. Furthermore, NPs do not elicit the neutrophils degranulation.

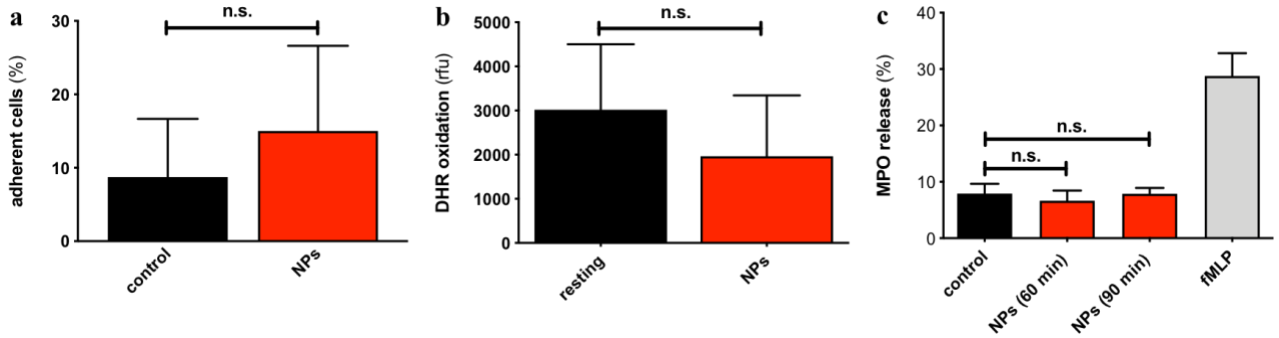

Figure 52. Effect of NPs (chitosan with F_A = 0.16 , M_v = 220 000 and CH/HA 1:1 w/w) on neutrophil adhesion (%) **(a)**, H_2O_2 production **(b)** and myeloperoxidase (MPO) release **(c)**. **(a, b)**: neutrophils were incubated for 60 min with NPs at 37 °C in FBG-coated wells. In (b) results are expressed as HRP-mediated, H_2O_2-dependent DHR oxidation. Data have been normalized for the number of adherent cells. **(c)** Neutrophils were incubated with NPs for 60 or 90 min at 37 °C in FBG-coated wells. The grey column shows the amount of MPO released by neutrophils stimulated with fMLP, a neutrophil secretagogue. Data are means (±SD) of four measurements. Student's *t*-test: n.s., not significant. Adapted with permission from Furlani *et al.*(Furlani, Sacco, Decleva, et al., 2019) Copyright 2019 American Chemical Society.

3.4.3.3 Evaluation of nanoparticles muco-adhesive properties

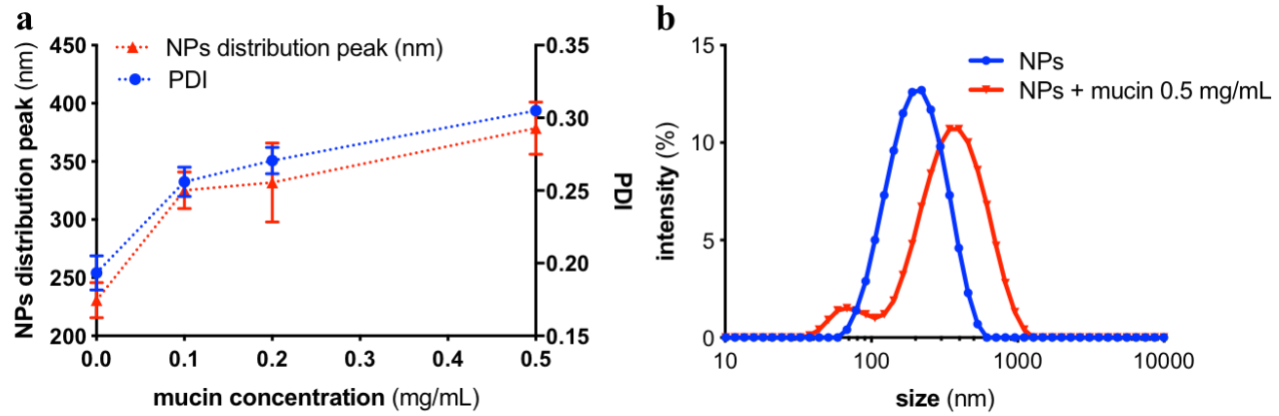

Figure 53. Interaction between NPs and mucin at pH ~ 5.5. NPs (chitosan with F_A = 0.16, M_v = 220 000 and CH/HA 1:1 w/w; 80 µg/mL final concentration) were added to mucin (0.1, 0.2, and 0.5 mg/mL final concentrations), and the resulting mixtures analyzed by DLS. Dotted lines are drawn to guide the eye. **(a)** NPs dimension (from distribution peak analysis) and PDI were reported as function of mucin concentration. Data are means (±SD) of three measurements. **(b)** Intensity size distribution of NPs diluted in water (blue curve) or in the presence mucin at the concentrations of 0.5 mg/mL (red curve). In the last case, the small peak centered at around 70 nm is attributed to mucin chains, according to Sogias *et al.*(Sogias, Williams, & Khutoryanskiy, 2008) Reprinted with permission from Furlani *et al.*(Furlani, Sacco, Decleva, et al., 2019) Copyright 2019 American Chemical Society.

Muco-adhesive properties of NPs were investigated by DLS analyses in the presence of mucin. A dose-dependent increase in NPs size was detected in the presence of mucin (Figure 53). Simultaneously, PDI values increased (Figure 53a), pointing to the formation of more heterogeneous aggregates. The origin of such interactions can be attributed to the electrostatic forces between the negatively charged mucin and the positively charged NPs.(Sogias et al., 2008)

3.4.3.4 Encapsulation of model molecule and drugs

The ability to encapsulate proper payloads represents another target that nanoparticles (NPs) should address. Centrifugation was used in order to promote NPs precipitation, then non-encapsulated free drug in the supernatant was quantified to investigate encapsulation efficiency of NPs. Indeed, centrifugation is the most widely used technique to evaluate encapsulation efficiency for nanoparticles based on chitosan, and several different conditions (*i.e.* centrifugation speed and centrifugation time) for NPs centrifugation were reported.(Almalik, Day, et al., 2013; Calvo et al., 1997; Oyarzun-Ampuero et al., 2009; Parajó et al., 2010) Precipitation efficiency was studied in order to find the best conditions allowing majority of NPs in the pellet. These conditions should avoid excessive centrifugation, preserving original physical properties of nanoparticles, *i.e.* avoid squeezing of NPs and releasing of encapsulated payloads.

A power law dependence of the scattering intensity as function of concentration of nanoparticles was detected (Figure 54a). Exploiting the fitting equation, it was possible to determine the precipitation efficiency, *i.e.* the percentage of NPs in the pellet after centrifugation. According to this approach, NPs are considered as a homogeneous population in which each NP is able to scatter light with the same intensity. This approximation can be acceptable since these NPs displayed a narrow size range (Figure 46a).

By using different centrifugation speeds and a constant centrifugation timeframe, *i.e.* 15 minutes, it was possible to detect a correlation between precipitation efficiency and centrifugation speed (Figure 54b). By using a low centrifugation speed, *i.e.* 3 000 g, the precipitation efficiency was close to 30%, instead in the case of the highest centrifugation speed, *i.e.* 12 000 g, the precipitation efficiency was almost doubled. After one hour at high constant speed, *i.e.* 12 000 g, it was possible to detect an almost complete (>90%) precipitation of NPs (Figure 54c). These results are in line with what recently reported by Cai and Lapitsky for chitosan/TPP NPs.(Cai & Lapitsky, 2019) These conditions, *i.e.* 12 000 g for one hour, seemed the best conditions to separate NPs encapsulating payload from free drug.

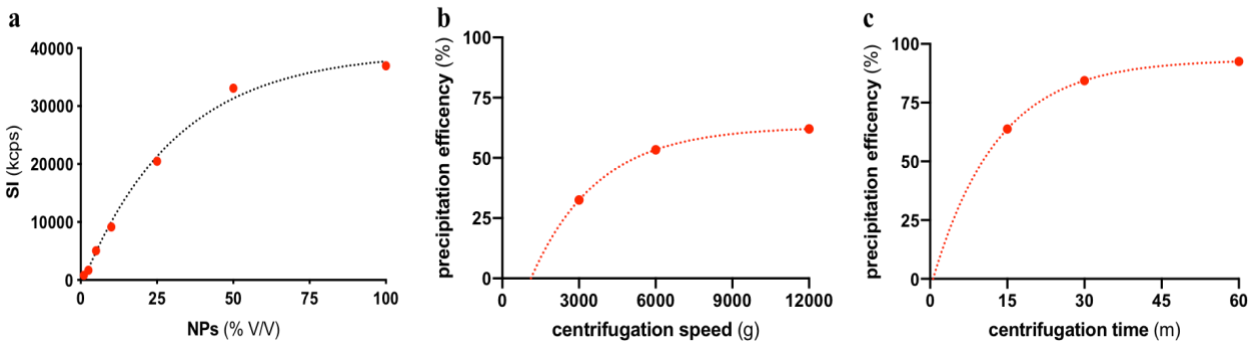

Figure 54. (a) Scattering intensity of NPs as function of their concentration (% V/V). The black dotted line is the best-fit of the experimental data points according to equation SI $\propto$ $(NPs)^{0.58}$ (R_2 > 0.95). **(b)** Precipitation efficiency as function of centrifugation speed, by using a constant centrifugation time (*i.e.* 15 minutes). The dotted line is drawn to guide the eye. **(c)** Precipitation efficiency as function of time by using a centrifugation speed equal to 12 000 g. The dotted line is drawn to guide the eye. CH/HA nanoparticles were prepared using chitosan with F_A = 0.16, M_v = 220 000 and CH/HA 1:1 w/w.

At first, fluoresceinamine isomer I was selected as model molecule. DLS measurements showed that the hydrodynamic diameter and PDI values of NPs were not affected by fluorophore loaded at different concentrations (data not shown). The encapsulation efficiency was equal to ~ 60% when the concentration of fluorophore was 1.0 μg/mL (Table 6). The encapsulation efficiency dropped around 40% by increasing the amount of payload to 2.0 μg/mL. Overall, our findings are in line with what already known for chitosan-based NPs.(Hu et al., 2008; Miladi, Sfar, Fessi, & Elaissari, 2015; Wu et al., 2005)

Table 6. Characterization of CH/HA nanoparticles prepared using chitosan with F_A = 0.16, M_v = 220 000 and CH/HA 1:1 w/w. The payload, the payload concentration and the corresponding encapsulation efficiency are reported. NPs were centrifugated for one hour at 12 000 g before supernatant analyses.

Payload	concentration (μg/mL)	EE (%)
Fluorescinamine isomer I	1	60.8 ± 1.0
	2	40.3 ± 4.2
Dexamethasone	20	9.1 ± 0.1
	50	3.5 ± 0.1
Aceclofenac	20	8.8 ± 0.4
	50	3.0 ± 0.1

Then, two anti-inflammatory drugs, *i.e.* dexamethasone and aceclofenac, were selected as payloads. The encapsulation efficiency, for both payloads concentrations, was lower than 10%. Such low encapsulation efficiency could be driven by an excessive centrifugation. Indeed, NPs are porous and centrifugation for one hour at high speed could induce a boost release of drugs, which can be squeezed out from the soft polymeric network. Unfortunately, it was not possible to find alternative techniques to evaluate encapsulation efficiency such as (*i*) filtration and (*ii*) dialysis. Filtration by using a syringe (or a pump) and a filter would requires high pression, which anyway can promote NPs squeezing, so cannot work for chitosan-based NPs. Dialysis by exploiting a semipermeable membrane could be very useful to separate only payloads covalently conjugated with NPs from free payloads (*e.g.* small proteins).

3.4.3.5 Drug release from nanocomposite networks

Nanoparticles encapsulating aceclofenac were then embedded in CTL-based networks in order to have a nanocomposite network able to slowly release drugs. The release of aceclofenac was evaluated in physiological conditions of pH, temperature and osmolarity and under shaking conditions. By UV-vis spectrophotometric analyses was possible to determine that nanocomposite networks were able to promote a drug release close to 20% after one day (Figure 55). The cumulative release of drug was almost complete (>90%) after three weeks. Thus, nanocomposite networks resulted suitable to promote a sustained release of drugs.

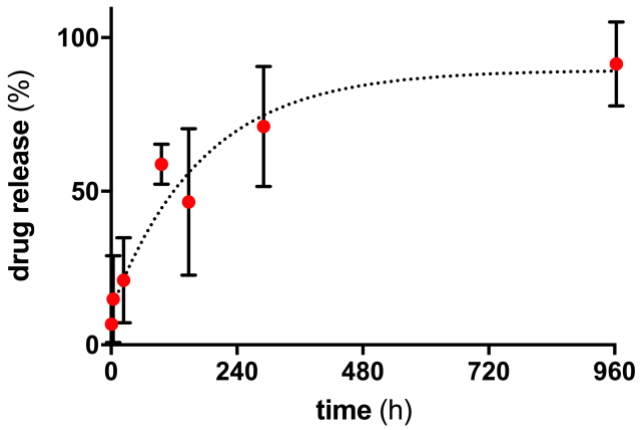

Figure 55. Cumulative release of aceclofenac as function of time at 37°C. NPs (chitosan with F_A = 0.16, M_v = 220 000 and CH/HA 1:1 w/w; 80 µg/mL final concentration) encapsulating aceclofenac were embedded in CTL-based networks ([CTL] = 10 g/L, [boric acid] = 8 mM, [mannitol] = 16 mM, $R_{M/B}$ = 2). The final concentration of aceclofenac in the resulting network was equal to 44.3 µg/mL. The dotted line is drawn to guide the eye.

Genta and collaborators reported for similar NPs (fabricated with a similar chitosan but a hyaluronic acid with high molecular weight) an almost complete release of drug after 1 day.(Chiesa et al., 2018) Similar results were reported by other research groups for other nanocomposite networks.(Asadi et al., 2018; Jeznach et al., 2018; Lim et al., 2010)

3.4.4 Main conclusions

This chapter was built upon knowledge about formation, stability and performance of chitosan/hyaluronan-based complex nanoparticles. Specifically, special attention was paid on the role played by chitosan molecular properties, *i.e.* molecular weight and F_A, in affecting nanoparticles dissolution/aggregation stability when dispersed in physiological medium. This aspect is of particular importance for potential translation of present system in fields such as nanomedicine. A systematic DLS investigation revealed that partial acetylation as well as medium molecular weight of chitosans are essential features to limit instability of resulting colloids. On the other side, SAXS analyses confirmed that osmotic swelling triggered by competition between phosphates of PBS buffer and TPP promoted an almost immediate macromolecular rearrangement with ensuing widening of network mesh and increase of porosity. When placed in physiological-simulated media in terms of pH and osmolarity, such as PBS or SBF, only NPs made with F_A = 0.16 chitosan and medium molecular weight (M_v = 220 000) maintained their integrity without dissolution or severe aggregation. The resulting NPs were analyzed in terms of activation of innate immune system cells, namely, macrophages and neutrophils. In detail, only stable NPs had no effect on TNF-α production by macrophages, whereas the other formulations enhanced such a production. Flow cytometry studies proved that most of the macrophages interacted with NPs immediately after their addition to the culture medium, albeit this association was weak. Furthermore, only a negligible fraction of the cell population internalized the NPs after three hours of incubation, whereas most cells displayed the internalized particles after 24 h. Resulting nanoparticles demonstrated to be stable up to three months and were able to host different payloads. Nanocomposite networks consisting of NPs embedding drugs and CTL-based networks were able to promote a sustained release of drugs. Resulting nanocomposite networks could be used as biomaterials in order to restore viscoelastic properties of native tissue and to soften chronic inflammation, *e.g.* for osteoarthritis.

4 CONCLUDING REMARKS

Macro- and micro/nano-hydrogels are highly hydrated networks consisting of polymers and solvents. They are widely studied and tested for different applications, especially for biomedical applications.

Cartilage degeneration represents one of the most common health problems worldwide, caused by different etiological agents. Cartilage regeneration approaches were widely studied over the last decades, and innovative biomaterials are needed to promote correct cartilage healing. To date, none of the proposed approaches fully satisfy patients' needs, probably since most of the products lack of peculiar mechanical properties of native tissues (*i.e.* non-linear response to stress - strain hardening). One emerging approach is the combination of nanoparticles encapsulating bioactive molecules (*e.g.* anti-inflammatory drugs) and a tridimensional network, with the final aim of finely tuning the release of these molecules. In this context, the present thesis has addressed the development of a nanocomposite biomimetic network showing the viscoelastic properties of native tissues, *e.g.* cartilage.

More in detail, the main goals reached in this thesis are summarized below.

(I) Boric acid fosters lactose-modified chitosan (CTL) structuring in physiological conditions of pH and osmolarity. Macromolecular association in dilute polymer solutions is dependent on crosslinker concentration: *(i)* for early cross-linking ion additions polymer chains form soluble aggregates, *(ii)* when further cross-linking agent is added to CTL solutions, a disruption of the chain−chain association occurs. Switching from dilute to concentrated solutions, rheological analyses have proved a strain-hardening behavior as a consequence of the formation of chain−chain cross−links. The present behavior observed for CTL−boric acid system, closely paralleled what already known for natural occurring biopolymers, *e.g.* collagen and neurofilaments. The inorganic component can act like a motor for the formation of the network, thus providing nucleation, reorganization and disassembly depending on curing and concentration. In this sense, the CTL-boric acid network can be seen as a synthetic chimera of natural occurring molecular motors.

(II) Two approaches, *i.e.* a pH- and a competitor-assisted gelation, have been developed for finely controlling gelation of CTL in the presence of boric acid as a cross-linker. Both approaches enable homogeneous networks. Notably, hydrogels display a strain-hardening behavior at large deformation, confirming their potential role as biomimetics of extracellular matrix. Resulting networks are multi-responsive toward different stimuli such as temperature or the presence of glucose and self-heal after breakage. Furthermore, different cells types, *i.e.* primary chondrocytes, and human

stem cells, are able to proliferate in contact and after embedding in CTL-boric acid gels. These gelation mechanisms may be easily translated to other diol-rich polymers for which boronic acids are used as a cross-linker.

(III) Genipin was used as alternative or combined crosslinker for CTL. Genipin, also at extremely low concentrations, boosts hydrogel formation in physiological conditions of pH and osmolarity. Surprisingly, a strain-hardening behavior was detected (also without boric acid). This behavior can be tentatively attributed - based on our preliminary data - to the formation and reorganization of intermolecular low-energy bounds (*e.g.* hydrogen bonding and hydrophobic interactions).

(IV) Special attention was paid on the role played by chitosan molecular properties, *i.e.* molecular weight and F_A, in affecting nanoparticles dissolution/aggregation stability when dispersed in physiological media. A systematic investigation revealed that partial acetylation (F_A = 0.16) as well as medium molecular weight ($\overline{M_v}$ = 220 000) of chitosans are essential features to limit dissolution or severe aggregation of resulting colloids. On the other side, in physiological media, osmotic swelling promotes an almost immediate macromolecular rearrangement with increase of porosity. The resulting NPs were analyzed in terms of activation of innate immune system cells, namely, macrophages and neutrophils. Strikingly, a structure-function relationship emerged, showing that instable NPs manifest a proinflammatory activity, linked to the instability (inhomogeneity) of the system. Conversely, stable homogeneous NPs neither modify the functional response of macrophages nor that of neutrophils. Of note, such NPs were found to possess additional properties potentially advantageous in applications such as delivery of therapeutics to target inflamed sites: *(i)* they are devoid of cytotoxic effects, *(ii)* they avoid engulfment during the early stage of interaction with macrophages, *(iii)* they are muco-adhesive, and *(iv)* they are able to host different payloads. Furthermore, nanocomposite networks consisting of NPs embedding drugs and CTL-based networks are able to promote a sustained release of drugs. The overall outcomes allow considering the present system as possible biomaterial suitable for tissue engineering and regenerative medicine, especially for cartilage regeneration.

5 REFERENCES

Abul Kalam, M., Khan, A. A., Khan, S., Almalik, A., & Alshamsan, A. (2016). Optimizing indomethacin-loaded chitosan nanoparticle size, encapsulation, and release using Box-Behnken experimental design. *International Journal of Biological Macromolecules*, *87*, 329–340. https://doi.org/10.1016/j.ijbiomac.2016.02.033

Agnihotri, S. A., Mallikarjuna, N. N., & Aminabhavi, T. M. (2004). Recent advances on chitosan-based micro- and nanoparticles in drug delivery. *Journal of Controlled Release*, Vol. 100, pp. 5–28. https://doi.org/10.1016/j.jconrel.2004.08.010

Ajun, W., Yan, S., Li, G., & Huili, L. (2009). Preparation of aspirin and probucol in combination loaded chitosan nanoparticles and in vitro release study. *Carbohydrate Polymers*, *75*(4), 566–574. https://doi.org/10.1016/j.carbpol.2008.08.019

Akizuki, S., Mow, V., Müller, F., Pita, J., Howell, D., & Manicourt, D. (1986). Tensile properties of human knee joint cartilage: I. Influence of ionic cartilage conditions, weight bearing and fibrillation on the tensile modulus. *J Orthop Res.*, (4), 379–392.

Albrecht, C., Tichy, B., Nürnberger, S., Hosiner, S., Zak, L., Aldrian, S., & Marlovits, S. (2011). Gene expression and cell differentiation in matrix-associated chondrocyte transplantation grafts: A comparative study. *Osteoarthritis and Cartilage*, *19*(10), 1219–1227. https://doi.org/10.1016/j.joca.2011.07.004

Ali, A., & Ahmed, S. (2018). A review on chitosan and its nanocomposites in drug delivery. *International Journal of Biological Macromolecules*, *109*, 273–286. https://doi.org/10.1016/j.ijbiomac.2017.12.078

Almalik, A., Day, P. J., & Tirelli, N. (2013). HA-coated chitosan nanoparticles for CD44-mediated nucleic acid delivery. *Macromolecular Bioscience*, *13*(12), 1671–1680. https://doi.org/10.1002/mabi.201300302

Almalik, A., Donno, R., Cadman, C. J., Cellesi, F., Day, P. J., & Tirelli, N. (2013). Hyaluronic acid-coated chitosan nanoparticles: Molecular weight-dependent effects on morphology and hyaluronic acid presentation. *Journal of Controlled Release*, *172*(3), 1142–1150. https://doi.org/10.1016/j.jconrel.2013.09.032

Almalik, A., Karimi, S., Ouasti, S., Donno, R., Wandrey, C., Day, P. J., & Tirelli, N. (2013). Hyaluronic acid (HA) presentation as a tool to modulate and control the receptor-mediated uptake of HA-coated nanoparticles. *Biomaterials*, *34*(21), 5369–5380.

https://doi.org/10.1016/j.biomaterials.2013.03.065

Almond, A. (2007). Hyaluronan. *Cellular and Molecular Life Sciences*, *64*(13), 1591–1596. https://doi.org/10.1007/s00018-007-7032-z

Amenitsch, H., Rappolt, M., Kriechbaum, M., Mio, H., Laggner, P., & Bernstorff, S. (1998). First performance assessment of the small-angle X-ray scattering beamline at ELETTRA. *Journal of Synchrotron Radiation*, *5*(3), 506–508. https://doi.org/10.1107/S090904959800137X

Andersson, M. (2009). *Patent No. WO/2009/056602*.

Annable, T., Buscall, R., Ettelaie, R., & Whittlestone, D. (1993). The rheology of solutions of associating polymers: Comparison of experimental behavior with transient network theory. *Journal of Rheology*, *37*(4), 695–726. https://doi.org/10.1122/1.550391

Aramwit, P., Ekasit, S., & Yamdech, R. (2015). The development of non-toxic ionic-crosslinked chitosan-based microspheres as carriers for the controlled release of silk sericin. *Biomedical Microdevices*, *17*(5), 1–9. https://doi.org/10.1007/s10544-015-9991-4

Argüelles-Monal, W., Recillas-Mota, M., & Fernández-Quiroz, D. (2017). Chitosan-Based Thermosensitive Materials. In *Biological Activities and Application of Marine Polysaccharides* (pp. 279–302). https://doi.org/http://dx.doi.org/10.5772/intechopen.68547

Asadi, N., Alizadeh, E., Salehi, R., Khalandi, B., Davaran, S., & Akbarzadeh, A. (2018). Nanocomposite hydrogels for cartilage tissue engineering: a review. *Artificial Cells, Nanomedicine and Biotechnology*, *46*(3), 465–471. https://doi.org/10.1080/21691401.2017.1345924

Ateshian, G., Warden, W., Kim, J., & Al., E. (1997). Finite deformation biphasic material properties of bovine articular cartilage from confined compression experiments. *J Biomech.*, (30), 1157–1164.

Backouche, F., Haviv, L., Groswasser, D., & Bernheim-Groswasser, A. (2006). Active gels: dynamics of patterning and self-organization. *Physical Biology*, *3*(4), 264–273.

Bainton, D. F. (1973). Sequential degranulation of the two types of polymorphonuclear leukocyte granules during phagocytosis of microorganisms. *The Journal of Cell Biology*, *58*(2), 249–264.

Barbosa, J. S., Ribeiro, A., Testera, A. M., Alonso, M., Arias, F. J., Rodríguez-Cabello, J. C., & Mano, J. F. (2010). Development of biomimetic chitosan-based hydrogels using an elastin-like polymer. *Advanced Engineering Materials*, *12*(1–2), 37–44.

https://doi.org/10.1002/adem.200980152

Barbosa, M. A., Pêgo, A. P., & Amaral, I. F. (2011). Materials of Biological Origin: Chitosan. In *Comprehensive Biomaterials* (pp. 221–237). https://doi.org/10.1016/B978-0-08-055294-1.00072-6

Beaucage, G. (1996). Small-Angle Scattering from Polymeric Mass Fractals of Arbitrary Mass-Fractal Dimension. *Journal of Applied Crystallography*, *29*(2), 134–146. https://doi.org/10.1107/S0021889895011605

Ben Messaoud, G., Promeneur, L., Brennich, M., Roelants, S. L. K. W., Le Griel, P., & Baccile, N. (2018). Complex coacervation of natural sophorolipid bolaamphiphile micelles with cationic polyelectrolytes. *Green Chemistry*, *20*(14), 3371–3385. https://doi.org/10.1039/c8gc01531g

Berth, G., & Dautzenberg, H. (2002). The degree of acetylation of chitosans and its effect on the chain conformation in aqueous solution. *Carbohydrate Polymers*, *47*, 39–51.

Bhattarai, N., Gunn, J., & Zhang, M. (2010). Chitosan-based hydrogels for controlled, localized drug delivery. *Advanced Drug Delivery Reviews*, *62*(1), 83–99. https://doi.org/10.1016/j.addr.2009.07.019

Bhattarai, N., Ramay, H. R., Gunn, J., Matsen, F. A., & Zhang, M. (2005). PEG-grafted chitosan as an injectable thermosensitive hydrogel for sustained protein release. *Journal of Controlled Release*, *103*(3), 609–624. https://doi.org/10.1016/j.jconrel.2004.12.019

Bi, L., Cao, Z., Hu, Y., Song, Y., Yu, L., Yang, B., … Han, Y. (2011). Effects of different cross-linking conditions on the properties of genipin-cross-linked chitosan/collagen scaffolds for cartilage tissue engineering. *Journal of Materials Science: Materials in Medicine*, *22*(1), 51–62. https://doi.org/10.1007/s10856-010-4177-3

Branco da Cunha, C., Klumpers, D. D., Li, W. A., Koshy, S. T., Weaver, J. C., Chaudhuri, O., … Mooney, D. J. (2014). Influence of the stiffness of three-dimensional alginate/collagen-I interpenetrating networks on fibroblast biology. *Biomaterials*, *35*(32), 8927–8936. https://doi.org/10.1016/j.biomaterials.2014.06.047

Brooks, W. L. A., & Sumerlin, B. S. (2016). Synthesis and Applications of Boronic Acid-Containing Polymers: From Materials to Medicine. *Chemical Reviews*, *116*(3), 1375–1397. https://doi.org/10.1021/acs.chemrev.5b00300

Brusatin, G., Panciera, T., Gandin, A., Citron, A., & Piccolo, S. (2018). Biomaterials and engineered

microenvironments to control YAP/TAZ-dependent cell behaviour. *Nature Materials*, *17*(12), 1063–1075. https://doi.org/10.1038/s41563-018-0180-8

Buckwalter, J. (1998). Articular cartilage: injuries and potential for healing. *J Orthop Sports Phys Ther.*, (28), 192–202.

Buckwalter, J., Hunzinker, E., & Rosenberg, L. (1988). Articular cartilage: composition and structure. In W. SLY & Buckwalter JA (Eds.), *Injury and Repair of the Musculoskeletal Soft Tissues* (pp. 405–425).

Buckwalter JA, M. H. (1997). Articular cartilage, part 1: tissue design and chondrocyte-matrix interaction. *J Bone Joint Surg Am.*, (79), 600–611.

Burdick, J. A., & Prestwich, G. D. (2011). Hyaluronic acid hydrogels for biomedical applications. *Advanced Materials*, *23*(12), 41–56. https://doi.org/10.1002/adma.201003963

Busetto, S., Trevisan, E., Patriarca, P., & Menegazzi, R. (2004). A single-step, sensitive flow cytofluorometric assay for the simultaneous assessment of membrane-bound and ingested Candida albicans in phagocytosing neutrophils. *Cytometry. Part A : The Journal of the International Society for Analytical Cytology*, *58*(2), 201–206. https://doi.org/10.1002/cyto.a.20014

Bushmann, M., Filion, D., & Lavertu, M. (2007). *Patent No. WO/2007/051311*.

Cai, Y., & Lapitsky, Y. (2019). Pitfalls in analyzing release from chitosan/tripolyphosphate micro- and nanoparticles. *European Journal of Pharmaceutics and Biopharmaceutics*, *142*(March), 204–215. https://doi.org/10.1016/j.ejpb.2019.06.020

Calvo, P., Remuñán-López, C., Vila-Jato, J. L., & Alonso, M. J. (1997). Novel hydrophilic chitosan-polyethylene oxide nanoparticles as protein carriers. *Journal of Applied Polymer Science*, *63*(1), 125–132. https://doi.org/10.1002/(SICI)1097-4628(19970103)63:1<125::AID-APP13>3.0.CO;2-4

Calvo, Pilar, RemunanLopez, C., VilaJato, J. L., Alonso, M. J., Remuñan-López, C., Vila-Jato, J. L., & Alonso, M. J. (1997). Chitosan and chitosan ethylene oxide propylene oxide block copolymer nanoparticles as novel carriers for proteins and vaccines. *Pharmaceutical Research*, Vol. 14, pp. 1431–1436. https://doi.org/10.1023/A:1012128907225

Carrillo, J.-M. Y., MacKintosh, F. C., & Dobrynin, A. V. (2013). Nonlinear Elasticity: From Single Chain to Networks and Gels. *Macromolecules*, *46*(9), 3679–3692.

https://doi.org/10.1021/ma400478f

Chandran, S., Dold, S., Buvignier, A., Krannig, K.-S., Schlaad, H., Reiter, G., & Reiter, R. (2015). Tuning Morphologies of Langmuir Polymer Films Through Controlled Relaxations of Non-Equilibrium States. *Langmuir*, *31*(23), 6426–6435. https://doi.org/10.1021/acs.langmuir.5b01212

Chang, F.-C., Levengood, S. L., Cho, N., Chen, L., Wang, E., Yu, J. S., & Zhang, M. (2018). Crosslinked Chitosan-PEG Hydrogel for Culture of Human Glioblastoma Cell Spheroids and Drug Screening. *Advanced Therapeutics*, *1*(7), 1800058. https://doi.org/10.1002/adtp.201800058

Chaudhuri, O., Gu, L., Darnell, M., Klumpers, D., Bencherif, S. A., Weaver, J. C., … Mooney, D. J. (2015). Substrate stress relaxation regulates cell spreading. *Nature Communications*, *6*, 1–7. https://doi.org/10.1038/ncomms7365

Chaudhuri, O., Gu, L., Klumpers, D., Darnell, M., Bencherif, S. A., Weaver, J. C., … Mooney, D. J. (2016). Hydrogels with tunable stress relaxation regulate stem cell fate and activity. *Nature Materials*, *15*(3), 326–334. https://doi.org/10.1038/nmat4489

Chen, Y., Diaz-dussan, D., Wu, D., Wang, W., Peng, Y., Asha, A. B., … Narain, R. (2018). *Bioinspired Self-Healing Hydrogel Based on Benzoxaborole- Catechol Dynamic Covalent Chemistry for 3D Cell Encapsulation*. https://doi.org/10.1021/acsmacrolett.8b00434

Chenite, A., Chaput, C., Wang, D., Combes, C., Buschmann, M. D., Hoemann, C. D., … Selmani, A. (2000). Novel injectable neutral solutions of chitosan form biodegradable gels in situ. *Biomaterials*, *21*(21), 2155–2161. https://doi.org/10.1016/S0142-9612(00)00116-2

Chiesa, E., Dorati, R., Conti, B., Modena, T., Cova, E., Meloni, F., & Genta, I. (2018). Hyaluronic acid-decorated chitosan nanoparticles for CD44-targeted delivery of everolimus. *International Journal of Molecular Sciences*, *19*(8). https://doi.org/10.3390/ijms19082310

Cooke, M. E., Simon, W. J., Horst, B. t., Moiemen, N., Snow, M., Chouhan, G., … Grover, M. L. (2018). Structuring of Hydrogels across Multiple Length Scales for Biomedical Applications. *Advanced Materials*, *30*(14), 1705013. https://doi.org/10.1002/adma.201705013

Correa, D., & Lietman, S. A. (2017). Articular cartilage repair: Current needs, methods and research directions. *Seminars in Cell and Developmental Biology*, *62*, 67–77. https://doi.org/10.1016/j.semcdb.2016.07.013

Coviello, T., Matricardi, P., Marianecci, C., & Alhaique, F. (2007). Polysaccharide hydrogels for modified release formulations. *Journal of Controlled Release*, *119*(1), 5–24. https://doi.org/10.1016/j.jconrel.2007.01.004

Crépet, A., Lalevée, G., Montembault, A., Sudre, G., Delair, T., Meadows, J., … Malaise, S. (2016). Polyelectrolyte complexes via desalting mixtures of hyaluronic acid and chitosan—Physicochemical study and structural analysis. *Carbohydrate Polymers*, *154*, 86–95. https://doi.org/10.1016/j.carbpol.2016.08.007

Croisier, F., & Jérôme, C. (2013). Chitosan-based biomaterials for tissue engineering. *European Polymer Journal*, *49*(4), 780–792. https://doi.org/10.1016/J.EURPOLYMJ.2012.12.009

Cross, M. M. (1965). Rheology of non-Newtonian fluids: A new flow equation for pseudoplastic systems. *Journal of Colloid Science*, *20*(5), 417–437. https://doi.org/10.1016/0095-8522(65)90022-X

D'Amelio, N., Esteban, C., Coslovi, A., Feruglio, L., Uggeri, F., Villegas, M., … Donati, I. (2013). Insight into the molecular properties of chitlac, a chitosan derivative for tissue engineering. *Journal of Physical Chemistry B*, *117*(43), 13578–13587. https://doi.org/10.1021/jp4067263

Danielsen, S. P. O., Sanoja, G. E., McCuskey, S. R., Hammouda, B., Bazan, G. C., Fredrickson, G. H., & Segalman, R. A. (2018). Mixed Conductive Soft Solids by Electrostatically Driven Network Formation of a Conjugated Polyelectrolyte. *Chemistry of Materials*, *30*(4), 1417–1426. https://doi.org/10.1021/acs.chemmater.7b05303

Dawber, J. G., Green, S. I. E., Dawber, J. C., & Gabrail, S. (1988). A polarimetric and 11B and 13C nuclear magnetic resonance study of the reaction of the tetrahydroxyborate ion with polyols and carbohydrates. *Journal of the Chemical Society, Faraday Transactions 1: Physical Chemistry in Condensed Phases*, *84*(1), 41–56. https://doi.org/10.1039/F19888400041

De Campos, A. M., Sanchez, A., & Alonso, M. J. (2001). Chitosan nanoparticles: a new vehicle for the improvement of the delivery of drugs to the ocular surface. Application to cyclosporin A. *Int J Pharm*, *224*(1–2), 159–168. https://doi.org/S0378517301007608 [pii]

de la Fuente, M., Seijo, B., & Alonso, M. J. (2008a). Design of novel polysaccharidic nanostructures for gene delivery. *Nanotechnology*, *19*(7), 075105. https://doi.org/10.1088/0957-4484/19/7/075105

de la Fuente, M., Seijo, B., & Alonso, M. J. (2008b). Novel hyaluronan-based nanocarriers for transmucosal delivery of macromolecules. *Macromolecular Bioscience*, *8*(5), 441–450.

https://doi.org/10.1002/mabi.200700190

de la Fuente, M., Seijo, B., & Alonso, M. J. (2008c). Novel hyaluronic acid-chitosan nanoparticles for ocular gene therapy. *Investigative Ophthalmology and Visual Science*, *49*(5), 2016–2024. https://doi.org/10.1167/iovs.07-1077

Debele, T. A., Mekuria, S. L., & Tsai, H. C. (2016). Polysaccharide based nanogels in the drug delivery system: Application as the carrier of pharmaceutical agents. *Materials Science and Engineering C*, *68*, 964–981. https://doi.org/10.1016/j.msec.2016.05.121

Deepthi, S., Gafoor, A. A. A., Sivashanmugam, A., Nair Shantikumar, V., & Jayakumar, R. (2016). Nanostrontium ranelate incorporated injectable hydrogel enhanced matrix production supporting chondrogenesis in vitro. *Journal of Materials Chemistry B*. https://doi.org/10.1039/b000000x

Demoor, M., Maneix, L., Ollitrault, D., Legendre, F., Duval, E., & Claus, S. (2012). Deciphering chondrocyte behaviour in matrix-induced autologous chondrocyte implantation to undergo accurate cartilage repair with hyaline matrix. *Pathol Biol*, (60), 199–207.

Deng, X., Cao, M., Zhang, J., Hu, K., Yin, Z., Zhou, Z., … Zeng, Y. (2014). Hyaluronic acid-chitosan nanoparticles for co-delivery of MiR-34a and doxorubicin in therapy against triple negative breast cancer. *Biomaterials*, *35*(14), 4333–4344. https://doi.org/10.1016/j.biomaterials.2014.02.006

Donati, I., Stredanska, S., Silvestrini, G., Vetere, A., Marcon, P., Marsich, E., … Vittur, F. (2005). The aggregation of pig articular chondrocyte and synthesis of extracellular matrix by a lactose-modified chitosan. *Biomaterials*, *26*(9), 987–998. https://doi.org/10.1016/j.biomaterials.2004.04.015

Donati, Ivan, Borgogna, M., Turello, E., Casàro, A., & Paoletti, S. (2007). Tuning supramolecular structuring at the nanoscale level: Nonstoichiometric soluble complexes in dilute mixed solutions of alginate and lactose-modified chitosan (Chitlac). *Biomacromolecules*, *8*(5), 1471–1479. https://doi.org/10.1021/bm0610828

Donati, Ivan, Feresini, M., Travan, A., Marsich, E., Lapasin, R., & Paoletti, S. (2011). Polysaccharide-Based Polyanion–Polycation–Polyanion Ternary Systems. A Preliminary Analysis of Interpolyelectrolyte Interactions in Dilute Solutions. *Biomacromolecules*, *12*(11), 4044–4056. https://doi.org/10.1021/bm201046p

Donati, Ivan, Huag, I. J., Scarpa, T., Borgogna, M., Draget, K. I., Skjåk-Bræk, G., & Paoletti, S. (2007). Synergistic effects in semidilute mixed solutions of alginate and lactose-modified

chitosan (chitlac). *Biomacromolecules*, *8*(3), 957–962. https://doi.org/10.1021/bm060856h

Dri, P., Cramer, R., Spessotto, P., Romano, M., & Patriarca, P. (1991). Eosinophil activation on biologic surfaces. Production of O2- in response to physiologic soluble stimuli is differentially modulated by extracellular matrix components and endothelial cells. *Journal of Immunology (Baltimore, Md. : 1950)*, *147*(2), 613–620. Retrieved from http://www.ncbi.nlm.nih.gov/pubmed/1712813

Dupont, S., Morsut, L., Aragona, M., Enzo, E., Giulitti, S., Cordenonsi, M., … Piccolo, S. (2011). Role of YAP/TAZ in mechanotransduction. *Nature*, *474*(7350), 179–184. https://doi.org/10.1038/nature10137

Elgadir, M. A., Uddin, M. S., Ferdosh, S., Adam, A., Chowdhury, A. J. K., & Sarker, M. Z. I. (2015). Impact of chitosan composites and chitosan nanoparticle composites on various drug delivery systems: A review. *Journal of Food and Drug Analysis*, *23*(4), 619–629. https://doi.org/10.1016/j.jfda.2014.10.008

Engler, A. J., Sen, S., Sweeney, H. L., & Discher, D. E. (2006). Matrix Elasticity Directs Stem Cell Lineage Specification. *Cell*, *126*(4), 677–689. https://doi.org/10.1016/j.cell.2006.06.044

Erk, K. A., Henderson, K. J., & Shull, K. R. (2010). Strain stiffening in synthetic and biopolymer networks. *Biomacromolecules*, *11*(5), 1358–1363. https://doi.org/10.1021/bm100136y

Esteban, C., Donati, I., Pantano, S., Villegas, M., Benegas, J., & Paoletti, S. (2018). Dissecting the conformational determinants of chitosan and chitlac oligomers. *Biopolymers*, *109*(6), e23221. https://doi.org/10.1002/bip.23221

Eyre, David. (2002). Collagen of articular cartilage. *Arthritis Research*, *4*(1), 30–35. https://doi.org/10.1186/ar380

Eyre, DR, & Wu, J. (1987). Type XI or 1α2α3α collagen. In R. Mayne & R. Burgeson (Eds.), *Structure and Function of Collagen Types* (pp. 261–281). New York: Academic Press.

Félix, L., Hernández, J., Argüelles, W. M., & Goycoolea, F. M. (2005). Kinetics of gelation and thermal sensitivity of N-isobutyryl chitosan hydrogels. *Biomacromolecules*, *6*(5), 2408–2415. https://doi.org/10.1021/bm0501297

Ferrante, A., Nandoskar, M., Walz, A., Goh, D. H., & Kowanko, I. C. (1988). Effects of tumour necrosis factor alpha and interleukin-1 alpha and beta on human neutrophil migration, respiratory burst and degranulation. *International Archives of Allergy and Applied Immunology*,

86(1), 82–91.

Fessel, G., Cadby, J., Wunderli, S., Van Weeren, R., & Snedeker, J. G. (2014). Dose- and time-dependent effects of genipin crosslinking on cell viability and tissue mechanics - Toward clinical application for tendon repair. *Acta Biomaterialia*, *10*(5), 1897–1906. https://doi.org/10.1016/j.actbio.2013.12.048

Franceschi, F., Longo, U., Ruzzini, L., Marinozzi, A., Maffulli, N., & Denaro, V. (2008). Simultaneous arthroscopic implantation of autologous chondrocytes and high tibial osteotomy for tibial chondral defects in the varus knee. *Knee*, (15), 309–313.

Freier, T., Koh, H. S., Kazazian, K., & Shoichet, M. S. (2005). Controlling cell adhesion and degradation of chitosan films by N-acetylation. *Biomaterials*, *26*(29), 5872–5878. https://doi.org/10.1016/j.biomaterials.2005.02.033

Furlani, F, Sacco, P., Marsich, E., Donati, I., & Paoletti, S. (2017). Highly monodisperse colloidal coacervates based on a bioactive lactose-modified chitosan: From synthesis to characterization. *Carbohydrate Polymers*. https://doi.org/10.1016/j.carbpol.2017.06.097

Furlani, Franco, Sacco, P., Cok, M., de Marzo, G., Marsich, E., Paoletti, S., & Donati, I. (2019). Biomimetic, Multiresponsive, and Self-Healing Lactose-Modified Chitosan (CTL)-Based Gels Formed via Competitor-Assisted Mechanism. *ACS Biomaterials Science & Engineering*. https://doi.org/10.1021/acsbiomaterials.9b01256

Furlani, Franco, Sacco, P., Decleva, E., Menegazzi, R., Donati, I., Paoletti, S., & Marsich, E. (2019). Chitosan Acetylation Degree Influences the Physical Properties of Polysaccharide Nanoparticles: Implication for the Innate Immune Cells Response. *ACS Applied Materials & Interfaces*, *11*, 9794−9803. https://doi.org/10.1021/acsami.8b21791

Furlani, Franco, Sacco, P., Scognamiglio, F., Asaro, F., Travan, A., Borgogna, M., … Donati, I. (2019). Nucleation, reorganization and disassembly of an active network from lactose-modified chitosan mimicking biological matrices. *Carbohydrate Polymers*, *208*, 451–456. https://doi.org/10.1016/j.carbpol.2018.12.096

Furlani, Franco, Sacco, P., Scognamiglio, F., Marsich, E., & Donati, I. (2019). *Patent No. 102019000006448*. Italy.

Gannon, J., Walker, G., Fischer, M., Carpenter, R., Thompson, R. J., & Oegema, T. (1991). Localization of type X collagen in canine growth plate and adult canine articular cartilage. *J Orthop Res*, (9), 485–494.

Giacalone, G., Hillaireau, H., Capiau, P., Chacun, H., Reynaud, F., & Fattal, E. (2014). Stabilization and cellular delivery of chitosan-polyphosphate nanoparticles by incorporation of iron. *Journal of Controlled Release*, *194*, 211–219. https://doi.org/10.1016/j.jconrel.2014.08.022

Gong, Z., Szczesny, S. E., Caliari, S. R., Charrier, E. E., Chaudhuri, O., Cao, X., … Shenoy, V. B. (2018). Matching material and cellular timescales maximizes cell spreading on viscoelastic substrates. *Proceedings of the National Academy of Sciences of the United States of America*, *115*(12), E2686–E2695. https://doi.org/10.1073/pnas.1716620115

Goycoolea, F. M., Brunel, F., Gueddari, N. E. El, Coggiola, A., Lollo, G., Moerschbacher, B. M., … Alonso, M. J. (2016). Physical Properties and Stability of Soft Gelled Chitosan-Based Nanoparticles. *Macromolecular Bioscience*, 1–10. https://doi.org/10.1002/mabi.201600298

Hall, D. G. (2011). Structure, Properties, and Preparation of Boronic Acid Derivatives. Overview of Their Reactions and Applications, in (ed D. G. Hall). In *Boronic Acids: Preparation and Applications in Organic Synthesis and Medicine* (pp. 1–133). https://doi.org/10.1002/9783527639328.ch1

Hall, L. D., & Yalpani, M. (1984). *Patent No. US4424346A*.

Hammersley, A. P., Svensson, S. O., Hanfland, M., Fitch, A. N., & Hausermann, D. (1996). Two-dimensional detector software: From real detector to idealised image or two-theta scan. *High Pressure Research*, *14*(4–6), 235–248. https://doi.org/10.1080/08957959608201408

Han, L., Wang, M., Li, P., Gan, D., Yan, L., Xu, J., … Lu, X. (2018). Mussel-Inspired Tissue-Adhesive Hydrogel Based on the Polydopamine-Chondroitin Sulfate Complex for Growth-Factor-Free Cartilage Regeneration. In *ACS Applied Materials and Interfaces* (Vol. 10). https://doi.org/10.1021/acsami.8b05314

Hardingham, T. (2004). *Chemistry and Biology of Hyaluronan* (E. Garg, H., Hales, C., Ed.). Elsevier.

He, J., Zhang, A., Zhang, Y., & Guan, Y. (2011). Novel redox hydrogel by in situ gelation of chitosan as a result of template oxidative polymerization of hydroquinone. *Macromolecules*, *44*(7), 2245–2252. https://doi.org/10.1021/ma1029532

Henderson, L. M., & Chappell, J. B. (1993). Dhydrorhodamine 123: a fluorescent probe for superoxide generation? *Eur J Biochem*, *217*, 973–980. https://doi.org/10.1111/j.1432-1033.1993.tb18328.x

Highley, C. B., Prestwich, G. D., & Burdick, J. A. (2016). Recent advances in hyaluronic acid

hydrogels for biomedical applications. *Current Opinion in Biotechnology*, *40*, 35–40. https://doi.org/10.1016/j.copbio.2016.02.008

Holly, E. E., Venkataraman, S. K., Chambon, F., & Henning Winter, H. (1988). Fourier transform mechanical spectroscopy of viscoelastic materials with transient structure. *Journal of Non-Newtonian Fluid Mechanics*, *27*(1), 17–26. https://doi.org/10.1016/0377-0257(88)80002-8

Hu, B., Pan, C., Sun, Y., Hou, Z., Ye, H., Hu, B., & Zeng, X. (2008). Optimization of fabrication parameters to produce chitosan-tripolyphosphate nanoparticles for delivery of tea catechins. *Journal of Agricultural and Food Chemistry*, *56*(16), 7451–7458. https://doi.org/10.1021/jf801111c

Huang, H., Zhang, X., Hu, X., Dai, L., Zhu, J., Man, Z., … Ao, Y. (2014). Directing chondrogenic differentiation of mesenchymal stem cells with a solid-supported chitosan thermogel for cartilage tissue engineering. *Biomedical Materials*, *9*(3), 035008. https://doi.org/10.1088/1748-6041/9/3/035008

Huang, Y., Cai, Y., & Lapitsky, Y. (2015). Factors affecting the stability of chitosan/tripolyphosphate micro- and nanogels: resolving the opposing findings. *J. Mater. Chem. B*, *3*(29), 5957–5970. https://doi.org/10.1039/C5TB00431D

Huang, Y., & Lapitsky, Y. (2011). Monovalent salt enhances colloidal stability during the formation of chitosan/tripolyphosphate microgels. *Langmuir : The ACS Journal of Surfaces and Colloids*, *27*(17), 10392–10399. https://doi.org/10.1021/la201194a

Huang, Y., & Lapitsky, Y. (2012). Salt-Assisted Mechanistic Analysis of Chitosan/Tripolyphosphate Micro- and Nanogel Formation. *Biomacromolecules*, *13*(11), 3868–3876. https://doi.org/10.1021/bm3014236

Huang, Y., & Lapitsky, Y. (2017). On the kinetics of chitosan/tripolyphosphate micro- and nanogel aggregation and their effects on particle polydispersity. *Journal of Colloid and Interface Science*, *486*, 27–37. https://doi.org/10.1016/j.jcis.2016.09.050

Huebsch, N. (2019). Translational mechanobiology: Designing synthetic hydrogel matrices for improved in vitro models and cell-based therapies. *Acta Biomaterialia*, *94*, 97–111. https://doi.org/10.1016/j.actbio.2019.05.055

Huebsch, N., Lippens, E., Lee, K., Mehta, M., Koshy, S. T., Darnell, M. C., … Mooney, D. J. (2015). *Matrix elasticity of void-forming hydrogels controls transplanted-stem-cell-mediated bone formation*. (September). https://doi.org/10.1038/NMAT4407

Hunter, D. J., & Bierma-Zeinstra, S. (2019). Osteoarthritis. *The Lancet*, *393*(10182), 1745–1759. https://doi.org/10.1016/S0140-6736(19)30417-9

Hunter, D., Schofield, D., & Callander, E. (2014). The individual and socioeconomic impact of osteoarthritis. *Nat Rev Rheumatol*, (10), 437–441.

Hunziker, E. B., & Rosenberg, L. C. (1996). Repair of partial-thickness defects in articularcartilage: cell recruitment from the synovial membrane. *J. Bone Joint Surg.Am.*, (78), 721–733.

Indei, T., & Takimoto, J. (2010). Linear viscoelastic properties of transient networks formed by associating polymers with multiple stickers. *The Journal of Chemical Physics*, *133*(19), 194902. https://doi.org/10.1063/1.3498779

Jacobi, M., Villa, V., Magnussen, R. A., & Neyret, P. (2011). MACI - a new era? *Sports Medicine, Arthroscopy, Rehabilitation, Therapy and Technology*, *3*(1), 1–7. https://doi.org/10.1186/1758-2555-3-10

Janes, K. A., & Alonso, M. J. (2003). Depolymerized chitosan nanoparticles for protein delivery: Preparation and characterization. *Journal of Applied Polymer Science*, *88*(12), 2769–2776. https://doi.org/10.1002/app.12016

Jeong, B., Bae, Y. H., & Kim, S. W. (1999). Thermoreversible gelation of PEG-PLGA-PEG triblock copolymer aqueous solutions. *Macromolecules*, *32*(21), 7064–7069. https://doi.org/10.1021/ma9908999

Jeznach, O., Kołbuk, D., & Sajkiewicz, P. (2018). Injectable hydrogels and nanocomposite hydrogels for cartilage regeneration. *Journal of Biomedical Materials Research - Part A*, *106*(10), 2762–2776. https://doi.org/10.1002/jbm.a.36449

Jiang, D., Liang, J., & Noble, P. W. (2007). Hyaluronan in tissue injury and repair. *Annual Review of Cell and Developmental Biology*, *23*, 435–461. https://doi.org/10.1146/annurev.cellbio.23.090506.123337

Jiang, Y., Chen, J., Deng, C., Suuronen, E. J., & Zhong, Z. (2014). Click hydrogels, microgels and nanogels: Emerging platforms for drug delivery and tissue engineering. *Biomaterials*, *35*(18), 4969–4985. https://doi.org/10.1016/j.biomaterials.2014.03.001

Jin, R., Moreira Teixeira, L. S., Dijkstra, P. J., Karperien, M., van Blitterswijk, C. A., Zhong, Z. Y., & Feijen, J. (2009). Injectable chitosan-based hydrogels for cartilage tissue engineering. *Biomaterials*, *30*(13), 2544–2551. https://doi.org/10.1016/j.biomaterials.2009.01.020

Johnson, R., & Halder, G. (2014). The two faces of Hippo: Targeting the Hippo pathway for regenerative medicine and cancer treatment. *Nature Reviews Drug Discovery*, *13*(1), 63–79. https://doi.org/10.1038/nrd4161

Khong, T. T., Aarstad, O. A., Skjåk-Bræk, G., Draget, K. I., & Vårum, K. M. (2013). Gelling concept combining chitosan and alginate-proof of principle. *Biomacromolecules*, *14*(8), 2765–2771. https://doi.org/10.1021/bm400610b

Kim, I. S., Kim, H. G., Hong, C. A., & Lee, S. Y. (2017). *Patent No. WO/2017/135498*.

Kim, S. K., Ravichandran, Y. D., Khan, S. B., & Kim, Y. T. (2008). Prospective of the cosmeceuticals derived from marine organisms. *Biotechnology and Bioprocess Engineering*, *13*(5), 511–523. https://doi.org/10.1007/s12257-008-0113-5

Kim, T. G., Shin, H., & Lim, D. W. (2012). Biomimetic Scaffolds for Tissue Engineering. *Advanced Functional Materials*, *22*(12), 2446–2468. https://doi.org/10.1002/adfm.201103083

Kim, T. H., Nah, J. W., Cho, M.-H., Park, T. G., & Cho, C. S. (2006). Receptor-mediated gene delivery into antigen presenting cells using mannosylated chitosan/DNA nanoparticles. *Journal of Nanoscience and Nanotechnology*, *6*(9–10), 2796–2803.

Klein, T., Rizzi, S., Reichert, J., Georgi, N, Malda, J., & Schuurman, W. (2009). Strategies for zonal cartilage repair using hydrogels. *Macromolecular Bioscience*, (9), 1049–1058.

Knutsen, G., Drogset, J., Engebretsen, L., Grontvedt, T., Isaksen, V., Ludvigsen, T., … Johansen, O. (2007). A randomized trial comparing autologous chondrocyte implantation with microfracture. Findings at five years. *J Bone Joint Surg Am.*, (89), 2105–2112.

Knutsen, G., Engebretsen, L., Ludvigsen, T., Drogset, J., Grøntvedt, T., & Solheim, E. (2004). Autologous chondrocyte implantation compared with microfracture in the knee—a randomised trial. *J Bone Joint Surg Am.*, (86), 455–464.

Kogan, G., Šoltés, L., Stern, R., & Gemeiner, P. (2007). Hyaluronic acid: A natural biopolymer with a broad range of biomedical and industrial applications. *Biotechnology Letters*, *29*(1), 17–25. https://doi.org/10.1007/s10529-006-9219-z

Kotsuchibashi, Y., Agustin, R. V. C., Lu, J. Y., Hall, D. G., & Narain, R. (2013). Temperature, pH, and glucose responsive gels via simple mixing of boroxole- and glyco-based polymers. *ACS Macro Letters*, *2*(3), 260–264. https://doi.org/10.1021/mz400076p

Kuo, C. K., & Ma, P. X. (2001). Ionically crosslinked alginate hydrogels as scaffolds for tissue

engineering: Part 1. Structure, gelation rate and mechanical properties. *Biomaterials*, *22*(6), 511–521. https://doi.org/10.1016/S0142-9612(00)00201-5

Lallana, E., Rios, J. M., Rosa, D., Tirella, A., Pelliccia, M., Gennari, A., … Tirelli, N. (2017). *Chitosan/Hyaluronic Acid Nanoparticles: Rational Design Revisited for RNA Delivery*. https://doi.org/10.1021/acs.molpharmaceut.7b00320

Lapasin, R. (2016). Rheological characterization of hydrogels. In P. Matricardi, F. Alhaique, & T. Coviello (Eds.), *Polysaccharide Hydrogels: Characterization and Biomedical Applications* (pp. 83–137). https://doi.org/10.4032/9789814613620

Lavertu, M., Filion, D., & Buschmann, M. D. (2008). Heat-induced transfer of protons from chitosan to glycerol phosphate produces chitosan precipitation and gelation. *Biomacromolecules*, *9*(2), 640–650. https://doi.org/10.1021/bm700745d

Lee, H., Gu, L., Mooney, D. J., Levenston, M. E., & Chaudhuri, O. (2017). Mechanical confinement regulates cartilage matrix formation by chondrocytes. *Nature Materials*, *16*, 1243.

Lee, H. P., Gu, L., Mooney, D. J., Levenston, M. E., & Chaudhuri, O. (2017). Mechanical confinement regulates cartilage matrix formation by chondrocytes. *Nature Materials*, *16*(12), 1243–1251. https://doi.org/10.1038/nmat4993

Lee, S., Stanton, A. E., Tong, X., & Yang, F. (2019). Hydrogels with enhanced protein conjugation efficiency reveal stiffness-induced YAP localization in stem cells depends on biochemical cues. *Biomaterials*, *202*(January), 26–34. https://doi.org/10.1016/j.biomaterials.2019.02.021

Leumann, A., Wiewiorski, M., Egelhof, T., Rasch, H., Magerkurth, O., Candrian, C., … Jakob, M, Valderrabano, V. (2009). Radiographic evaluation of frontal talar edge configuration for osteochondral plug transplantation. *Clin Anat*, (22), 261–266.

Levett, P. A., Melchels, F. P. W., Schrobback, K., Hutmacher, D. W., Malda, J., & Klein, T. J. (2014). A biomimetic extracellular matrix for cartilage tissue engineering centered on photocurable gelatin, hyaluronic acid and chondroitin sulfate. *Acta Biomaterialia*, *10*(1), 214–223. https://doi.org/10.1016/j.actbio.2013.10.005

Li, H., Zhao, X., Ma, Y., Zhai, G., Li, L., & Lou, H. (2009). Enhancement of gastrointestinal absorption of quercetin by solid lipid nanoparticles. *Journal of Controlled Release*, *133*(3), 238–244. https://doi.org/10.1016/j.jconrel.2008.10.002

Li, L., Eyckmans, J., & Chen, C. S. (2017). Designer biomaterials for mechanobiology. *Nature*

Materials, *16*(12), 1164–1168. https://doi.org/10.1038/nmat5049

Lieleg, O., Schmoller, K. M., Cyron, C. J., Luan, Y., Wall, W. A., & Bausch, A. R. (2009). Structural polymorphism in heterogeneous cytoskeletal networks. *Soft Matter*, *5*(9), 1796–1803. https://doi.org/10.1039/B814555P

Lietman, S., Miyamoto, S., Brown, P., Inoue, N., & Reddi, A. (2002). The temporalsequence of spontaneous repair of osteochondral defects in the knees ofrabbits is dependent on the geometry of the defect. *J. Bone Joint Surg. Br.*, (84), 600–606.

Lim, S. M., Oh, S. H., Lee, H. H., Yuk, S. H., Im, G. Il, & Lee, J. H. (2010). Dual growth factor-releasing nanoparticle/hydrogel system for cartilage tissue engineering. *Journal of Materials Science: Materials in Medicine*, *21*(9), 2593–2600. https://doi.org/10.1007/s10856-010-4118-1

Liu, F., Li, F., Deng, G., Chen, Y., Zhang, B., Zhang, J., & Liu, C.-Y. (2012). Rheological Images of Dynamic Covalent Polymer Networks and Mechanisms behind Mechanical and Self-Healing Properties. *Macromolecules*, *45*(3), 1636–1645. https://doi.org/10.1021/ma202461e

Liu, K., Mihaila, S. M., Rowan, A., Oosterwijk, E., & Kouwer, P. H. J. (2019). Synthetic Extracellular Matrices with Nonlinear Elasticity Regulate Cellular Organization. *Biomacromolecules*, *20*(2), 826–834. https://doi.org/10.1021/acs.biomac.8b01445

López-león, T., Carvalho, E. L. S., Seijo, B., Ortega-vinuesa, J. L., & Bastos-González, D. (2005). Physicochemical characterization of chitosan nanoparticles : electrokinetic and stability behavior. *Journal of Colloid and Interface Science*, *283*, 344–351. https://doi.org/10.1016/j.jcis.2004.08.186

Lou, J., Stowers, R., Nam, S., Xia, Y., & Chaudhuri, O. (2018). Stress relaxing hyaluronic acid-collagen hydrogels promote cell spreading, fiber remodeling, and focal adhesion formation in 3D cell culture. *Biomaterials*, *154*, 213–222. https://doi.org/10.1016/j.biomaterials.2017.11.004

Luo, Y., & Wang, Q. (2014). Recent development of chitosan-based polyelectrolyte complexes with natural polysaccharides for drug delivery. *International Journal of Biological Macromolecules*, *64*, 353–367. https://doi.org/10.1016/j.ijbiomac.2013.12.017

Ma, L., Xu, J., Coulombe, P. A., & Wirtz, D. (1999). Keratin filament suspensions show unique micromechanical properties. *Journal of Biological Chemistry*, *274*(27), 19145–19151. https://doi.org/10.1074/jbc.274.27.19145

Maleki, A., Kjøniksen, A. L., & Nyström, B. (2007). Characterization of the chemical degradation of

hyaluronic acid during chemical gelation in the presence of different cross-linker agents. *Carbohydrate Research*, *342*(18), 2776–2792. https://doi.org/10.1016/j.carres.2007.08.021

Mankin, H. (1982). The response of articular cartilage to mechanical injury. *J Bone Joint Surg Am.*, (64), 460–466.

Manna, U., Bharani, S., & Patil, S. (2009). Layer-by-layer self-assembly of modified hyaluronic acid/chitosan based on hydrogen bonding. *Biomacromolecules*, *10*(9), 2632–2639. https://doi.org/10.1021/bm9005535

Marcon, P., Marsich, E., Vetere, A., Mozetic, P., Campa, C., Donati, I., … Paoletti, S. (2005). The role of Galectin-1 in the interaction between chondrocytes and a lactose-modified chitosan. *Biomaterials*, *26*(24), 4975–4984. https://doi.org/10.1016/j.biomaterials.2005.01.044

Marsich, E., Borgogna, M., Donati, I., Mozetic, P., Strand, B. L., Salvador, S. G., … Paoletti, S. (2008). Alginate/lactose-modified chitosan hydrogels: a bioactive biomaterial for chondrocyte encapsulation. *Journal of Biomedical Materials Research. Part A*, *84*(2), 364–376. https://doi.org/10.1002/jbm.a.31307

Marsich, E., Travan, A., Feresini, M., Lapasin, R., Paoletti, S., & Donati, I. (2013). Polysaccharide-based polyanion-polycation-polyanion ternary systems in the concentrated regime and hydrogel form. *Macromolecular Chemistry and Physics*, *214*(12), 1309–1320. https://doi.org/10.1002/macp.201300057

Masarudin, M. J., Cutts, S. M., Evison, B. J., Phillips, D. R., & Pigram, P. J. (2015). Factors determining the stability, size distribution, and cellular accumulation of small, monodisperse chitosan nanoparticles as candidate vectors for anticancer drug delivery: Application to the passive encapsulation of [14C]-doxorubicin. *Nanotechnology, Science and Applications*, *8*, 67–80. https://doi.org/10.2147/NSA.S91785

Matricardi, P., Alhaique, F., & Coviello, T. (2016). Polysaccharide hydrogels: Characterization and biomedical applications. In P. Matricardi, F. Alhaique, & T. Coviello (Eds.), *Polysaccharide Hydrogels: Characterization and Biomedical Applications*. https://doi.org/10.4032/9789814613620

Mauch, L., Lun, A., O'Gorman, M. R. G., Harris, J. S., Schulze, I., Zychlinsky, A., … Roesler, J. (2007). Chronic granulomatous disease (CGD) and complete myeloperoxidase deficiency both yield strongly reduced dihydrorhodamine 123 test signals but can be easily discerned in routine testing for CGD. *Clinical Chemistry*, *53*(5), 890–896.

https://doi.org/10.1373/clinchem.2006.083444

Mauck, R. L., Soltz, M. A., Wang, C. C. B., Wong, D. D., Chao, P. H. G., Valhmu, W. B., … Ateshian, G. A. (2000). Functional tissue engineering of articular cartilage through dynamic loading of chondrocyte-seeded agarose gels. *Journal of Biomechanical Engineering*, *122*(3), 252–260. https://doi.org/10.1115/1.429656

Mayumi, K., Marcellan, A., Ducouret, G., Creton, C., & Narita, T. (2013). Stress–Strain Relationship of Highly Stretchable Dual Cross-Link Gels: Separability of Strain and Time Effect. *ACS Macro Letters*, *2*(12), 1065–1068. https://doi.org/10.1021/mz4005106

McKinnon, D. D., Domaille, D. W., Cha, J. N., & Anseth, K. S. (2014). Biophysically defined and cytocompatible covalently adaptable networks as viscoelastic 3d cell culture systems. *Advanced Materials*, *26*(6), 865–872. https://doi.org/10.1002/adma.201303680

Medelin, M., Porrelli, D., Aurand, E. R., Scaini, D., Travan, A., Borgogna, M. A., … Ballerini, L. (2018). Exploiting natural polysaccharides to enhance in vitro bio-constructs of primary neurons and progenitor cells. *Acta Biomaterialia*, *73*, 285–301. https://doi.org/10.1016/j.actbio.2018.03.041

Menegazzi, R., Busetto, S., Dri, P., Cramer, R., & Patriarca, P. (1996). Chloride ion efflux regulates adherence, spreading, and respiratory burst of neutrophils stimulated by tumor necrosis factor-alpha (TNF) on biologic surfaces. *The Journal of Cell Biology*, *135*(2). Retrieved from http://jcb.rupress.org/content/135/2/511

Menegazzi, R., Zabucchi, G., Knowles, A., Cramer, R., & Patriarca, P. (1992). A new, one-step assay on whole cell suspensions for peroxidase secretion by human neutrophils and eosinophils. *Journal of Leukocyte Biology*, *52*(6), 619–624.

Menzel, E. J., & Farr, C. (1998). Hyaluronidase and its substrate hyaluronan: Biochemistry, biological activities and therapeutic uses. *Cancer Letters*, *131*(1), 3–11. https://doi.org/10.1016/S0304-3835(98)00195-5

Mero, A., & Campisi, M. (2014). Hyaluronic acid bioconjugates for the delivery of bioactive molecules. *Polymers*, *6*(1), 346–369. https://doi.org/10.3390/polym6020346

Mi, F. L., Sung, H. W., Shyu, S. S., Su, C. C., & Peng, C. K. (2003). Synthesis and characterization of biodegradable TPP/genipin co-crosslinked chitosan gel beads. *Polymer*, *44*(21), 6521–6530. https://doi.org/10.1016/S0032-3861(03)00620-7

Miladi, K., Sfar, S., Fessi, H., & Elaissari, A. (2015). Enhancement of alendronate encapsulation in chitosan nanoparticles. *Journal of Drug Delivery Science and Technology*, *30*, 391–396. https://doi.org/10.1016/j.jddst.2015.04.007

Mobasheri, A., Shakibaei, M., Mobasheri, R., Richardson, S., & Hoyland, J. (2006). Glucose Sensing in Chondrocytes via GLUT1 and GLUT3: Implications for Articular Cartilage and Intervertebral Disc Metabolism. *Current Rheumatology Reviews*, *2*(2), 109–121. https://doi.org/10.2174/157339706776876071

Moghimi, E., Jacob, A. R., Koumakis, N., & Petekidis, G. (2017). Colloidal gels tuned by oscillatory shear. *Soft Matter*, *13*(12), 2371–2383. https://doi.org/10.1039/C6SM02508K

Montanari, E., Capece, S., Di Meo, C., Meringolo, M., Coviello, T., Agostinelli, E., & Matricardi, P. (2013). Hyaluronic acid nanohydrogels as a useful tool for BSAO immobilization in the treatment of melanoma cancer cells. *Macromolecular Bioscience*, *13*(9), 1185–1194. https://doi.org/10.1002/mabi.201300114

Montanari, E., Meo, C. Di, Coviello, T., Gueguen, V., Pavon-djavid, G., & Matricardi, P. (2019). *Intracellular Delivery of Natural Antioxidants via Hyaluronan Nanohydrogels*.

Moore, G. K., & Roberts, G. A. F. (1980). Chitosan gels: 2. Mechanism of gelation. *International Journal of Biological Macromolecules*, *2*(2), 78–80. https://doi.org/10.1016/0141-8130(80)90032-X

Mow, V., Holmes, M., & Lai, W. (1984). Fluid transport and mechanical properties of articular cartilage: a review. *J Biomech.*, (17), 377–394.

Muzzarelli, R. A. A. (2009). Genipin-crosslinked chitosan hydrogels as biomedical and pharmaceutical aids. *Carbohydrate Polymers*, *77*(1), 1–9. https://doi.org/10.1016/j.carbpol.2009.01.016

Muzzarelli, R. A. A., El Mehtedi, M., Bottegoni, C., Aquili, A., & Gigante, A. (2015). Genipin-crosslinked chitosan gels and scaffolds for tissue engineering and regeneration of cartilage and bone. *Marine Drugs*, *13*(12), 7314–7338. https://doi.org/10.3390/md13127068

Mwale, F., Iordanova, M., Demers, C. N., Steffen, T., Roughley, P., & Antoniou, J. (2005). Biological evaluation of chitosan salts cross-linked to genipin as a cell scaffold for disk tissue engineering. *Tissue Engineering*, *11*(1–2), 130–140. https://doi.org/10.1089/ten.2005.11.130

Nam, S., Hu, K. H., Butte, M. J., & Chaudhuri, O. (2016). *Strain-enhanced stress relaxation impacts*

nonlinear elasticity in collagen gels. *113*(20), 1–6. https://doi.org/10.1073/pnas.1523906113

Narita, T., Mayumi, K., Ducouret, G., & Hébraud, P. (2013). Viscoelastic properties of poly(vinyl alcohol) hydrogels having permanent and transient cross-links studied by microrheology, classical rheometry, and dynamic light scattering. *Macromolecules*, *46*(10), 4174–4183. https://doi.org/10.1021/ma400600f

Nguyen, L. H., Kudva, A. K., Guckert, N. L., Linse, K. D., & Roy, K. (2011). Unique biomaterial compositions direct bone marrow stem cells into specific chondrocytic phenotypes corresponding to the various zones of articular cartilage. *Biomaterials*, *32*(5), 1327–1338. https://doi.org/10.1016/j.biomaterials.2010.10.009

Niaz, T., Shabbir, S., Manzoor, S., Rehman, A., Rahman, A., Nasir, H., & Imran, M. (2016). Antihypertensive nano-ceuticales based on chitosan biopolymer: Physico-chemical evaluation and release kinetics. *Carbohydrate Polymers*, *142*, 268–274. https://doi.org/10.1016/j.carbpol.2016.01.047

Nilsen-Nygaard, J., Strand, S. P., Vårum, K. M., Draget, K. I., & Nordgård, C. T. (2015). Chitosan: Gels and interfacial properties. *Polymers*, *7*(3), 552–579. https://doi.org/10.3390/polym7030552

Oliver-De La Cruz, J., Nardone, G., Vrbsky, J., Pompeiano, A., Perestrelo, A. R., Capradossi, F., … Forte, G. (2019). Substrate mechanics controls adipogenesis through YAP phosphorylation by dictating cell spreading. *Biomaterials*, *205*(November 2018), 64–80. https://doi.org/10.1016/j.biomaterials.2019.03.009

Oyarzun-Ampuero, F. A., Brea, J., Loza, M. I., Torres, D., & Alonso, M. J. (2009). Chitosan-hyaluronic acid nanoparticles loaded with heparin for the treatment of asthma. *International Journal of Pharmaceutics*, *381*(2), 122–129. https://doi.org/10.1016/j.ijpharm.2009.04.009

Pandit, V., Zuidema, J. M., Venuto, K. N., Macione, J., Dai, G., Gilbert, R. J., & Kotha, S. P. (2013). Evaluation of multifunctional polysaccharide hydrogels with varying stiffness for bone tissue engineering. *Tissue Engineering - Part A*, *19*(21–22), 2452–2463. https://doi.org/10.1089/ten.tea.2012.0644

Paoletti, S., Donati, I., & Marsich, E. (2007). *Polymer Mixtures of Anionic and Cationic Polysaccharides and use thereof: WO/2007/135116A1; US8951991B2; EP2021408B1*.

Paoletti, S., Donati, I., & Marsich, E. (2009). *Patent No. EP2021408B1*.

Parajó, Y., D'Angelo, I., Welle, A., Garcia-Fuentes, M., & Alonso, M. J. (2010). Hyaluronic

acid/Chitosan nanoparticles as delivery vehicles for VEGF and PDGF-BB. *Drug Delivery*, *17*(November 2009), 596–604. https://doi.org/10.3109/10717544.2010.509357

Park, J. H., Saravanakumar, G., Kim, K., & Kwon, I. C. (2010). Targeted delivery of low molecular drugs using chitosan and its derivatives. *Advanced Drug Delivery Reviews*, *62*(1), 28–41. https://doi.org/10.1016/j.addr.2009.10.003

Peters, J. A. (2014). Interactions between boric acid derivatives and saccharides in aqueous media: Structures and stabilities of resulting esters. *Coordination Chemistry Reviews*, *268*, 1–22. https://doi.org/https://doi.org/10.1016/j.ccr.2014.01.016

Pettignano, A., Grijalvo, S., Häring, M., Eritja, R., Tanchoux, N., Quignard, F., & Díaz Díaz, D. (2017). Boronic acid-modified alginate enables direct formation of injectable, self-healing and multistimuli-responsive hydrogels. *Chemical Communications*, *53*(23), 3350–3353. https://doi.org/10.1039/c7cc00765e

Poole, A. R., Kojima, T., Yasuda, T., Mwale, F., Kobayashi, M., & Laverty, S. (2001). Composition and structure of articular cartilage: A template for tissue repair. *Clinical Orthopaedics and Related Research*, (391 SUPPL.). https://doi.org/10.1097/00003086-200110001-00004

Qin, L. X., & Tang, Z. Y. (2002). The prognostic molecular markers in hepatocellular carcinoma. *World Journal of Gastroenterology*, *8*(3), 385–392.

Rabea, E. I., Stevens, C. V, Smagghe, G., & Steurbaut, W. (2003). Chitosan as Antimicrobial Agent: Applications and Mode of Action. *Biomacromolecules*, *4*(6).

Racine, L., Texier, I., & Auzély-Velty, R. (2017). Chitosan-based hydrogels: recent design concepts to tailor properties and functions. *Polymer International*, *66*(7), 981–998. https://doi.org/10.1002/pi.5331

Raemdonck, K., Martens, T. F., Braeckmans, K., Demeester, J., & De Smedt, S. C. (2013). Polysaccharide-based nucleic acid nanoformulations. *Advanced Drug Delivery Reviews*, *65*(9), 1123–1147. https://doi.org/10.1016/j.addr.2013.05.002

Rao, W., Wang, H., Han, J., Zhao, S., Dumbleton, J., Agarwal, P., … He, X. (2015). Chitosan-Decorated Doxorubicin-Encapsulated Nanoparticle Targets and Eliminates Tumor Reinitiating Cancer Stem-like Cells. *ACS Nano*, *9*(6), 5725–5740. https://doi.org/10.1021/nn506928p

Reguzzoni, M., Manelli, A., Ronga, M, Raspanti, M., & Grassi, F. (2005). Histology and ultrastructure of a tissue-engineered collagen meniscus before and after implantation. *J Biomed*

Mater Res B Appl Biomater, (74), 808–816.

Repetto, G., del Peso, A., & Zurita, J. L. (2008). Neutral red uptake assay for the estimation of cell viability/cytotoxicity. *Nature Protocols*, *3*(7), 1125–1131. https://doi.org/10.1038/nprot.2008.75

Richardson, J., Caterson, B., Evans, E., Ashton, B., & Roberts, S. (1999). Repair of human articular cartilage after implantation of autologous chondrocytes. *J Bone Joint Surg Br*, (81), 1064–1068.

Rinaldi, M., Moroni, P., Paape, M. J., & Bannerman, D. D. (2007). Evaluation of assays for the measurement of bovine neutrophil reactive oxygen species. *Veterinary Immunology and Immunopathology*, *115*(1–2), 107–125. https://doi.org/10.1016/j.vetimm.2006.09.009

Rinaudo, M. (2006). Chitin and chitosan: Properties and applications. *Progress in Polymer Science (Oxford)*, *31*(7), 603–632. https://doi.org/10.1016/j.progpolymsci.2006.06.001

Rinaudo, M. (2008). Main properties and current applications of some polysaccharides as biomaterials. *Polym Int*, *57*(57), 397–430.

Rios de la Rosa, J. M., Tirella, A., Gennari, A., Stratford, I. J., & Tirelli, N. (2017). The CD44-Mediated Uptake of Hyaluronic Acid-Based Carriers in Macrophages. *Advanced Healthcare Materials*, *6*(4), 1601012. https://doi.org/10.1002/adhm.201601012

Robert, A., Rossow, M. J., Hookway, C., Adam, S. A., & Gelfand, V. I. (2015). Vimentin filament precursors exchange subunits in an ATP-dependent manner. *Proceedings of the National Academy of Sciences*, *112*(27), E3505 LP-E3514.

Rowley, J. A., Madlambayan, G., & Mooney, D. J. (1999). Alginate hydrogels as synthetic extracellular matrix materials. *Biomaterials*, *20*(1), 45–53. https://doi.org/10.1016/S0142-9612(98)00107-0

Ruel-Gariepy, E., Chenite, A., Chaput, C., Guirguis, S., & Leroux, J. (2000). *Characterization of thermosensitive chitosan gels for the sustained delivery of drugs*. *203*, 89–98.

Sacco, P., Furlani, F., Cok, M., Travan, A., Borgogna, M., Marsich, E., … Donati, I. (2017). Boric Acid Induced Transient Cross-Links in Lactose-Modified Chitosan (Chitlac). *Biomacromolecules*, *18*(12), 4206–4213. https://doi.org/10.1021/acs.biomac.7b01237

Sacco, Pasquale, Borgogna, M., Travan, A., Marsich, E., Paoletti, S., Asaro, F., … Donati, I. (2014). Polysaccharide-based networks from homogeneous chitosan-tripolyphosphate hydrogels: Synthesis and characterization. In *Biomacromolecules* (Vol. 15).

https://doi.org/10.1021/bm500909n

Sacco, Pasquale, Brun, F., Donati, I., Porrelli, D., Paoletti, S., & Turco, G. (2018). On the Correlation between the Microscopic Structure and Properties of Phosphate-Cross-Linked Chitosan Gels. *ACS Applied Materials & Interfaces*, *10*(13), 10761–10770. https://doi.org/10.1021/acsami.8b01834

Sacco, Pasquale, Cok, M., Asaro, F., Paoletti, S., & Donati, I. (2018). The role played by the molecular weight and acetylation degree in modulating the stiffness and elasticity of chitosan gels. *Carbohydrate Polymers*, *196*(May), 405–413. https://doi.org/10.1016/j.carbpol.2018.05.060

Sacco, Pasquale, Decleva, E., Tentor, F., Menegazzi, R., Borgogna, M., Paoletti, S., … Marsich, E. (2017). Butyrate-Loaded Chitosan/Hyaluronan Nanoparticles: A Suitable Tool for Sustained Inhibition of ROS Release by Activated Neutrophils. *Macromolecular Bioscience*, *17*(11). https://doi.org/10.1002/mabi.201700214

Sacco, Pasquale, Furlani, F., Cok, M., Travan, A. A., Borgogna, M., Marsich, E., … Donati, I. (2017). Boric Acid Induced Transient Cross-Links in Lactose-Modified Chitosan (Chitlac). *Biomacromolecules*, *18*(12), 4206–4213. https://doi.org/10.1021/acs.biomac.7b01237

Sacco, Pasquale, Furlani, F., Paoletti, S., & Donati, I. (2019). pH-Assisted Gelation of Lactose-Modified Chitosan. *Biomacromolecules*, acs.biomac.9b00636. https://doi.org/10.1021/acs.biomac.9b00636

Sannan, T., Kurita, K., & Iwakura, Y. (1976). Studies on chitin, 2. Effect of deacetylation on solubility. *Die Makromolekulare Chemie*, *177*(12), 3589–3600. https://doi.org/10.1002/macp.1976.021771210

Setton, L., Mow, V., & Howell, D. (1995). Changes in the sheer properties of the canine knee cartilage resulting from anterior cruciate transaction. *J Orthop Res.*, (13), 473–482.

Silva, S. S., Oliveira, J. M., Sá-Lima, H., Sousa, R. A., Mano, J. F., & Reis, R. L. (2011). Polymers of biological origin. In *Comprehensive Biomaterials* (Vol. 2). https://doi.org/10.1016/b978-0-08-055294-1.00069-6

Smithmyer, M. E., Deng, C. C., Cassel, S. E., LeValley, P. J., Sumerlin, B. S., & Kloxin, A. M. (2018). Self-Healing Boronic Acid-Based Hydrogels for 3D Co-cultures. *ACS Macro Letters*, 1105–1110. https://doi.org/10.1021/acsmacrolett.8b00462

Sogias, I. A., Williams, A. C., & Khutoryanskiy, V. V. (2008). Why is chitosan mucoadhesive? *Biomacromolecules*, *9*(7), 1837–1842. https://doi.org/10.1021/bm800276d

Sorlier, P., Denuzière, A., Viton, C., & Domard, A. (2001). Relation between the Degree of Acetylation and the Electrostatic Properties of Chitin and Chitosan. *Biomacromolecules*, *2*(3), 765–772. https://doi.org/10.1021/bm015531+

Springsteen, G., & Wang, B. (2002). A detailed examination of boronic acid–diol complexation. *Tetrahedron*, *58*(26), 5291–5300. https://doi.org/https://doi.org/10.1016/S0040-4020(02)00489-1

Stanton, A. E., Tong, X., Lee, S., & Yang, F. (2019). Biochemical Ligand Density Regulates Yes-Associated Protein Translocation in Stem Cells through Cytoskeletal Tension and Integrins [Research-article]. *ACS Applied Materials and Interfaces*, *11*(9), 8849–8857. https://doi.org/10.1021/acsami.8b21270

Steadman, J. R., Briggs, K. K., Rodrigo, J. J., Kocher, M. S., Gill, T. J., & Rodkey, W. G. (2003). Outcomes of microfracture for traumatic chondral defects of the knee:average 11-year follow-up. *Arthroscopy*, (19), 477–484.

Steadman, J., Rodkey, W., Briggs, K., & Rodrigo, J. (1999). The microfracture technic in the management of complete cartilage defects in the knee joint. *Orthopade*, (28), 26–32.

Storm, C., Pastore, J. J., MacKintosh, F., Lubensky, T., & Jamney, P. A. (2005). Nonlinear elasticity in biological gels. *Nature*, *435*(May), 191–194. https://doi.org/10.1038/nature03497.1.

Sundström, C., & Nilsson, K. (1976). Establishment and characterization of a human histiocytic lymphoma cell line (U-937). *International Journal of Cancer*, *17*(5), 565–577. https://doi.org/10.1002/ijc.2910170504

Sung, H. W., Huang, R. N., Huang, L. H., & Tsai, C. C. (1999). In vitro evaluation of cytotoxicity of a naturally occurring cross-linking reagent for biological tissue fixation. *Journal of Biomaterials Science, Polymer Edition*, *10*(1), 63–78. https://doi.org/10.1163/156856299X00289

Supper, S., Anton, N., Boisclair, J., Seidel, N., Riemenschnitter, M., Curdy, C., & Vandamme, T. (2014). Chitosan/glucose 1-phosphate as new stable in situ forming depot system for controlled drug delivery. *European Journal of Pharmaceutics and Biopharmaceutics*, *88*(2), 361–373. https://doi.org/10.1016/j.ejpb.2014.05.015

Supper, S., Anton, N., Seidel, N., Riemenschnitter, M., Curdy, C., & Vandamme, T. (2014).

Thermosensitive chitosan/glycerophosphate-based hydrogel and its derivatives in pharmaceutical and biomedical applications. *Expert Opinion on Drug Delivery*, *11*(2), 249–267. https://doi.org/10.1517/17425247.2014.867326

Swierczewska, M., Han, H. S., Kim, K., Park, J. H., & Lee, S. (2016). Polysaccharide-based nanoparticles for theranostic nanomedicine. *Advanced Drug Delivery Reviews*, *99*, 70–84. https://doi.org/10.1016/j.addr.2015.11.015

Ta, H. T., Han, H., Larson, I., Dass, C. R., & Dunstan, D. E. (2009). Chitosan-dibasic orthophosphate hydrogel: A potential drug delivery system. *International Journal of Pharmaceutics*, *371*(1–2), 134–141. https://doi.org/10.1016/j.ijpharm.2009.01.018

Tallian, C., Herrero-Rollett, A., Stadler, K., Vielnascher, R., Wieland, K., Weihs, A. M., … Guebitz, G. M. (2018). Structural insights into pH-responsive drug release of self-assembling human serum albumin-silk fibroin nanocapsules. *European Journal of Pharmaceutics and Biopharmaceutics*, *133*(October), 176–187. https://doi.org/10.1016/j.ejpb.2018.10.002

Tam, K. C., Jenkins, R. D., Winnik, M. A., & Bassett, D. R. (1998). A Structural Model of Hydrophobically Modified Urethane−Ethoxylate (HEUR) Associative Polymers in Shear Flows. *Macromolecules*, *31*(13), 4149–4159. https://doi.org/10.1021/ma980148r

Tan, H., Gao, X., Sun, J., Xiao, C., & Hu, X. (2013). Double stimulus-induced stem cell aggregation during differentiation on a biopolymer hydrogel substrate. *Chemical Communications*, *49*(98), 11554. https://doi.org/10.1039/c3cc47101b

Tang, S., Habicht, A., Li, S., Seiffert, S., & Olsen, B. D. (2016). Self-Diffusion of Associating Star-Shaped Polymers. *Macromolecules*, *49*(15), 5599–5608. https://doi.org/10.1021/acs.macromol.6b00959

Tang, S., Ma, H., Tu, H.-C. C., Wang, H.-R. R., Lin, P.-C. C., & Anseth, K. S. (2018). Adaptable Fast Relaxing Boronate-Based Hydrogels for Probing Cell-Matrix Interactions. *Advanced Science*, *1800638*, 1–8. https://doi.org/10.1002/advs.201800638

Tarus, D., Hachet, E., Messager, L., Catargi, B., Ravaine, V., & Auzély-Velty, R. (2014). Readily prepared dynamic hydrogels by combining phenyl boronic acid-and maltose-modifi ed anionic polysaccharides at neutral pH. *Macromolecular Rapid Communications*, *35*(24), 2089–2095. https://doi.org/10.1002/marc.201400477

Thu, B., Bruheim, P., Espevik, T., Smidsrød, O., Soon-Shiong, P., & Skjåk-Bræk, G. (1996). Alginate polycation microcapsules: I. Interaction between alginate and polycation. *Biomaterials*, *17*(10),

1031–1040. https://doi.org/10.1016/0142-9612(96)84680-1

Tibbitt, M. W., & Anseth, K. S. (2009). Hydrogels as extracellular matrix mimics for 3D cell culture. *Biotechnology and Bioengineering*, *103*(4), 655–663. https://doi.org/10.1002/bit.22361

Torzilli, P., Grigiene, R., Borrelli, J. J., & Helfet, D. (1999). Effect of impact load on articular cartilage: cell metabolism and viability, and matrix water content. *J Biomech Eng.*, (121), 433–441.

Travan, A., Marsich, E., Donati, I., Foulc, M.-P., Moritz, N., Aro, H. T., & Paoletti, S. (2012). Polysaccharide-Coated Thermosets for Orthopedic Applications: From Material Characterization to In Vivo Tests. *Biomacromolecules*, *13*(5), 1564–1572. https://doi.org/10.1021/bm3002683

Tripodo, G., Trapani, A., Torre, M. L., Giammona, G., Trapani, G., & Mandracchia, D. (2015). Hyaluronic acid and its derivatives in drug delivery and imaging: Recent advances and challenges. *European Journal of Pharmaceutics and Biopharmaceutics*, *97*(Pt B), 400–416. https://doi.org/10.1016/j.ejpb.2015.03.032

Udalova, I. A., Mantovani, A., & Feldmann, M. (2016). Macrophage heterogeneity in the context of rheumatoid arthritis. *Nature Reviews Rheumatology*. https://doi.org/10.1038/nrrheum.2016.91

Vafaei, S. Y., Esmaeili, M., Amini, M., Atyabi, F., Ostad, S. N., & Dinarvand, R. (2016). Self assembled hyaluronic acid nanoparticles as a potential carrier for targeting the inflamed intestinal mucosa. *Carbohydrate Polymers*, *144*, 371–381. https://doi.org/10.1016/j.carbpol.2016.01.026

Varelas, X., Abercrombie, M., Alarcön, C., Zaromytidou, A.-I., Xi, Q., Gao, S., … Yang, X. (2014). The Hippo pathway effectors TAZ and YAP in development, homeostasis and disease. *Development (Cambridge, England)*, *141*(8), 1614–1626. https://doi.org/10.1242/dev.102376

Vårum, K M, Anthonsen, M. W., Grasdalen, H., & Smidsrød, O. (1991). Determination of the degree of N-acetylation and the distribution of N-acetyl groups in partially N-deacetylated chitins (chitosans) by high-field n.m.r. spectroscopy. *Carbohydrate Research*, *211*(1), 17–23.

Vårum, Kjell M., Ottøy, M. H., & Smidsrød, O. (1994). Water-solubility of partially N-acetylated chitosans as a function of pH: effect of chemical composition and depolymerisation. *Carbohydrate Polymers*, *25*(2), 65–70. https://doi.org/10.1016/0144-8617(94)90140-6

Vårum, Kjell M, & Smidsrød, O. (2004). Structure-Property Relationship in Chitosans. In S. Dumitriu

(Ed.), *Polysaccharides: Structural Diversity and Functional Versatility* (Vol. 30, pp. 625–642). https://doi.org/10.1201/9781420030822.ch26

Vasiliadis, H. S., Wasiak, J., & Salanti, G. (2010). Autologous chondrocyte implantation for the treatment of cartilage lesions of the knee: A systematic review of randomized studies. *Knee Surgery, Sports Traumatology, Arthroscopy, 18*(12), 1645–1655. https://doi.org/10.1007/s00167-010-1050-3

Vatankhah-Varnosfaderani, M., Daniel, W. F. M., Everhart, M. H., Pandya, A. A., Liang, H., Matyjaszewski, K., … Sheiko, S. S. (2017). Mimicking biological stress–strain behaviour with synthetic elastomers. *Nature, 549*(7673), 497–501. https://doi.org/10.1038/nature23673

Vecchies, F., Sacco, P., Decleva, E., Menegazzi, R., Porrelli, D., Donati, I., … Marsich, E. (2018). Complex Coacervates between a Lactose-Modified Chitosan and Hyaluronic Acid as Radical-Scavenging Drug Carriers. *Biomacromolecules, 19*(10), 3936–3944. https://doi.org/10.1021/acs.biomac.8b00863

Vimal, S., Abdul Majeed, S., Taju, G., Nambi, K. S. N., Sundar Raj, N., Madan, N., … Sahul Hameed, A. S. (2013). Chitosan tripolyphosphate (CS/TPP) nanoparticles: Preparation, characterization and application for gene delivery in shrimp. *Acta Tropica*, *128*(3), 486–493. https://doi.org/10.1016/j.actatropica.2013.07.013

Wang, C., Lau, T. T., Loh, W. L., Su, K., & Wang, D. A. (2011). Cytocompatibility study of a natural biomaterial crosslinker-Genipin with therapeutic model cells. *Journal of Biomedical Materials Research - Part B Applied Biomaterials*, *97 B*(1), 58–65. https://doi.org/10.1002/jbm.b.31786

Wang, L., & Stegemann, J. P. (2010). Thermogelling chitosan and collagen composite hydrogels initiated with β-glycerophosphate for bone tissue engineering. *Biomaterials, 31*(14), 3976–3985. https://doi.org/10.1016/j.biomaterials.2010.01.131

Wang, S. (1992). Transient Network Theory for Shear-Thickening Fluids and Physically Cross-Linked Systems. *Macromolecules*, 7003–7010.

Wang, T., Lacik, I., Brissova, M., Anilkumar, A. V, Prokop, A., Hunkeler, D., … Powers, A. C. (1997). Immunoisolation of pancreatic islets. *Nature Biotechnology*, *15*(April), 358–403.

Webber, M. J., Khan, O. F., Sydlik, S. A., Tang, B. C., & Langer, R. (2015). A perspective on the clinical translation of scaffolds for tissue engineering. *Annals of Biomedical Engineering*, *43*(3), 641–656. https://doi.org/10.1007/s10439-014-1104-7

Woo, S., Mow, V., & Lai, W. (1987). Biomechanical properties of articular cartilage. In E. Skalak R, Chen S (Ed.), *Handbook of Bioengineering.* (pp. 4.1-4.44). New York, NY: McGraw-Hill Book Co.

Wu, D., & Delair, T. (2015). Stabilization of chitosan/hyaluronan colloidal polyelectrolyte complexes in physiological conditions. *Carbohydrate Polymers*, *119*, 149–158. https://doi.org/10.1016/j.carbpol.2014.11.042

Wu, X., Li, Z., Chen, X.-X., Fossey, J. S., James, T. D., & Jiang, Y.-B. (2013). Selective sensing of saccharides using simple boronic acids and their aggregates. *Chemical Society Reviews*, *42*(20), 8032–8048. https://doi.org/10.1039/C3CS60148J

Wu, Y., Yang, W., Wang, C., Hu, J., & Fu, S. (2005). Chitosan nanoparticles as a novel delivery system for ammonium glycyrrhizinate. *International Journal of Pharmaceutics*, *295*(1–2), 235–245. https://doi.org/10.1016/j.ijpharm.2005.01.042

Xu, Jingyuan, Schwarz, W. H., Käs, J. A., Stossel, T. P., Janmey, P. A., & Pollard, T. D. (1998). Mechanical properties of actin filament networks depend on preparation, polymerization conditions, and storage of actin monomers. *Biophysical Journal*, *74*(5), 2731–2740. https://doi.org/10.1016/S0006-3495(98)77979-2

Xu, Jinke, Strandman, S., Zhu, J. X. X., Barralet, J., & Cerruti, M. (2015). Genipin-crosslinked catechol-chitosan mucoadhesive hydrogels for buccal drug delivery. *Biomaterials*, *37*, 395–404. https://doi.org/10.1016/j.biomaterials.2014.10.024

Yang, J., Han, S., Zheng, H., Dong, H., & Liu, J. (2015). Preparation and application of micro/nanoparticles based on natural polysaccharides. *Carbohydrate Polymers*, *123*, 53–66. https://doi.org/10.1016/j.carbpol.2015.01.029

Yao, N. Y., Broedersz, C. P., Depken, M., Becker, D. J., Pollak, M. R., MacKintosh, F. C., & Weitz, D. A. (2013). Stress-Enhanced Gelation: A Dynamic Nonlinearity of Elasticity. *Physical Review Letters*, *110*(1), 18103. https://doi.org/10.1103/PhysRevLett.110.018103

Yesilyurt, V., Webber, M. J., Appel, E. A., Godwin, C., Langer, R., & Anderson, D. G. (2016). Injectable Self-Healing Glucose-Responsive Hydrogels with pH- Regulated Mechanical Properties. *Advanced Materials*, *91*(2), 165–171. https://doi.org/10.1016/j.chemosphere.2012.12.037.Reactivity

Yin, L., Ding, J., He, C., Cui, L., Tang, C., & Yin, C. (2009). Drug permeability and mucoadhesion properties of thiolated trimethyl chitosan nanoparticles in oral insulin delivery. *Biomaterials*,

30(29), 5691–5700. https://doi.org/10.1016/j.biomaterials.2009.06.055

Ying, G., Xiong, W., Wang, H., Sun, Y., & Liu, H. (2011). Preparation, water solubility and antioxidant activity of branched-chain chitosan derivatives. *Carbohydrate Polymers*, *83*(4), 1787–1796. https://doi.org/10.1016/J.CARBPOL.2010.10.037

Zambito, Y., Felice, F., Fabiano, A., Di Stefano, R., & Di Colo, G. (2013). Mucoadhesive nanoparticles made of thiolated quaternary chitosan crosslinked with hyaluronan. *Carbohydrate Polymers*, *92*(1), 33–39. https://doi.org/10.1016/j.carbpol.2012.09.029

Zhang, H., Oh, M., Allen, C., & Kumacheva, E. (2004). Monodisperse Chitosan Nanoparticles for Mucosal Drug Delivery. *Biomacromolecules*, *5*, 2461–2468. https://doi.org/10.1021/bm0496211

Zhang, Y. S., & Khademhosseini, A. (2017). Advances in engineering hydrogels. *Science*, *356*(6337). https://doi.org/10.1126/science.aaf3627

Zhang, Y., Tao, L., Li, S., & Wei, Y. (2011). Synthesis of multiresponsive and dynamic chitosan-based hydrogels for controlled release of bioactive molecules. *Biomacromolecules*, *12*, 2894–2901. https://doi.org/10.1021/bm200423f

Zhong, W., Li, Y., Li, L., Zhang, W., Wang, S., & Zheng, X. (2013). YAP-mediated regulation of the chondrogenic phenotype in response to matrix elasticity. *Journal of Molecular Histology*, *44*(5), 587–595. https://doi.org/10.1007/s10735-013-9502-y

Zhou, H. Y., Jiang, L. J., Cao, P. P., Li, J. B., & Chen, X. G. (2015). Glycerophosphate-based chitosan thermosensitive hydrogels and their biomedical applications. *Carbohydrate Polymers*, *117*, 524–536. https://doi.org/10.1016/j.carbpol.2014.09.094

6 AKNOWLEDGEMENTS

I’d like to thank all the people who have supported me during the whole Ph.D.

First of all I’d like to thank Prof. Sergio Paoletti and Prof. Ivan Donati for giving me the possibility to pursue the doctoral degree in the lab headed by them at the University of Trieste. I’d like to thank my co-supervisors Prof. Eleonora Marsich and Dr. Pasquale Sacco for the extraordinary help in the experimental activity. Scientific discussions with all of them greatly helped me to grow as a “researcher”.

I’d like to thank my labmates Massimiliano, Andrea, Federica, Michela, Francesca, and Chiara for sharing time in the lab (and also outside the lab) and for their advices and help. It was a pleasure to be part of this group.

I’d like to thank Dr. Giancarlo Forte for hosting me at FNUSA-ICRC (Brno, CZ). I’d like to thank my labmates at FNUSA-ICRC, Stefania, Jorge, Ruby, Pamela, Vlada, Honza, Hanka, Ece, Nives, Helca, and Jana for their advices and help in the experimental activity.

I’d like to thank my master degree students, Gaia and Andrea, and my bachelor degree student Simone, for helping me in the experimental activity.

I’d like to thank Prof. Fioretta Asaro, Prof. Paolo Macor, Prof. Gianluca Turco, Prof. Renzo Menegazzi, Dr. Eva Decleva, Dr. Pietro Parisse, Dr. Jolanda Spadavecchia, Dr. Dan Cojoc, Davide, Martina, and everyone I worked with during these years.

I’d like to thank also my officemates Mario, Riccardo, Adriana, and Federica.

Finally, I’d like to thank my family, who always supported and encouraged me during this route.